

Modeling and Optimization of a Solar Assisted Heat Pump Using Ice Slurry as a Latent Storage
Material

Justin Tamasauskas

A Thesis

in

The Department of

Building, Civil and Environmental Engineering

Presented in Partial Fulfillment of the Requirements

for the Degree of Master of Applied Science (Building Engineering) at

Concordia University

Montreal, Quebec, Canada

August, 2011

© Justin Tamasauskas, 2011

CONCORDIA UNIVERSITY

School of Graduate Studies

This is to certify that the thesis prepared

By: Justin Tamasauskas

Entitled: Modeling and Optimization of a Solar Assisted Heat Pump Using Ice Slurry as a Latent Storage Material

and submitted in partial fulfillment of the requirements for the degree of

Master of Applied Science (Building Engineering)

complies with the regulations of the University and meets the accepted standards with respect to originality and quality.

Signed by the final Examining Committee:

<u>Dr. P. Fazio</u>	Chair
<u>Dr. G. Vatistas</u>	Examiner
<u>Dr. L. Wang</u>	Examiner
<u>Dr. R. Zmeureanu</u>	Co-Supervisor
<u>Dr. M. Poirier</u>	Co-Supervisor

Approved by J. Drapeau
Graduate Program Director

Dr. R. Drew
Dean of the Faculty

Date August 22nd, 2011

ABSTRACT

Modeling and Optimization of a Solar Assisted Heat Pump Using Ice Slurry as a Latent Storage Material

Justin Tamasauskas

The use of a solar assisted heat pump has the potential to significantly reduce the amount of energy required for home heating. This study examines the viability of using a solar assisted heat pump operating with ice slurry to heat a high performance home in Montreal, QC.

A new mathematical model is first developed to predict the performance of an ice slurry storage tank. The model is integrated into the TRNSYS 16 simulation environment, and validated using experimental data. Results show that the proposed model is able to accurately predict tank performance in all phases of operations.

A computer model of the proposed heat pump system is then created in TRNSYS using both standard and custom components. The TRNSYS model is used in conjunction with the GenOPT computer program to perform an optimization of the system with the goal of minimizing the operating energy use over a heating season. The proposed system shows significant potential as it leads to an 86% reduction in the operating energy use in comparison to a base case home operating with electrical heaters, and a 26% reduction in the operating energy use in comparison to a solar assisted heat pump operating using only sensible storage.

Acknowledgements

I would like to express my gratitude to my two co-supervisors. First, thank you to Dr. Radu Zmeureanu for his patience, encouragement and support during the preparation of this thesis. I will never forget the dedication and generosity he has shown. I would also like to thank Dr. Michel Poirier for his constructive comments and feedback. His attention to detail and willingness to help are greatly appreciated.

A special thanks to Roberto Sunyé and everyone at CanmetENERGY in Varennes for their assistance, and for providing me with the opportunity to work on such an interesting project.

I would like to acknowledge the financial assistance I have received from NRCan/CanmetENERGY, NSERC, and Concordia University.

Thank you to all my friends at Concordia. They have made the last two years a truly unforgettable experience.

Finally, a special thanks to my parents for their love and encouragement. This thesis would not have been possible without their continuous support.

Table of Figures

List of Tables	ix
List of Figures.....	xi
Nomenclature.....	xiv
1. Introduction	1
1.1 Background	1
1.2 Research Objectives	2
2. Literature Review	3
2.1 Advanced Housing Design in the Canadian Market	3
2.2 Thermal Storage in Buildings	5
2.3 Methods of Ice Storage	7
2.3.1 Ice-On-Coil Design Alternatives.....	7
2.3.2 Encapsulated Ice Designs Alternatives	9
2.3.3 Ice Harvester Systems.....	11
2.3.4 Ice Slurry Systems.....	12
2.4 Ice Storage in Buildings.....	15
2.5 Ice Storage Integration with Solar Thermal Systems	18
2.6 Simulation Studies.....	24
2.6.1 Ice Storage Models	24
2.6.2 Whole-Building Simulation	30
2.6.3 Summary of Models.....	35

2.7 Conclusions	37
2.8 Thesis Objectives	39
2.9 Methodology.....	39
3. Development of an Ice Storage Tank Mathematical Model.....	42
3.1 Development Assumptions.....	42
3.2 Mathematical Model	43
3.2.1 Energy Balances.....	43
3.2.2 Effectiveness Coefficient Approach.....	45
3.2.3 Discretization of Energy Balance Equations.....	49
3.2.4 Calculation Assumptions.....	49
3.3 TRNSYS Integration.....	50
3.3.1 TRNSYS Component Development	50
3.3.2 Description of TRNSYS Proforma	54
3.3.3 Description of Iterative Approach	56
3.4 Validation of Simulation Results	57
3.4.1 Validation of the Charging (Ice Building) Process.....	58
3.4.2 Validation of the Discharge (Ice Melting) Process.....	61
3.5 Summary.....	64
4. Modeling of a Solar Assisted Heat Pump Using Ice Slurry.....	65
4.1 TRNSYS Overview	65

4.2 System Description.....	67
4.3 Modeling of Solar Assisted Heat Pump in TRNSYS.....	70
4.3.1 Summary of TRNSYS Components Used	70
4.3.2 Description of TRNSYS Modeling Approach.....	73
4.4 Summary.....	108
5. Optimization of a Solar Assisted Heat Pump using Ice Slurry.....	109
5.1 Optimization Variables	109
5.1.1 Independent Design Variables	109
5.1.2 Dependant Design Variables.....	111
5.2 Optimization Objective Function	113
5.3 Optimization Algorithm	113
5.3.1 Description of Algorithm.....	114
5.3.2 Demonstration of Optimization Algorithm.....	117
5.3.3 Optimization Parameters.....	119
5.4 Optimization using GenOPT and TRNSYS	119
5.5 Optimization Results	121
5.5.1 Comparison of Optimization Results using Different Control Strategies.....	121
5.5.2 Sensitivity Analysis.....	125
5.6 Summary.....	132
6. Simulated Performance of a Solar Assisted Heat Pump Using Ice Slurry.....	133

6.1 System Comparison.....	133
6.2 Ice Slurry System Performance	135
6.2.1 General Performance.....	135
6.2.2 Component Performance	139
6.2.3 Daily System Performance	148
6.3 Summary.....	154
7. Conclusions.....	155
7.1 Contributions	157
7.2 Future Work.....	157
References.....	159
Appendix A1: Heat Pump Performance	170
Appendix A2: DHW Temperature Profile	171
Appendix A3: Demonstration of Sample Optimization.....	172

List of Tables

Table 2-1: Summary of Latent Heat Values for Selected Phase Change Materials	6
Table 3-1: Experimental Parameters for Effectiveness Function Development (ASHRAE, 1993) .	47
Table 3-2: Summary of Parameters for Type 213	54
Table 3-3: Summary of Derivatives for Type 213	55
Table 3-4: Summary of Inputs for Type 213	55
Table 3-5: Summary of Outputs for Type 213	56
Table 3-6: Key Discharge Test Parameters (ASHRAE, 1993).....	61
Table 4-1: TRNSYS Storage Components.....	70
Table 4-2: TRNSYS Hydronic Components.....	71
Table 4-3: TRNSYS System Control Components	71
Table 4-4: TRNSYS HVAC Components.....	71
Table 4-5: TRNSYS Data Input/Output and Calculation Components.....	72
Table 4-6: TRNSYS Weather and Temperature Components	72
Table 4-7: TRNSYS Miscellaneous Components	72
Table 4-8: Description of Physical Parameters of Home.....	75
Table 4-9: Summary of Window Area for Home	75
Table 4-10: Summary of Thermal Performance of Key Building Materials	76
Table 4-11: Energy Consumption of Base Case Home	76
Table 4-12: Soil Properties Input to Type 701	78
Table 4-13: Kasuda Correlation Properties	78
Table 4-14: Ground Reflectance Values	79
Table 4-15: Summary of Collector Array Properties	92
Table 4-16: Piping Parameters.....	93

Table 4-17: Outlet Loop Connections to WWST	94
Table 4-18: Heat Exchanger Properties.....	94
Table 4-19: Circulation Pump Properties for Heat Pump Loop	98
Table 4-20: PID Controller Parameters	101
Table 4-21: Radiant Floor Piping Properties.....	102
Table 4-22: HRU Properties	105
Table 4-23: Summary of Ventilation Pump Parameters	105
Table 5-1: Study Range of Independent Design Variables	110
Table 5-2: Optimization Parameters for Sample Function.....	118
Table 5-3: Algorithm Parameters for Ice Slurry Study	119
Table 5-4: Initial Values of Optimization Variables.....	119
Table 5-5: Optimization Results for Two Control Strategies	122
Table 5-6: Optimization Results for Modified Control Strategy	124
Table 5-7: Design Variables for Further Analysis	131
Table 6-1: Distribution of Electricity by End Use	135
Table 6-2: Monthly Thermal Energy Input	137
Table 6-3: Energy Inputs/Extractions to WWST over Heating Season.....	143
Table 6-4: Summary of Heat Pump Performance	144
Table 6-5: Summary of Solar Loop Performance	145

List of Figures

Figure 1-1-Greenhouse Gas Emissions in Canada.....	2
Figure 2-1: Ice-On-Coil Internal Melt System Schematic	8
Figure 2-2: System Schematic for External Melt System	8
Figure 2-3(a): Charging of Encapsulated Ice Design Alternative	10
Figure 2-4(a): Charging of Ice Harvester Alternative	12
Figure 2-5: Ice Slurry Schematic	13
Figure 2-6: Solar Assisted Heat Pump with Latent Storage (Qi et al, 2008)	19
Figure 2-7: Combined Latent Store with Solar Collectors and Geothermal Loop (Han et al, 2008)	21
Figure 2-8: Ice Storage combined with Solar Collectors (Trinkl et al, 2009)	22
Figure 3-1: Ice and Water Layer Control Volumes.....	43
Figure 3-2: Effectiveness Function Proposed by Behschnitt (1996)	46
Figure 3-3: Calculated Effectiveness Coefficient as a Function of Ice Fraction	48
Figure 3-4: Effectiveness Function for Type 213	48
Figure 3-5: TRNSYS Component Approach.....	51
Figure 3-6: Comparison of Simulated and Experimental Ice Fraction During Charging Process... 60	
Figure 3-7: Comparison of Simulated and Experimental Tank Fluid Temperatures During Charging Process (IGR=1.96 kg/min, $T_{fluid0}=-1.5^{\circ}\text{C}$, $m_{ice0}=0$ kg).....	60
Figure 3-8: Comparison of Simulated and Experimental Ice Fraction During Discharge Process for Run#4 ($T_{o, col}=7.8^{\circ}\text{C}$, $m_{col}=2730$ kg/h, $T_{fluid0}=0^{\circ}\text{C}$, $m_{ice0}=1205$ kg).....	62
Figure 3-9: Comparison of Simulated and Experimental Ice Fraction During Discharge Process for Run #8 ($T_{o, col}=19.4^{\circ}\text{C}$, $m_{col}=2730$ kg/h, $T_{fluid0}=0^{\circ}\text{C}$, $m_{ice0}=1499$ kg)	62

Figure 3-10: Comparison of Simulated and Experimental Fluid Temperature During Discharge Process for Run #4 ($T_{o, col}=7.8^{\circ}\text{C}$, $m_{col}=2730\text{ kg/h}$, $T_{fluid0}=0^{\circ}\text{C}$, $m_{ice0}=1205\text{ kg}$).....	63
Figure 3-11: Comparison of Simulated and Experimental Fluid Temperature During Discharge Process for Run #8 ($T_{o, col}=19.4^{\circ}\text{C}$, $m_{col}=2730\text{ kg/h}$, $T_{fluid0}=0^{\circ}\text{C}$, $m_{ice0}=1499\text{ kg}$).....	63
Figure 4-1: Impact of System Layout on Solar Collector Performance	67
Figure 4-2: Proposed System Layout of Solar Assisted Heat Pump with Ice Slurry	69
Figure 4-3: House Portion of TRNSYS Simulation Model	73
Figure 4-4: Solar Loop Portion of the TRNSYS Simulation Model	80
Figure 4-5: Heat Pump Portion of TRNSYS Simulation Model	95
Figure 4-6: Radiant Floor Loop Portion of TRNSYS Simulation Model	99
Figure 4-7: Supply Fluid Temperature to Radiant Floor Loop	100
Figure 4-8: Ventilation Loop Portion of TRNSYS Simulation Model.....	103
Figure 4-9: TRNSYS Modeling of DHW Simulation Loop	105
Figure 4-10: Simulated DHW Flow Profile for Jan. 2 nd	107
Figure 5-1: Search Path of Sample Optimization	118
Figure 5-2: Information Exchange between GenOPT and TRNSYS	121
Figure 5-3: Impact of T_{set} on Heating Operating Energy Use.....	123
Figure 5-4: Impact of A_{col} on Heating Operating Energy Use	126
Figure 5-5: Impact of V_{WWSST} on Heating Operating Energy Use.....	127
Figure 5-6: Impact of β on Heating Operating Energy Use	128
Figure 5-7: Impact of m_{col}, s on Heating Operating Energy Use	129
Figure 5-8: Impact of V_{ice} on Heating Operating Energy Use.....	130
Figure 6-1: Comparison of Heating Operating Energy Use over Heating Season.....	134
Figure 6-2: Distribution of Electricity Use over Heating Season.....	136

Figure 6-3: Ice Inventory in Ice Tank over Heating Season	140
Figure 6-4: Fluid Temperature in Ice Tank over Heating Season	141
Figure 6-5: Average Fluid Temperatures in WWST over Heating Season	142
Figure 6-6: Monthly Solar Collector Efficiencies over Heating Season	147
Figure 6-7: Average Monthly Solar Collector Outlet Temperatures over Heating Season	147
Figure 6-8: Pump and Heat Pump Control Signals for October 25 th	149
Figure 6-9: WWST Fluid Temperatures for October 25 th	150
Figure 6-10: Ice Tank Fluid Temperatures for October 25 th	150
Figure 6-11: Pump and Heat Pump Control Signals for January 5 th	151
Figure 6-12: WWST Fluid Temperatures for January 5 th	152
Figure 6-13: Ice Inventory in Ice Tank for January 5 th	153

Nomenclature

Symbol	Description	Unit
0	Superscript referring to initial conditions	-
A_c	Contact area between the ice and water layers	m^2
A_{col}	Collector area	m^2
A_{floor}	Floor area	m^2
$A_{s,fluid}$	Surface area of fluid in contact with the sides of the storage tank	m^2
$A_{s,ice}$	Surface area of ice in contact with the sides of the storage tank	m^2
a	DHW temperature profile correlation coefficient	-
b_0	First order incidence angle modifier	-
b_1	Second order incidence angle modifier	-
COP_{sys}	System coefficient of performance	-
CS	Control signal to pump	-
c	Mesh exponent increment	-
c_p	Specific heat of the fluid	$kJ/kg \cdot ^\circ C$
d_{pipe}	Pipe diameter	m
$E_{A,DHW}$	Auxiliary energy input to meet DHW demand	$kW \cdot h$
$E_{A,RF}$	Auxiliary energy input to the radiant floor	$kW \cdot h$
$E_{A,Vent}$	Auxiliary energy input to the water in ventilation loop	$kW \cdot h$
$E_{i,aux}$	Energy input to auxiliary heaters	$kW \cdot h$
$E_{i,HP}$	Energy input to the heat pump	$kW \cdot h$
$E_{i,pump}$	Energy input to the circulation pumps	$kW \cdot h$
E_{Op}	Heating operating energy use	$kW \cdot h$
e	Search direction	-

F'	Collector efficiency parameter	-
F_R	Heat removal factor	-
F_{solar}	Solar fraction	-
G_{beam}	Beam radiation incident on the collector	W/m^2
G_{dif}	Diffuse radiation incident on the collector	W/m^2
G_{gnd}	Ground reflected radiation incident on the collector	W/m^2
G_T	Total incident radiation on the surface	W/m^2
h	Convective heat transfer coefficient between the ice and water layers	$kJ/h \cdot m^2 \cdot ^\circ C$
IGR	Ice generation rate	kg/h
K_θ	Incidence angle modifier	-
$K_{\theta,beam}$	Incidence angle modifier for beam radiation	-
$K_{\theta,dif}$	Incidence angle modifier for diffuse radiation	-
$K_{\theta,gnd}$	Incidence angle modifier for ground reflected radiation	-
k	Optimization iteration	-
L	Latent heat of ice	kJ/kg
\dot{m}_{calc}	Calculated mass flow rate from the PID controller	kg/h
\dot{m}_{col}	Mass flow rate of fluid from the solar collectors	kg/h
$\dot{m}_{col,s}$	Specific solar collector flow rate	kg/h
\dot{m}_{HP}	Mass flow rate of fluid from the heat pump	kg/h
\dot{m}_{rated}	Rated flow rate of the pump	kg/h
\dot{m}_{test}	Fluid mass flow rate at test conditions	kg/h
m_{fluid}	Mass of fluid in the ice tank	kg
m_{glycol}	Mass of glycol in tank	kg
m_{ice}	Mass of ice in the ice tank	kg

$m_{ice,max}$	Maximum ice storage capacity of the ice tank	kg
m_{tank}	Total mass storage capacity of the ice tank	kg
N	Day of year	-
N_{Loops}	Number of piping loops in the zone	-
N_{series}	Number of collectors in series	-
n	Ice tank solver iteration	-
\dot{P}	Pump power	W
\dot{P}_{rated}	Rated pump power	W
Q_{col}	Volumetric flow rate through the pump	m^3/s
$Q_{gain,col}$	Heat gain from collector	W
Q_{load}	Combined heating and DHW load of the home	kW
R_1	Flow correction factor	-
R_2	Series correction factor	-
R_{test}	Test correction factor	-
r	Mesh size divider	-
rd_{tank}	Radius of ice storage tank	m
S_{pipe}	Length of the piping segment	m
S_{ice}	Ice mass storage array	-
S_{Temp}	Ice tank fluid temperature storage array	-
s	Variable step size	-
T_{amb}	Temperature of ambient air	$^{\circ}C$
T_{cont}	Control temperature difference	$^{\circ}C$

T_{env}	Temperature of the ambient air surrounding the tank	$^{\circ}\text{C}$
T_{city}	Temperature of water from the city main	$^{\circ}\text{C}$
T_{fluid}	Fluid temperature in the ice tank	$^{\circ}\text{C}$
T_{glycol}	Glycol freeze point temperature	$^{\circ}\text{C}$
$T_{i,col}$	Inlet fluid temperature into the collector	$^{\circ}\text{C}$
$T_{i,HP}$	Inlet fluid temperature to the heat pump	$^{\circ}\text{C}$
T_{ice}	Temperature of the ice layer	$^{\circ}\text{C}$
$T_{o,col}$	Fluid temperature exiting the solar collectors	$^{\circ}\text{C}$
$T_{o,col,LoopB}$	Anticipated outlet collector temperature in the Loop B configuration	$^{\circ}\text{C}$
$T_{o,HP}$	Fluid temperature exiting the heat pump evaporator	$^{\circ}\text{C}$
$T_{o,ice}$	Fluid temperature exiting the ice layer	$^{\circ}\text{C}$
T_{set}	User defined setpoint temperature	$^{\circ}\text{C}$
T_{sup}	Radiant floor supply temperature	$^{\circ}\text{C}$
T_{WWST}	Temperature at the bottom of the WWST	$^{\circ}\text{C}$
t	Time	h
t_{LoopA}	Duration of time in Loop A mode	h
t_{LoopB}	Duration of time in Loop B mode	h
U	Tank loss coefficient	$\text{kJ}/\text{h}\cdot\text{m}^2\cdot^{\circ}\text{C}$
U_L	Collector heat loss coefficient	$\text{W}/\text{m}^2\cdot^{\circ}\text{C}$
U_L'	Modified first order collector efficiency coefficient	$\text{W}/\text{m}^2\cdot^{\circ}\text{C}$
$U_{L/T}$	Temperature dependency of collector heat loss coefficient	$\text{W}/\text{m}^2\cdot^{\circ}\text{C}^2$
V_{ice}	Ice tank volume	m^3
V_{pipe}	Flow velocity in pipe	m/s
V_{tank}	Maximum storage volume of the ice tank	m^3

V_{WWST}	WWST volume	m^3
$v_{1..17}$	DHW temperature profile coefficients	-
$w_{1..17}$	DHW temperature profile coefficients	-
X	Set of constraints	-
X_o	Outlet ice fraction	-
x'	Exploration vector	-
x_b	Optimization base point	-
x_k	Vector corresponding to the lowest value of the objective function	-
Y_{Pipe}	Pipe spacing	m
y	Mesh size exponent	-
z	DHW temperature profile correlation coefficient	-

Greek Symbol

Symbol	Description	Unit
Φ	Refrigeration capacity of the heat pump	kJ/h
Δ	Mesh size factor	-
ΔP	Pump head	Pa
$\Delta T_{col,LoopA}$	Anticipated fluid temperature rise across the solar collectors in Loop A mode	$^{\circ}C$
$\Delta T_{col,LoopB}$	Anticipated fluid temperature rise across the solar collectors in Loop B mode	$^{\circ}C$
Δt	Simulation time step	h
β	Collector tilt angle	$^{\circ}$
ϵ	Effectiveness coefficient	-
γ	Fraction of ice mass in the storage tank	-
λ_{glycol}	Glycol concentration	-
η_{col}	Solar collector efficiency	-
$\eta_{overall}$	Overall collector efficiency	-
η_{LoopA}	Loop A collector efficiency	-
η_{LoopB}	Loop B collector efficiency	-
η_{pump}	Combined electrical and mechanical pump efficiency	-
θ	Incidence angle	$^{\circ}$
θ_{dif}	Effective incidence angle for diffuse radiation	$^{\circ}$
θ_{gnd}	Effective incidence angle for ground reflected radiation	$^{\circ}$
ρ_{fluid}	Density of storage fluid in ice tank	kg/m ³
ρ_{ice}	Density of ice	kg/m ³
$(\tau\alpha)$	Combined transmittance/absorptance product	-
ω_{gnd}	Ground reflectance	-

Abbreviations

ASHRAE	American Society of Heating, Refrigeration, and Air-Conditioning Engineers
CS	Control Signal
COP	Coefficient of Performance
IGR	Ice Gain Rate
IPCC	Intergovernmental Panel on Climate Change
NRCan	Natural Resources Canada
PCM	Phase Change Material
UNFCCC	United Nations Framework Convention on Climate Change
WWST	Warm Water Storage Tank

1. Introduction

1.1 Background

Climate change is one of the greatest issues facing our society today. Global temperatures have increased by an average of 0.7°C since 1950, and are anticipated to rise a further 1.8°C to 4°C over the next 100 years (IPCC, 2007). These temperature rises are expected to have a significant impact on the global population, resulting in higher sea levels and an increase in extreme weather events such as cyclones and droughts (IPCC, 2007).

The Intergovernmental Panel on Climate Change (IPCC) suggests that the increase in global temperatures over the last 50 years is “most likely due to the observed increase in anthropogenic greenhouse gas emissions” (IPCC, 2007). Recognition of the anthropogenic component of climate change has led to several international accords aimed at dealing with this issue. Of particular significance is the Kyoto Protocol, which was adopted in 1997 and entered into effect in 2005. This Protocol sets forth emissions targets for 37 industrialized nations, with the goal of achieving an overall 5.2% reduction in greenhouse gas emissions (relative to 1990 levels) over the period 2008-2012 (UNFCCC, 2011).

As part of the Protocol, Canada agreed to reduce greenhouse gas emissions by 6%. However, as shown in Figure 1-1, Canadian greenhouse gas emissions have risen by an additional 24% over 1990 levels, meaning that an overall reduction of 31.5% is required (Environment Canada, 2010). Clearly, significant action is needed to approach the targeted reductions.

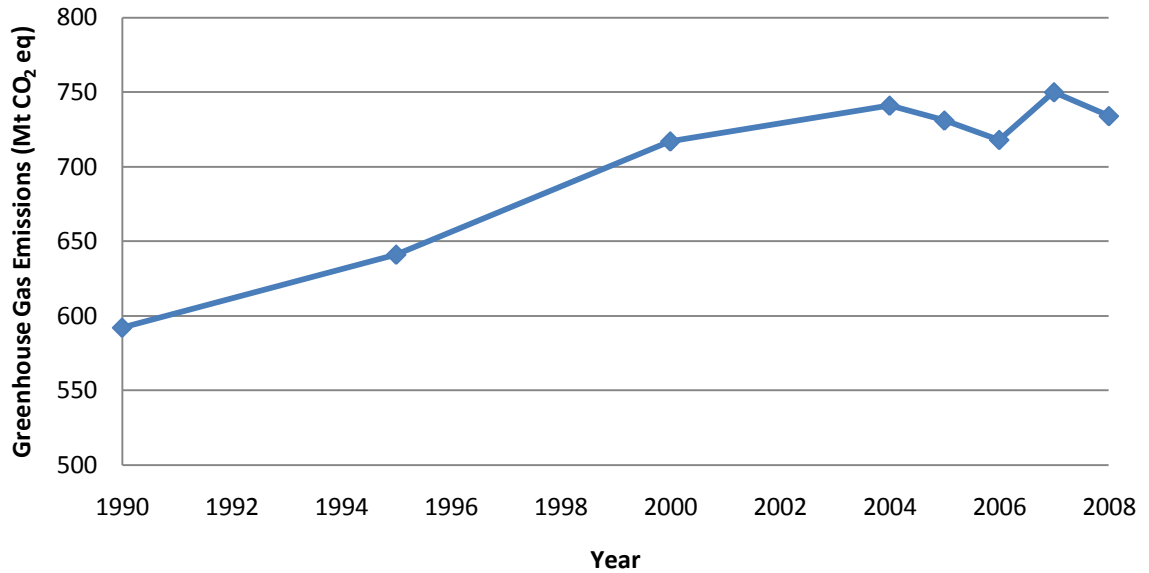


Figure 1-1-Greenhouse Gas Emissions in Canada

Energy use is closely linked with greenhouse gas emissions, as a large proportion of energy in Canada is supplied by fossil fuels (NRCAN, 2011a). In Canada, residential buildings account for 17% of all secondary energy usage, with home and water heating comprising 80% of the total (NRCAN, 2010a). By reducing the amount of energy used for residential home and water heating, Canada can make significant progress towards its emission reduction targets.

1.2 Research Objectives

The objective of the proposed research is to examine the potential of using a solar assisted heat pump to heat a high performance Canadian home. In particular, the use of latent storage will be examined because of the higher energy storage densities available in this type of design (Hasnain, 1998).

2. Literature Review

This section outlines important concepts regarding thermal storage and its use in low energy buildings. The advanced housing market in Canada is first introduced, followed by an introduction to ice-based thermal storage systems serving in both building heating and cooling operational modes. Various models for simulating ice-based storage are presented, followed by an examination of ice-storage simulation in the whole-building context. The goal is to define the current level of knowledge, and highlight the need for further analysis, experimental work and detailed simulation of these systems in the built environment.

2.1 Advanced Housing Design in the Canadian Market

Increasing concern over climate change and greenhouse gas (GHG) emissions has brought about a deeper awareness of energy use in our society. In particular, much attention has been paid to energy use in the residential sector, as this accounts for 17% of total consumption in Canada (NRCan, 2010a). A number of incentive and demonstration programs have been implemented in Canada to promote innovative and energy efficient technologies in the residential housing sector. One of the most widespread is the R-2000 program, which was created in 1981 through a collaboration between Natural Resources Canada (NRCan) and the Canadian Home Builders' Association (NRCan, 2010b). A voluntary program currently in operation, it aims at improving energy efficiency, indoor air quality, and environmental awareness in the home building sector. The specifications listed in the standard encompass wall insulation, the maximum amount of air leakage in the home, and ventilation system design. They also set the maximum energy consumption in terms of electricity and hot water usage. Strictly applicable to low-rise residential buildings, it requires extensive certification to ensure proper implementation, and represents a benchmark in Canadian home construction.

While the R-2000 program focused solely on reducing the energy used to provide space conditioning and domestic hot water, the Advanced Houses Program was introduced by NRCan in 1991 with the primary goal of demonstrating the use of available environmentally friendly and energy efficient technologies (CalRecycle, 1998). A total of 10 demonstration homes were constructed across Canada, with the aim of reducing the amount of energy purchased (for electrical appliances, space heating and cooling, and domestic hot water) to half of what is consumed in a typical R-2000 home. Each home represented a unique design aimed at implementing technologies including solar thermal systems, seasonal thermal storage, and geothermal heat pumps. Gerbasi (2000) analyzed the energy use of the NOVTEC advanced home in Laval, QC. The home used an innovative Exterior Insulation and Finish System (EIFS), along with a ground source heat pump and a radiant slab heating system. The annual energy consumption was $60 \text{ kW}\cdot\text{h}/\text{m}^2$, which represented an over 40% reduction in comparison to an R-2000 home. Mayo and Sinha (1996) presented monitored energy usage for five additional Advanced Homes (The Nova Scotia EnviroHome, Waterloo Green Home, Ottawa Innova House, and the Manitoba and Saskatchewan Advanced Homes). Each home used an upgraded building envelope and a water based integrated mechanical system. On average, annual energy use was found to be $81 \text{ kW}\cdot\text{h}/\text{m}^2$, which fell short of the targeted 50% reduction in comparison to an R-2000 home. Although the program was unable to fully obtain the desired reductions in annual energy consumption, it allowed researchers to examine how best to implement various energy efficient technologies into a single family Canadian home.

2.2 Thermal Storage in Buildings

Thermal storage is based on the idea that the excess thermal energy produced by plant equipment or collected solar radiation can be stored in some form of storage material for later use. These storage materials can range from the rock and concrete used as thermal mass in passive solar buildings to water and phase change materials used in cool and hot storage systems. The concept of thermal storage is vital to the efficient operations of buildings. Often the thermal energy available to a building (from plant equipment or captured solar radiation) is much greater than what is required to meet the space heating, space cooling or domestic hot water (DHW) loads. Equipment such as chillers and boilers are generally sized to meet the peak load of a building which may occur for only a small fraction of operations. In the case of solar energy, daily incident radiation is usually non-coincident with heating demand. Peak radiation levels occur near midday and increase significantly during the summer months, while the demand for thermal energy is highest in a cold-climate home in the winter months during the early morning or evening hours. Thermal storage allows some of this excess energy to be kept for future use, whether this is short term (on the order of hours) or long term storage (on the order of days/weeks/months).

One form of this technology is cool storage, in which thermal energy is stored below the space or usage temperature (ASHRAE, 2007). Cool storage systems fall into two classifications: sensible or latent storage. Sensible storage uses the temperature change of a single-phase substance to store thermal energy. While simple, the large storage volumes required often limit its application.

Latent storage systems using phase change materials (PCM) take advantage of the latent heat of melting or solidification during a phase change to store thermal energy at a much higher density. In general, heat is extracted to form a solid or added to produce a low temperature liquid. The latent storage material can be integrated into various components of the building envelope (Feldman et al, 1991), or simply kept in a storage tank (Feldman et al, 1988). The higher storage densities and larger temperature ranges available make latent storage a preferred method in comparison to sensible storage (Hasnain, 1998). These types of storage systems can also lead to a significant reduction in tank sizes. For example, with a 50% ice storage fraction combined with sensible storage from 0°C to 13°C, the overall storage volume can be reduced to 1/9th of a pure sensible water storage system with a temperature range of 7°C to 13°C (Wang and Kusumoto, 2001).

One of the most important properties is the latent heat of fusion of the phase change material. A wide range of values exist, with the latent heat of fusion for selected PCMs summarized below in Table 2-1 (Values from ((Hawes et al, 1993))).

Table 2-1: Summary of Latent Heat Values for Selected Phase Change Materials

Phase Change Material	Latent Heat of Fusion (kJ/kg)	Phase Change Temperature (°C)
Paraffin (CH ₃ (CH ₂) _n (CH ₃))	200.0	20.0-60.0
1-tetradecanol (CH ₃ (CH ₂) ₁₂ OH)	205.0	38.0
Calcium Chloride Hexahydrate (CaCl ₂ ·6H ₂ O)	171.0	29.7
Sodium Orthophosphate Dedecahydrate (Na ₂ HPO ₄ ·12H ₂ O)	281.0	35.0
Water (H ₂ O)	333.5	0.0

Ice-based latent heat storage provides a number of advantages over other types of phase change materials. Firstly, the latent heat of fusion for water/ice is significantly higher than most other PCMs, meaning that thermal energy can be stored at a higher density. Water is also a naturally available substance, making it easy to obtain the storage material and replenish the tank in case of any leaks. In addition, water represents a low cost and environmentally safe storage material.

2.3 Methods of Ice Storage

Latent storage is often preferred due to the high energy storage density available in the storage tank. Several methods exist for the charging (extracting thermal energy to freeze the PCM) or discharging (adding thermal energy to the tank to melt the PCM) of a latent storage tank. This section examines a few common approaches to this problem, focusing strictly on water based systems due to their prevalence in the marketplace.

2.3.1 Ice-On-Coil Design Alternatives

Ice-on-coil designs involve locating the evaporator of a refrigeration system directly within the storage tank (ASHRAE, 2007). During charging, heat is extracted from the water in the storage tank by refrigerant circulating through the evaporator coils, eventually leading to ice formation on the coils. The system can also use a secondary loop (with brine or glycol), with the secondary fluid circulating through a coiled heat exchanger located in the ice tank. Discharging can be accomplished using two different methods. In an internal melt system, the refrigerant cycle is reversed, with the coils located in the storage tank becoming the condenser of the unit. Ice layers closest to the coils are melted first with the melting front moving radially outward. The water remains in the tank, and the storage container acts as a heat sink. A basic system schematic for the internal melt system can be seen in Figure 2-1.

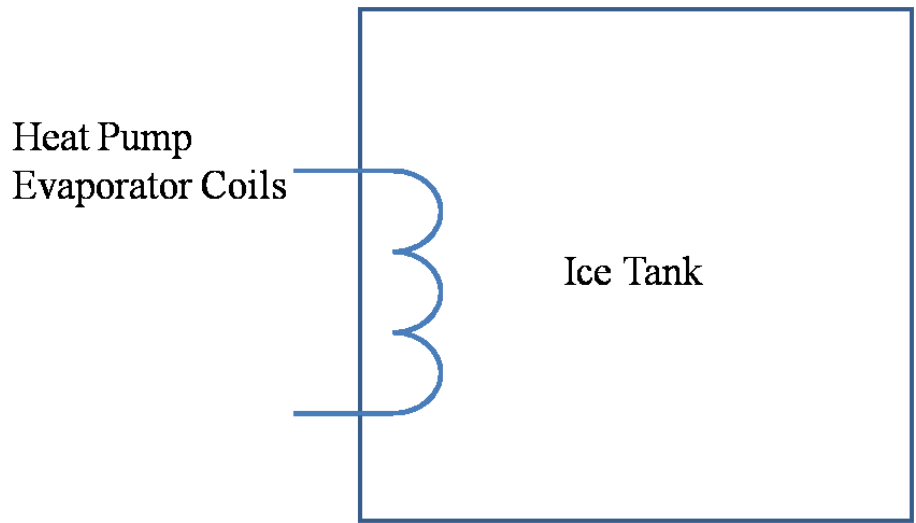


Figure 2-1: Ice-On-Coil Internal Melt System Schematic

In external melt designs, the water remaining in the tank after charging is circulated to a cooling coil. Warmer return water from the cooling coil is then circulated in the tank, melting the outer portions of the ice first. The system is shown in Figure 2-2.

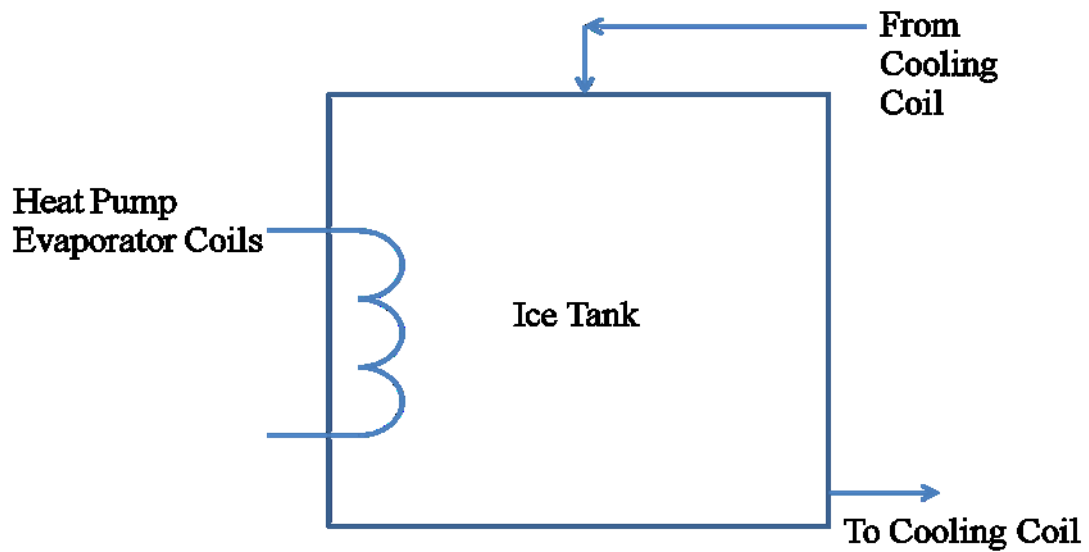


Figure 2-2: System Schematic for External Melt System

The main disadvantage of this system, in both approaches, is the reduced performance during charging due to the added resistance of the growing ice layer (ASHRAE, 2007). The charging process needs to be carefully controlled to ensure ice thickness is not too great, as larger ice layers lead to lower heat transfer to the refrigerant in the evaporator coils and thus reduced overall performance. Furthermore, locating the evaporator coil inside the ice tank also reduces the available storage volume.

2.3.2 Encapsulated Ice Designs Alternatives

An encapsulated ice system generally involves the use of three different fluids: water, brine, and a refrigerant. Water is generally stored in spherical enclosures located inside the storage tank (ASHRAE, 2007), acting as the PCM storage material for the system.

A general system layout in the charging mode is shown in Figure 2-3(a), while the system layout in the discharge mode can be seen in Figure 2-3(b). Charging and discharging are controlled by circulating a brine solution through the storage tank, with this solution flowing over the outside of the storage capsules. During the charging process the brine solution is circulated through the ice tank, absorbing heat from the spherical enclosures. This brine solution then passes to a chiller, with the brine rejecting its heat to a refrigerant flowing in the evaporator. During the discharge process the circulating brine is cooled by passing through the ice tank. The brine then absorbs heat at a cooling coil before being reintroduced into the ice bank tank.

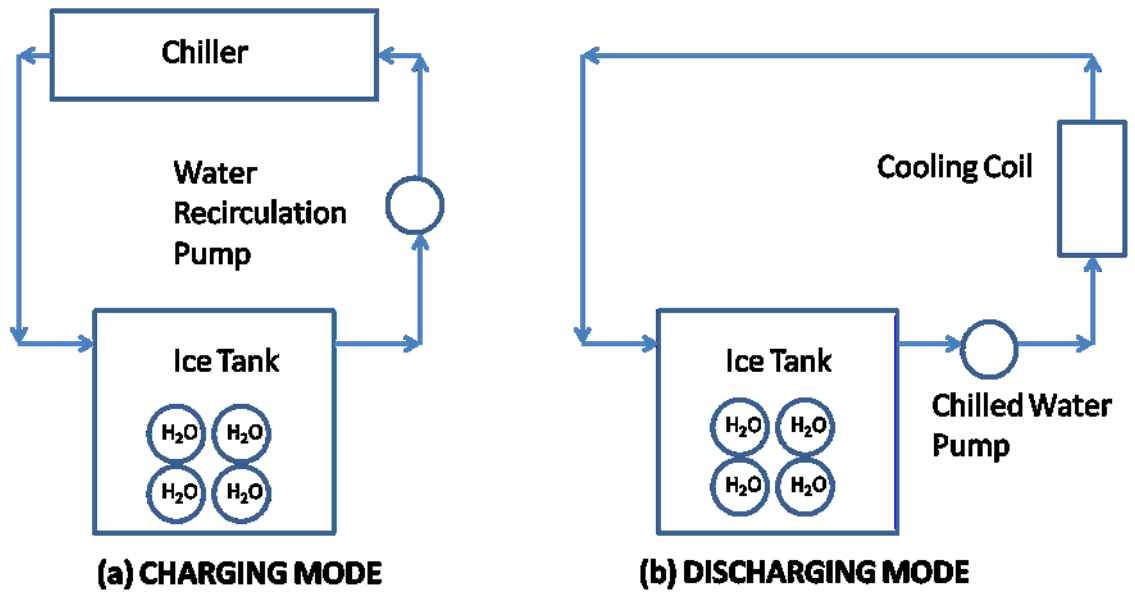


Figure 2-3(a): Charging of Encapsulated Ice Design Alternative

(b): Discharging of Encapsulated Ice Design Alternative

One of the main issues with this type of design is the subcooling effect often encountered in the absence of a nucleating agent inside the PCM enclosure (Wulfinghoff, 1999). This can lead to lower required freezing temperatures and consequently higher energy consumption for the refrigeration system. The spherical storage enclosures are often randomly arranged within the tank (Wulfinghoff, 1999). Since the primary mode of heat transfer between the brine and storage enclosure is convection, any flow irregularities caused by this random packing can lead to varying heat transfer rates at different locations in the tank. This can result in situations where some enclosures freeze or discharge at a faster rate than those in a different part of the tank, making capacity prediction and storage control a challenge.

2.3.3 Ice Harvester Systems

Ice harvester systems work in a similar manner to ice-on-coil designs, utilizing the evaporator of a refrigeration cycle to produce ice (ASHRAE, 2007). In the case of the ice harvester system this evaporator is located external to the tank.

A general system layout for charging mode is shown in Figure 2-4(a), with the discharging layout shown in Figure 2-4(b). In the charging mode a water recirculation pump directs a water-antifreeze brine mixture from the storage tank to an ice-maker. The liquid brine is then allowed to run through a plate heat exchanger operating as an evaporator, with ice forming on the evaporator surface. The evaporator is periodically defrosted through the use of bypass gases from the compressor or by reversing the refrigeration cycle. This defrost operation is required to limit the buildup of ice on the evaporator surface and thus allow for higher and less variable heat transfer to the refrigerant. The ice removed from the evaporator then falls into a storage tank located underneath the harvester, thus charging the storage tank with ice.

In the discharging mode a chilled water pump is used to transport liquid brine from the storage tank to a cooling coil. Return brine from the cooling coil is then reintroduced to the tank above 0°C, melting some of the existing ice in the storage tank.

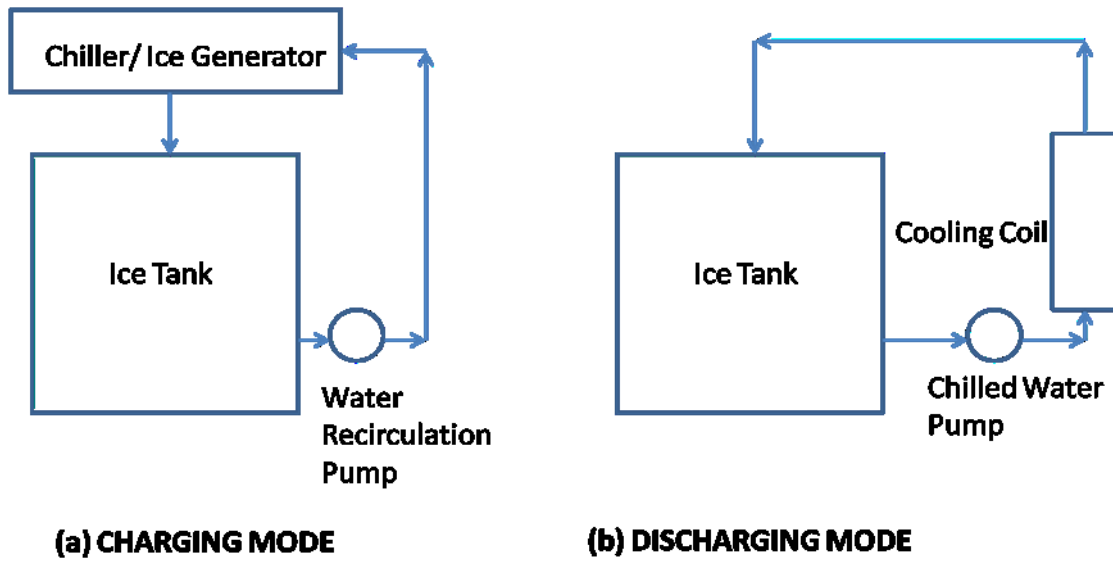


Figure 2-4(a): Charging of Ice Harvester Alternative

(b): Discharging of Ice Harvester Alternative

While this method keeps the evaporator relatively free of ice and separates the storage tank and ice generation equipment, the system is highly inefficient due to the energy used during defrost operations (Wulfinghoff, 1999).

2.3.4 Ice Slurry Systems

Ice slurry systems are similar to harvester systems in that the ice is produced outside of the storage tank (ASHRAE, 2007). In the case of ice slurry, heat is extracted from a water or antifreeze brine circulating through the evaporator of a refrigeration cycle until ice crystals begin to form. The sides of the evaporator are mechanically scraped to prevent ice from adhering to the surface, creating a two phase water-ice mixture which is stored in the storage tank and can then be pumped to a cooling coil. A general schematic of the system is shown in Figure 2-5.

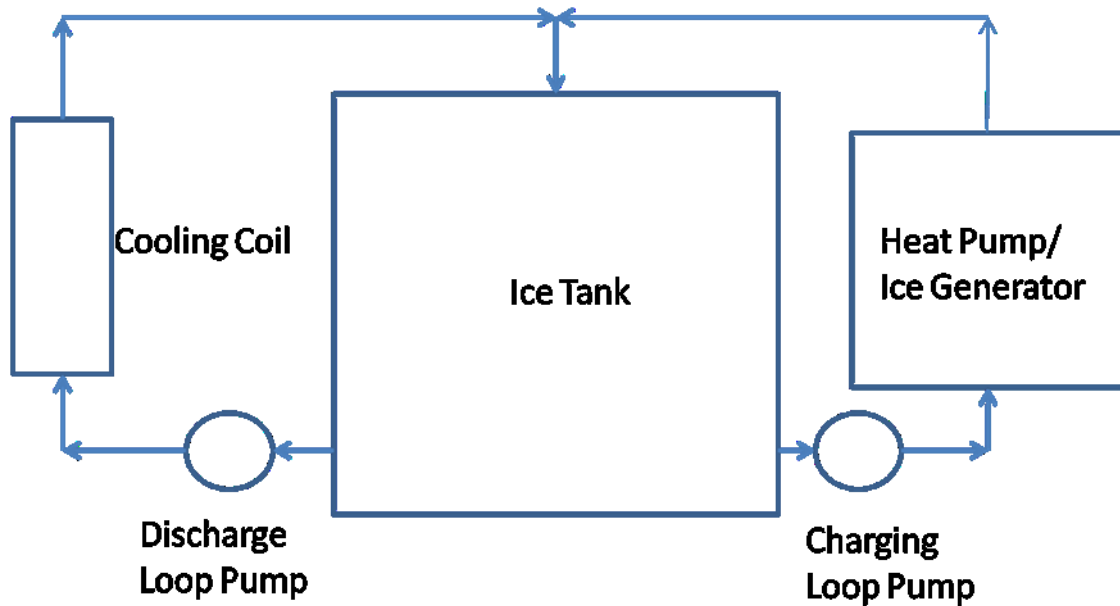


Figure 2-5: Ice Slurry Schematic

Discharging of the tank can be performed in two ways (Ure, 1999). The slurry mixture can be allowed to stratify in the storage tank, yielding a low temperature liquid at the bottom of the tank which can be used as the working fluid in a cooling coil. Alternatively, a homogenous two-phase slurry mixture can also be circulated. This requires that the tank be mechanically stirred to prevent ice agglomeration, or that the ice and water that has stratified be mixed external to the storage tank before being directed to the cooling coil.

In both methods of discharge, the water or ice/water mixture absorbs heat at the cooling coil. The return water or slurry mixture is then reintroduced at the top of the storage tank at a temperature above 0°C, melting existing ice in the tank.

More complex methods of slurry generation have also been proposed, mainly focusing on the use of super-cooled water. Li et al. (2009) proposed a system in which cold, low humidity air is introduced to a water spray chamber, super-cooling the water and precipitating ice particles through the use of a super-cooling water releaser.

Ice slurry has a number of advantages over the above mentioned ice storage systems. One of the primary benefits of ice slurry is its capability to absorb large amounts of thermal energy (Ure, 1999) due to the increased ice surface area available in the mixture. The ice slurry mixture can be pumped directly to applications throughout a building, or simply stored in a stratified ice tank in an arrangement similar to the ice harvester. The storage tank also avoids the need for any heat exchangers within its structure, yielding a simpler and easier to maintain system. Since the storage tank does not have to be located directly underneath the ice generator, more flexibility is provided to the designer in terms of system layout.

A number of studies have examined the impact of ice slurry on pumps and piping components. Niezgodna-Zelakso and Zalewski (2006), Grozdek et al. (2009), and Illan and Viedma (2009) all examined the pressure losses associated with ice slurry in horizontal piping. In general, the pressure drop of the ice slurry mixture increased with flow velocity and ice fraction. However, the relationship between these three variables (pressure drop, velocity and ice content) was complex. At a constant flow velocity, a laminar flow at 0% ice fraction exhibited a gradual increase in pressure drop as the ice content was raised. For flows that were turbulent at 0% ice fraction, the pressure drop remained similar to that of a liquid solution until a critical ice fraction is reached. This critical ice fraction marked the transition from turbulent to laminar flow, with the pressure drop at a constant flow velocity increasing significantly beyond this point.

Norgaard et al. (2005) and Frei and Huber (2005) studied the performance of circulation pumps operating using ice slurry. In general, ice slurry use resulted in a lower pump head and efficiency due to the higher viscosity of the operating fluid in comparison to a single phase liquid. However, the difference in performance between ice slurry and a single phase liquid was very

small for ice fractions below 15%, with Frei and Huber (2005) suggesting that centrifugal pumps be used up to an ice fraction of 25% because of their low cost and consistent performance.

While ice slurries hold much promise, their proper application to buildings has been limited due to a relative lack of information regarding the design, system implementation, performance, and mathematical modeling.

2.4 Ice Storage in Buildings

Ice storage has become increasingly popular in buildings due to the lower tank volumes required to store an equivalent amount of energy in comparison to sensible systems. One of the best documented applications of ice storage can be found in the Oak Ridge National Laboratory report on the Knoxville Demonstration House (Fischer, 1981). The home, located in the southeastern United States, incorporated a heat pump along with an ice storage tank. The mechanical system could be operated in three different modes: space heating mode, domestic hot water heating mode, and heat rejection (cooling) mode. In heating mode thermal energy from the ice storage tank was transferred to a refrigerant circulating in the heat pump evaporator, creating ice and thus charging the tank. This energy was then transferred via the heat pump to a stratified storage tank, from which the space and domestic hot water needs of the home could be met. Cooling was performed by using chilled water in the ice storage tank directly in the supply air coils. An analysis of system performance over a four year period revealed an annual Coefficient of Performance (COP) of 2.8. While the study is limited to a single building, it demonstrates the feasibility of an ice storage system in the North American marketplace.

A similar mechanical system incorporating ice storage was implemented in the Brampton Advanced House (Enermodal, 1992). Like the Knoxville home, the mechanical system consisted

of a heat pump operating between ice storage and stratified hot water tanks. In heating mode thermal energy was extracted from the ice storage tank using in-tank evaporator coils. The thermal energy was subsequently upgraded using the heat pump and stored in a warm-side storage tank to satisfy heating and domestic hot water requirements. Cooling of the home was achieved by pumping the liquid water in the ice storage tank to the cooling coil, with the warmer return water rejecting its heat to the ice remaining in the tank.

The home incorporated a number of energy recovery systems, including grey water heat exchangers and exhaust air coils to recover heat from the outgoing air. Performance was analyzed over a two year operational period. The seasonal performance factor (SPF, defined as the useful heating and cooling obtained over the energy demands of the mechanical system and auxiliary heating) was found to be 1.54 while the heat pump COP ranged from 1.7 to 2.1. Both indices were significantly less than the predicted values of 2.0 for the SPF and the 2.5 to 3.0 for the heat pump COP. The lower than expected heat pump performance combined with higher than predicted pump power requirements led to an annual energy usage of 19834 kW·h (48.6 kW·h/m²) during the second year of operations, approximately 60% greater than predicted using the ENERPASS simulation program. Although overall performance did not meet initial expectations, energy usage was still half of an equivalent R-2000 home.

The last decade has seen an increase in the use of ice slurry systems due to their high heat transfer capabilities and the availability of improved slurry generation systems. Wang and Kusumoto (2001) described the ice slurry system used in the Herbis Osaka complex, a multi-purpose building consisting of shops, offices, exhibition spaces, and a hotel. Located in Osaka, Japan, the building comprised 40 above ground floors, 5 underground floors, and a tower floor with a total floor area of 136823 m². The high density of electrical equipment in the office

spaces resulted in a cooling dominated structure, with the cooling load approximately double the heating load.

The variety of space uses led the designers to select a distributed ice-slurry based heating and cooling system. A total of 31 ice slurry generation units (260 kW each) were installed, providing half of the peak load of the building. The remainder of the peak load was provided using an ice slurry thermal storage system, with 16 tanks (volume 70 m³ or 140 m³) installed throughout the building for a total storage capacity of 80750 kW·h.

The HERBIS building used ice slurry to drive a natural refrigeration cycle operating with a Freon refrigerant. During heating operations, heat rejected from the ice generation process was used to evaporate liquid Freon returning from an air coil via a liquid/liquid coiled heat exchanger. The vapourized refrigerant then returned to the air handling unit through buoyancy forces, rejecting its heat and transferring thermal energy to the incoming ventilation air.

The cooling cycle worked in a similar manner, with ice slurry from the bottom of the tank being circulated to an ice slurry/refrigerant coiled heat exchanger. Refrigerant vapour entering this heat exchanger from the air handling unit rejected its thermal energy to the ice slurry, cooling until it became a single phase liquid. This liquid refrigerant then reentered the air handling unit cooling coil via gravity, absorbing thermal energy and cooling the incoming air.

Coupling the ice slurry system with a gravity driven refrigeration cycle yielded a 60% reduction in the energy required to transport air and the heating and cooling fluids. The designers were also able to reduce the energy consumption of pumps and air conditioning equipment from 12.5 W/m² to 8 W/m². In addition, a comparison of actual building performance to a simulated building operating with same heat pump system but no thermal storage showed that the

selected design reduced the peak energy demand by approximately $1/3^{\text{rd}}$, yielding significant economic benefits for the building owners.

2.5 Ice Storage Integration with Solar Thermal Systems

Ice storage systems can also be integrated with solar thermal collectors operating within a building. This integration has a number of potential benefits. One of the main issues with any solar thermal system is the discrepancy in time between incident radiation and thermal energy demand within the building. The latent heat of ice can be used as a storage material to help bridge this gap, offering significant volume reductions over purely sensible heat storage systems. The majority of the thermal energy obtained from solar thermal panels occurs near noon when occupancy levels and heating loads are lowest. By using an integrated ice storage/solar thermal system this thermal energy can be stored in an ice storage tank for later use, whether this is short term (hours, days) or long term (weeks, months). Existing ice in the tank absorbs the thermal energy from the circulating collector fluid, melting the ice and producing a low temperature liquid. When required, the stored thermal energy can be extracted from the ice storage tank using a heat pump, thus providing heating and DHW for the building. The evaporator of the heat pump serves as the ice generator in this mode of operation, producing an ice/water mixture at the evaporator exit when the cooling capacity is sufficient to initiate a phase change.

Using an integrated ice storage/solar thermal system can also significantly improve collector performance (Trinkl et al, 2009). The efficiency of a solar collector is highly dependent on the inlet fluid temperature (Duffie and Beckman, 2006): Colder inlet fluid temperatures result in reduced thermal losses to the ambient and increased collector efficiencies. Using an ice storage system allows a low temperature fluid to be circulated in the collector loop, increasing the

thermal efficiency and extending the period of time that useful thermal gains can be obtained (in comparison to a system in which the collectors operate against a warm water storage tank).

The main disadvantage of this type of system is that it degrades the quality of energy obtained from the solar collectors due to the low storage temperatures used. The heat pump is thus required to upgrade the quality of energy to meet the demand quality.

A few publications provide an insight into the overall layout of these systems operating in heating modes. Qi et al. (2008) examined a latent heat store integrated with solar thermal collectors. The layout, shown below in Figure 2-6, consisted of solar thermal collectors (Item 1) in series with a latent heat store (Item 2) using $\text{CaCl}_2 \cdot 6\text{H}_2\text{O}$ as the storage material. In the summer the solar thermal collectors were operated, collecting thermal energy which was then stored in the latent heat storage tank. During the winter this energy was extracted by circulating a heat transfer fluid through the latent heat store. The heat transfer fluid then served as the source for a heat pump evaporator (Item 3) which provided heating to the home through the use of an air heating coil (Item 5). This work provides insight into how solar thermal panels can be integrated with latent heat stores in a heating only mode.

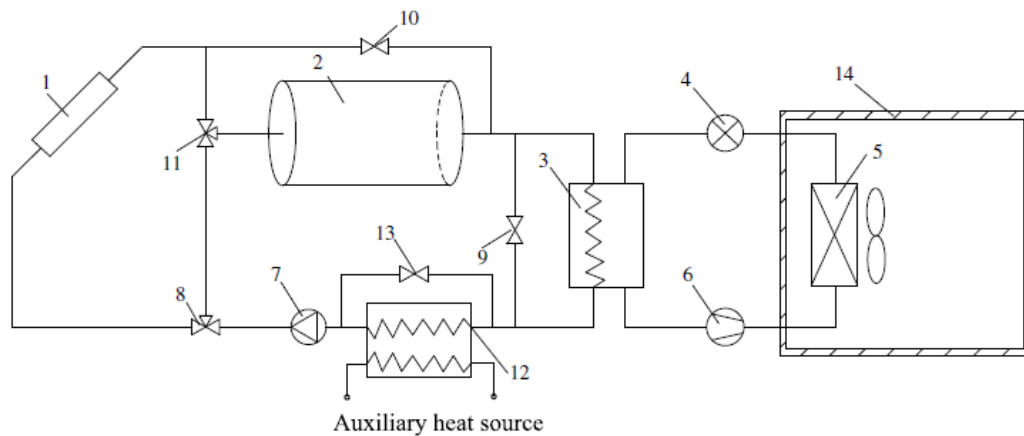


Figure 2-6: Solar Assisted Heat Pump with Latent Storage (Qi et al, 2008)

Han et al. (2008) examined a solar thermal system integrated with a geothermal loop and latent heat storage tank using $\text{CaCl}_2 \cdot 6\text{H}_2\text{O}$. The system was designed only for heating operations, with the basic layout consisting of the latent heat storage tank in series with the solar thermal panels as shown in Figure 2-7. While much of the focus was on using the thermal energy collected from the solar thermal panels to limit the long term effects of the geothermal loop, a number of important operating modes were in evidence. When the fluid temperature available from the solar thermal collectors (Item A) or latent heat storage tank (Item B) was high enough, this fluid was used directly at the fan coil unit (Item E). This allowed the system to bypass the heat pump, reducing the amount of electrical energy consumption in the home. If the thermal energy available from the solar collectors or heat store was not high enough, a heat pump (Item D) operating between the latent heat store and the fan coil unit was used. The use of $\text{CaCl}_2 \cdot 6\text{H}_2\text{O}$ as the storage material means that some of the operational modes studied would not be feasible in ice storage systems. In particular, direct use of the latent heat store for heating would be unlikely in ice storage due to the high degree of additional sensible storage that would be required in the ice tank.

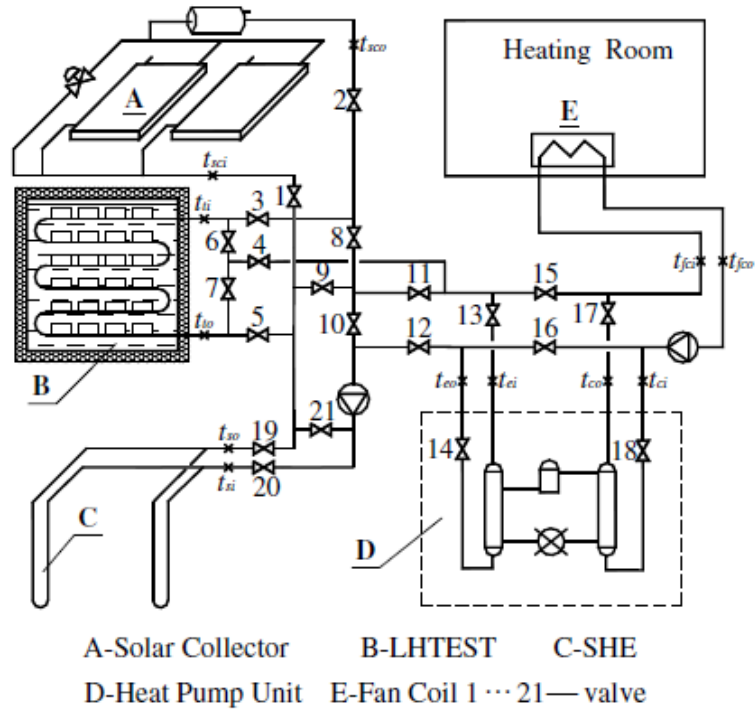


Figure 2-7: Combined Latent Store with Solar Collectors and Geothermal Loop (Han et al, 2008)

Trinkl et al. (2009) proposed a solar thermal system operating in conjunction with an ice storage system as shown in Figure 2-8. Two solar loops were implemented: an indirect configuration, with the collectors operating against the ice storage tank; and a direct configuration, with the collectors operating against a warm water storage tank. A heat pump was used to transfer thermal energy from the ice tank to the warm water storage tank, which served as the heat distribution point for the home.

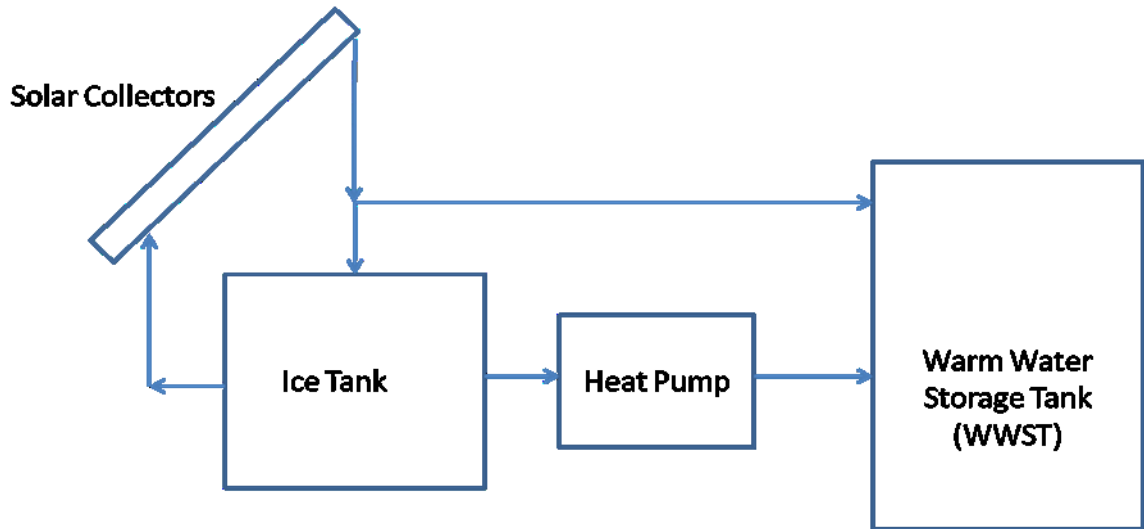


Figure 2-8: Ice Storage combined with Solar Collectors (Trinkl et al, 2009)

Selection of the appropriate solar loop was based on calculating the potential solar collector efficiency in the direct configuration. Collector efficiency is inversely proportional to the temperature difference between the inlet fluid and the ambient air (Duffie and Beckman, 2006). As such, Trinkl et al. (2009) used the temperature difference between the bottom of the warm water storage tank (T_{WWST}) and the ambient air (T_{amb}) to estimate potential solar collector efficiencies.

Collectors were operated against the ice storage tank when:

$$T_{WWST} - T_{amb} > T_{cont} \quad (2-1)$$

where:

T_{WWST} is the temperature at the bottom of the WWST (°C)

T_{amb} is the ambient air temperature (°C)

T_{cont} is a designer specified temperature difference (°C)

When eqn. (2-1) is satisfied the collector efficiency is deemed to be too low to operate the collectors in the direct configuration. Collectors are instead operated against the ice storage tank to improve efficiencies and extend the collector utilization period.

Collectors were operated against the warm water tank when:

$$T_{WWST} - T_{amb} \leq T_{cont} \quad (2-2)$$

In this case the estimated collector efficiency is high enough to allow the solar collectors to operate directly against the warm water tank.

The dual loop system proposed by Trinkl et al. (2009) offers a number of potential benefits. The ice storage loop allows the operator to increase the solar collector efficiency as needed, particularly during the winter months when colder temperatures and lower solar radiation result in the direct collector configuration obtaining minimal thermal gains. The warm water loop allows the operator to bypass the heat pump when it is not required, reducing the mechanical system energy consumption.

Selection of the appropriate solar loop is a major challenge. Trinkl et al. (2009) focused on using the temperature difference ($T_{WWST} - T_{amb}$) to estimate the solar collector efficiency and subsequently select the appropriate solar loop. While straightforward to implement, using this temperature difference does not provide a direct measure of the solar collector efficiency, as the efficiency is also a function of the collector design, mass flow rate, and number of panels in series. This may lead to inaccurate estimations of the solar collector efficiency, potentially leading the system to operate in a non-optimal configuration. Furthermore, a control scheme based only on the solar collector efficiency does not take into account the potential quality of energy in each solar configuration. While the collector efficiency in the direct configuration may

be below the control setpoint, the potential quality of energy obtained may still be high enough to directly meet heating and DHW loads. Focusing only on the collector efficiency may result in missed opportunities to save energy by bypassing the heat pump.

2.6 Simulation Studies

Accurate simulation tools are vital to the successful design, analysis and implementation of any building integrated system. They allow the engineer to examine various equipment layouts and investigate the effects of equipment parameters on overall performance. This section will review existing models for ice storage, and their subsequent use in whole building performance studies.

2.6.1 Ice Storage Models

Much of the current literature on ice storage centers on the development of computer models for the ice generation and storage processes. While the amount of literature on ice slurry systems is limited, the present study of the available ice storage tank models provides an indication of the processes and challenges involved in the simulation these systems.

Silver et al. (1989) created a number of component models to simulate the performance of an ice-on-coil external melt system with a water/ice mixture inside the storage tank. Water from the tank was circulated and used for cooling. Warmer return water was re-introduced into the tank and rejected heat to the ice/water mixture. The heat re-introduced to the tank from the cooling coil acted as a source for the ice generator evaporator during the ice creation mode of operation. The computer models of different components such as the storage tank and evaporator were developed for the DOE-2 energy analysis program, allowing engineers to easily add and configure the ice generation system to their building model. The evaporator model was based on a simple thermal circuit. Resistance terms included convective heat transfer from the

water in the tank to the ice on the evaporator coils, convective transfer from the inner coil wall to the circulating refrigerant, and conduction through the ice layer and coil wall. Capacitance (storage) terms were also added to the thermal circuit model, allowing the user to account for the sub cooling of the existing ice layer below 0°C as well as for the latent heat of ice formation during new ice production. The latent heat capacitance term accounted for the absorption of energy at a near constant temperature (0°C) that occurs during the phase change from solid to liquid, while the sub cooling capacitance term was needed to approximate the additional thermal energy that can be extracted from the ice layer initially at 0°C. The thermal circuit was divided into finite segments along the flow direction of the coil, with the output flow parameters of each segment (refrigerant temperature, pressure and quality) becoming the input parameters to the next axial segment. The evaporator model was coupled to a simple storage tank model, which was based on a single node energy balance between the heat transferred to the evaporator, the heat input into the tank from the return water, and the environmental losses.

While the model allows users to simulate an ice storage system in DOE-2, it is only applicable to ice-on-coil systems. The use of a fixed one hour time step limits examination of the system on shorter time scales. Furthermore, the model is derived for systems in which the liquid water in the ice storage tank is used directly at the cooling coil, limiting the applicability of this model to external-melt systems only. Finally, the model requires detailed knowledge of the evaporator geometry including coil thickness, internal radius and length. This may become a possible source of uncertainty or error if work is at a preliminary design stage and these quantities are unknown.

ASHRAE Report RP707 (ASHRAE, 1993) presented a model of a rectangular ice storage tank connected to an ice harvester. The harvester evaporator coil was located above the storage

tank, with the liquid water in the tank being used directly at the cooling coil. The ice was divided up into unsaturated (above the water line, in which the porous gaps in the ice are not fully filled with liquid water) and saturated (below the water line, in which the porous portions of the ice are fully saturated with water) sections, with return water entering the top portion of the tank either through a uniformly introduced spray or rectangular inlet openings. For the unsaturated section the tank water flow was assumed to be in the downward direction only, with a coefficient (itself dependant on ice particle shape, permeability and porosity) used to relate the length of segment to the temperature rise and inlet flow velocity. The saturated section also utilized a coefficient to relate the segment length to temperature rise and velocity. For the saturated elements a three-dimensional flow field was analyzed through the use of a program previously developed by Wilson et al. (1988). The overall exit temperature of the water in the tank was then calculated by averaging the outlet temperature of each of the saturated elements located along the exit plane. While the general modeling approach is applicable to a wide variety of systems, including ice slurries, the coupling of the tank model with an external program makes this model difficult to implement as an individual component in a building simulation program. Furthermore, the use of a three dimensional grid with multiple control volumes increases the computational time for the model.

One of the primary results of the experimental and simulation work in ASHRAE RP707 was that the exit temperature of water from the ice tank approached 0°C when the ice content was high. This result formed the basis of the TRNSYS Type 207 component (Behschnitt, 1996), which is the ice storage tank model available for version 16 of the TRNSYS building simulation program (Klein et al, 2004). The model was initially designed to be used with an ice harvester system, with discharging of the tank achieved through the direct use of liquid water from the storage tank at

the cooling coil. The higher temperature return water was then sprayed uniformly over the top of the ice tank, melting existing ice and releasing additional cooling.

Type 207 allows users to input a variety of tank parameters, including ice generation rate, tank geometry, and return water flow rate from the cooling coil. Using the entire tank as a control volume, an energy balance is performed taking into account the heat transfer to the tank from the ambient and from the incoming flow stream. An effectiveness coefficient is used to relate the amount of thermal energy transferred from the circulating water stream with the amount of ice remaining in the tank. The model assumes that if the ice fraction in the tank is greater than 20% of the storage capacity (on a mass basis), the exit water temperature will be 0°C and the effectiveness coefficient will be 1. As the ice fraction goes below the 20% threshold, the effectiveness coefficient reduces linearly to 0 (at which point no ice remains in the tank). The resultant heat transfer is then scaled back from the maximum heat transfer (when the exit water temperature is 0°C) by multiplying by this effectiveness coefficient. Type 207 performs energy balance calculations at each time step, providing the user with output variables including the ice usage rate, remaining ice inventory, and exiting chilled water temperature

While simple and easy to implement within the TRNSYS structure, Type 207 does not directly take into account the thermal capacitance of the fluid in the tank. When no ice remains in the tank, the outlet fluid temperature is calculated to be the same as the inlet fluid temperature, regardless of the inlet flow rate or the tank fluid temperature at the end of the previous time step. This can lead to large fluctuations in the predicted tank outlet temperature, which is particularly significant if the ice tank is used as a source for heating or cooling energy.

Tanino et al. (2001) developed a model of a non-agitated ice slurry storage tank in which the ice and water were allowed to stratify into a non-homogenous mixture. Both ice slurry and return

water were introduced to the top of the storage tank through a supply pipe, while liquid water was drawn out through openings cut into the bottom of the storage tank and used to provide cooling or produce additional ice slurry. The model was divided into two subsections: one defining the ice storage process, and one defining the ice melting process. The storage subsection contained a two-dimensional model, taking into effect the movement of ice slurry in the vertical and radial directions of the tank, and accounting for deformation and compaction of the agglomerated ice layer. The second section dealt with the melting processes involved in an already-charged ice slurry tank. Energy balances were performed on both the ice and water layers, with the output temperature and amount of ice melted calculated at each time step of the simulation.

The complexity of the model limits its use to studies focused primarily on ice tank performance. While the ice profiles during the charging and melting process can provide useful information to the designer, this level of tank performance prediction may not be required if the purpose is to examine how the tank performs as part of a larger system. The model is further limited in that it assumes that no heat transfer occurs during the charging process of the tank. This means that an additional energy balance equation would need to be implemented to use the model in a study of a heating or cooling system.

Flick et al. (2007) created a model to examine the behavior of an ice slurry storage tank. Liquid water from the bottom of the tank was used as a source for the slurry generator, while slurry for use at the cooling coil was drawn from an outlet at the midpoint of the tank. Ice slurry from the slurry generator was introduced to the top of the tank, with a stirring device operating to prevent agglomeration of the ice in the upper portion of the storage container. Slurry returning after being circulated in the cooling coil was added through openings in both the top and

bottom of the tank. The model used three governing equations: an energy balance on the fluid along with mass balances on the ice crystals and solute. The tank was divided into elements along the axial direction, and the three governing mass and energy balance equations used to calculate the temperature, ice fraction, and particle diameter distribution profiles for the entire tank at a particular time step.

While the model has the ability to accurately predict the temperature and ice fraction in both the charging and discharging modes of operation, the high level of detail provided may not be required for systems level research.

Egolf et al. (2008) created a numerical model to account for ice stratification inside a non-agitated ice slurry storage tank. The slurry/water mixture remains in the tank, with the sole purpose of the study to determine how this mixture stratifies over time. There is no generation of ice slurry, or heat transferred through the circulation of the slurry/water mixture. The model centered on the use of particle conservation equations applied to differential mass elements in the tank. These conservation expressions contained terms for the diffusion of particles, melting/freezing of ice, and particle movement due to buoyancy within the ice slurry mixture. For a given mass element, the rate of change of the number of particles in the element must be equal to the particles added or subtracted through diffusion, phase changes and buoyancy. The governing conservation equations were then combined with empirical correlations for density (a function of temperature and ice concentration) and viscosity (a function of ice concentration and packing factor). The conservation expression was solved for mass elements oriented axially along the tank, with the resulting model outputs allowing users to analyze the propagation front and ice concentration distribution in the tank over time.

One of the main drawbacks of this model is that it is developed solely for stratification analysis. No heat is rejected to the tank, no ice slurry is generated, and no slurry or liquid tank water is used for cooling or heating purposes. The use of particle conservation expressions as the basis for the model neglects the effects of temperature changes that would occur if the tank was used within a heating or cooling system, and means that an additional energy balance equation would need to be added for this model to be appropriate for overall system simulations.

2.6.2 Whole-Building Simulation

The primary purpose of developing complex computer models is to accurately predict the performance of systems integrated into a building. To this end a number of studies have been carried out examining the integration of ice storage systems into a structure and the subsequent effect on energy usage.

2.6.2.1 Ice Storage in Cooling Operations

The majority of simulation studies using ice storage focus on cooling only applications. While the purpose of this thesis is to examine system operations in a heating mode, these studies provide important insights into the integration of ice tank models within a complex building system.

Kondo et al. (1999) examined the performance of an ice storage system integrated into a building with radiant cooling. The ice storage tank was designed to provide water at a temperature of 1°C to 2°C to a forced air cooling unit, as well as being coupled to an air source heat pump to provide heating during the winter months. A simulation study of the system integrated into a typical Tokyo office building showed that the use of ice storage could provide significant electrical energy and cost savings when combined with a radiant cooling system.

While this study allows for the combination of two technologies, it is focused on the application of ice storage to commercial buildings in cooling dominated climates. As well, the exact methods

of producing ice and providing heating during the winter months is not mentioned, making it difficult to determine if the results are applicable to a wide range of systems.

Adam et al. (2003) utilized the TRNSYS building simulation program to analyze the performance of a university building equipped with an ice-on-coil storage system. The component model used for the storage tank was initially developed for a paraffin phase change material, and utilized a range of fusion temperatures (-2°C to -0.5°C) when calculating the specific enthalpy at a given ice/water temperature. The performance of the building under three different control sequences was analyzed by examining the energy costs incurred during operations and the deviation of room temperature from the thermostat set point. While results showed significant cost savings were obtained by using the ice storage system, the economic savings were often countered by larger deviations from the set point temperature targeted in the simulation.

One of the main drawbacks of this study is that it utilized a simplified model of the building being simulated. The simulation model was based on a degree-hours calculation instead of the more complex multi-zone TRNSYS Type 56 model available for simulation. This limits the ability to analyze the effect that high performance building envelopes and multi-zone structures have on the performance of ice storage systems. The model used to simulate the storage tank is also adapted from a previous application, and showed large relative simulation errors in temperature prediction at certain points during discharge operations.

Chan et al. (2005) performed a study of ice storage in a district cooling application for a fictional development in Hong Kong. A central plant with an ice harvester thermal storage system was used to delay the peak electrical demand for refrigeration systems and thereby level electrical loads. The authors utilized the TRNSYS building simulation program, as well as the TRNSYS Type 207 storage tank model discussed above, to simulate system performance for various storage

capacities and control sequences. The resulting simulation showed that all of the ice storage systems consumed more energy in comparison to a standard refrigeration system with vapor compression chillers due to the lower operational efficiencies encountered when operating in the ice-creation mode. The main benefits of the ice storage system were evident when examining the effects of load leveling on the energy costs. Cost savings were found to be highly dependent on the rate structures offered by local utilities, with more pronounced price reductions for off-peak electrical usage correlating well with increased cost savings for ice storage.

The study again focused on the use of ice storage in a cooling only application. While an interesting case study of the integration of an ice storage model into the TRNSYS energy simulation program, the scope of the study is limited by the development assumptions inherent with Type 207.

2.6.2.2 Solar Assisted Heat Pumps using Latent Storage

One of the main objectives of this work is to determine the viability of a solar assisted heat pump operating using latent storage. Several studies have focused on examining this issue through computer simulations.

Both Qi et al. (2008) and Han et al. (2008) highlighted the potential of using latent heat storage in combination with a solar assisted heat pump as discussed in Section 2.5. Qi et al. (2008) studied the performance of a proposed system located in Beijing, China. The home had a total floor area of 325 m², and was heated from mid-November to mid-March. System simulations were based on a simplified mathematical model, with the authors calculating a heat pump COP of 4.2 over the heating period. A sensitivity analysis highlighted the importance of properly

selecting the latent storage tank volume and solar collector area to balance the amounts of energy input and extracted on an annual basis.

Han et al. (2008) examined a more complex system using a latent heat storage tank in combination with solar collectors and a ground heat exchanger. System performance was analyzed for a building in Harbin, China, with a design heating load of 10 kW and heating season from mid-October to mid-April. Mathematical models for each component were developed and simulated in Matlab, with the authors reporting an annual system COP of 4.67 when the latent storage tank was used as a source for the heat pump.

While Qi et al. (2008) and Han et al. (2008) presented important findings regarding the integration of latent heat storage into a solar system, both studies use $\text{CaCl}_2 \cdot 6\text{H}_2\text{O}$ as a latent storage material. The melting point and latent heat capacity of $\text{CaCl}_2 \cdot 6\text{H}_2\text{O}$ differ significantly from water, meaning that the findings presented in each study cannot be applied directly to an ice storage system. Both studies also use simplified models for determining the thermodynamic performance of the building, limiting the ability to simulate more complex interactions between the heating system and the structure. Furthermore, in the case of Han et al. (2008), latent heat storage is used as part of a more complex system involving ground heat exchangers. While the authors present a system COP for the case when the heat pump operates against the latent storage tank, it is difficult to decouple this value from overall system operations.

Trinkl et al. (2009) performed a simulation study on a solar thermal/ice storage system operating in a heating mode. As discussed in Section 2.5, two distinct solar loops allowed the solar collectors to operate against the ice storage tank or warm water storage tank. A heat pump was used as required to transfer thermal energy from the ice storage tank to the warm water storage tank. The warm water tank acted as the heat distribution point for the home, with

the bottom of the tank maintained at 35°C for space heating while the top of the tank was maintained at 45°C for DHW preparation.

Standard components from the MATLAB/Simulink library were used to simulate the heat pump and solar collectors. A simplified ice storage tank model was developed which assumed no sub-cooling of the ice and ignored ice stratification effects within the tank. The study focused on a parametric evaluation of important system properties and how they affect the seasonal performance factor (defined as the overall demand for heating and DHW divided by the heat pump electricity demand) of a high efficiency house in Germany. Results using a single zone house model showed that the system had a high sensitivity to solar collector area and ice storage tank size, suggesting that these factors should be the focus of design efforts. The system was found to have a SPF of 4.6 when operating at the recommended set of design variables.

While the study is unique in that it focuses on the use of ice storage for heating purposes, a number of limitations still exist. The authors focus solely on the use of an ice-on-coil ice generation system, with this method shown to experience reduced performance as the ice fraction increases. As well, the solar loop control strategy focuses primarily on maintaining the solar collector efficiency in the direct configuration above a user defined setpoint. Although the collector efficiency is an important indicator of system performance, its use as a control parameter may cause the system to miss opportunities to directly meet heating and DHW loads. Furthermore, while a parametric analysis provided suggested design values for system components such as the solar collectors and storage tank volumes, a complete mathematical optimization would be better suited to defining a set of recommended design variables.

2.6.3 Summary of Models

The increasing popularity of ice as a PCM storage material has led to the development of simulation models examining the performance of both the ice storage tank and its integration into buildings. The development of each of these models is based on assumptions which limit their general applicability. One of the main constraints is often system configuration and tank geometry. The model of Silver et al. (1989) allowed DOE-2 users to simulate ice-on-coil systems through solving an analogous thermal circuit. While simple to understand and apply, the model required an in-depth knowledge of the evaporator geometry and was developed for systems in which the evaporator coil was located directly within the ice tank. The issue of evaporator geometry and the impact of estimating these model parameters was also encountered by Adam et al. (2003).

Models can also be classified by their representation of the physical processes occurring inside the storage tank. TRNSYS Type 207 presents a simplified tank model, with a single energy balance performed on the tank control volume. This allows for a simple and computationally efficient solution method, with the heat transfer from the inlet fluid stream to the ice tank calculated using an effectiveness coefficient. The main issue with this model is that it does not include the thermal capacitance of the tank fluid in the energy balance equation, leading to rapid fluctuations in the tank fluid temperature when there is no ice in the tank.

More complex models in the literature focus on dividing the tank into a number of smaller elements. Stewart et al. (1995), Tanino et al. (2001), Flick et al. (2007), and Egolf et al. (2008) all examined the performance of ice storage tanks by using multiple control volumes. While this detailed approach allowed for an in-depth analysis of the velocity, temperature and ice profiles within the tank, the level of detail provided by each model is higher than required for simulations in a whole-building context. Furthermore, solving multiple equations at each time

step can be computationally expensive, particularly when the analysis program must simulate a variety of other system components.

A number of simulation studies also exist examining the integration of ice storage into buildings. Of these, the majority are focused on the use of ice storage as a means of load leveling during the cooling season. Adam et al. (2003) used TRNSYS to simulate an ice storage system serving a university complex. The study was limited to cooling only applications and the use of a degree-day based building model instead of the more complex multi-zone models which can be developed in TRNSYS. Chan et al. (2005) used TRNSYS to study the use of ice storage as a load leveling technique for a fictional development in Hong Kong. Again, the study focused only on cooling applications and how ice storage can be implemented into large buildings and developments.

Qi et al. (2008) and Han et al. (2008) both examined solar assisted heat pump systems using latent storage. Each study used $\text{CaCl}_2 \cdot 6\text{H}_2\text{O}$ as a storage material, preventing the direct application of the findings to an ice storage system. As well, in the case of Han et al. (2008), latent heat storage was used as part of a larger system including ground heat exchangers, making it difficult to separate the performance of the latent storage system from overall operations.

Trinkl et al. (2009) analyzed a solar assisted heat pump system using ice storage. While the study highlighted the potential benefits of ice storage for heating a residential building, it was limited to an ice-on-coil system. Furthermore, while a direct connection was possible between the solar collectors and warm water tank, the use of a control scheme focused on maximizing the solar collector efficiency could lead to the system missing opportunities to meet the heating and DHW loads directly.

2.7 Conclusions

Increasing energy demand due to the heating and cooling requirements of buildings has led to a strong desire to integrate renewable energy technologies into the built environment. While solar energy is particularly promising, peak supply and demand are often non-coincident. Ice storage allows home owners to lower their purchased energy by storing excess thermal energy captured by solar collectors through the latent and sensible heat capacities of a water/ice mixture. Ice storage also has the potential to significantly improve solar collector efficiencies, increasing the thermal input into the system and allowing the collectors to be used for a longer period of time.

The method used for simulating the ice tank is an important decision. A number of mathematical models exist for simulating ice storage tanks. However, very few appear applicable for simulating an ice slurry tank in a whole building context, either to due to limitations in the system configuration, defining equations, or computational resources. Based on the available ice tank simulation models in the literature, it can be concluded that a new ice tank model is needed which should include the following characteristics:

1. Appropriate level of detail for system simulations. The primary purpose of the new model is to provide the average tank fluid temperature and ice mass at each time step during the heating season. As such, detailed information regarding the temperature gradient and ice mass profile in the tank can be neglected (Trinkl et al, 2009). This reduces the amount of control volumes and defining equations required, thus improving the computational efficiency of the model.
2. Separate treatment of ice and water layers. A common point in many of the ice tank models ((Stewart et al, 1995), (Tanino et al, 2001), (Flick et al, 2007)) is the separate

treatment of ice and water elements. The new ice tank model should allow for the separate modeling of the heat transfer in each of these two distinct layers.

3. Ability to model the thermal capacitance of the water layer. The main disadvantage of TRNSYS Type 207 is that it does not take into account the thermal capacitance of the fluid within the ice storage tank. The new model should include a thermal capacitance term within the energy balance on the water layer, thus making the tank model applicable for use when there is no ice in the tank.

One of the primary questions faced by the designer is how best to integrate the solar collectors with the ice storage system. A review of the literature provides two main conclusions regarding the combination of solar thermal collectors and latent heat storage tanks:

1. A connection should allow for the solar collectors to operate in series with the latent storage tank when needed. Thermal energy collected from the solar panels is then stored in the latent storage tank, where it is eventually extracted using a heat pump to provide DHW or space heating to the building.
2. A second connection should allow the solar collectors to directly meet heating and DHW loads. This direct connection allows the system to bypass the heat pump when it is not required to upgrade the quality of thermal energy obtained from the solar collectors.

There is a clear need for further simulation work regarding solar assisted heat pumps operating using ice storage. While Trinkl et al. (2009) presented important findings regarding the use of ice storage in combination with solar collectors, there is still the potential to further reduce energy consumption based on the use of ice slurry and a new control strategy.

The need for proper selection of system parameters such as the solar collector area and ice tank volume has also been outlined by Qi et al. (2008), and Trinkl et al. (2009). Although a number of mathematical optimization studies have been performed on heat pump systems, none have

examined a solar assisted heat pump using ice storage. The application of optimization techniques to this type of system would provide designers with a better understanding of how to optimally configure the system in a cold climate such as Montreal, QC.

2.8 Thesis Objectives

The objectives of this thesis are as follows:

1. Develop a new mathematical model for the simulation of a non-agitated ice slurry storage tank.
2. Use a simulation based approach to examine the potential of using a solar assisted heat pump with ice slurry to heat a high performance home in Montreal, QC.
3. Determine the optimal combination of solar collectors and thermal storage capacity that minimizes the energy used for heating and DHW purposes.

2.9 Methodology

The following methodology will be used to achieve the goals of the study:

1. Energy balance equations will be developed to define the heat transfer processes in the ice storage tank. These equations will then be discretized and integrated into a component model for the TRNSYS energy simulation program.
2. The new mathematical model will be verified using available experimental data to ensure that it accurately predicts tank performance in all operational modes.
3. A computer model will be created in TRNSYS to simulate the proposed solar assisted heat pump operating using ice slurry.

4. Optimizations will be performed on a set of design variables defining the solar collectors and the thermal storage capacity of the system. The goal will be to minimize the energy required for home heating and DHW over a single heating season.
5. A one-dimensional sensitivity analysis will be performed to determine the impact of each design variable on system performance.
6. The optimized system will be compared with two other heating methods to determine its viability in heating a high performance home in Montreal, QC.

Chapter 3 presents the development of a mathematical model for the ice slurry tank. The defining equations are presented along with all assumptions made during the development process. The energy balance equations are then used to develop a new component model for the TRNSYS energy simulation program. The performance of the component model is verified with experimental data to ensure that it accurately predicts the ice mass and tank fluid temperature over time.

Chapter 4 presents the computer modeling of the solar assisted heat pump system in TRNSYS. The concept and system layout are first presented. The TRNSYS simulation model is then discussed in terms of the components used and the control strategies implemented.

Chapter 5 presents the optimization of the solar assisted heat pump system. The design variables and optimization parameters are first defined. Optimizations are then performed using three different control strategies, with the goal of minimizing the energy use for heating and DHW purposes. A sensitivity analysis is used to examine the impact of each design variable on the heating operating energy.

Chapter 6 presents the simulated performance of the solar assisted heat pump system. The system is compared with two other heating methods to determine its viability in the Canadian

marketplace. The ice slurry system is then examined in detail, including a presentation of system performance on a seasonal, monthly, and daily level.

3. Development of an Ice Storage Tank Mathematical Model

This chapter presents the development of the custom ice storage tank model. Key development assumptions are first introduced, followed by a description of the mathematical model employed. The new TRNSYS component model (Type 213) is then discussed, including a description of the solving algorithm and component inputs, outputs, and parameters. The chapter concludes with the results of verification tests comparing simulated results with available experimental data.

3.1 Development Assumptions

The development of the ice tank model is based on the following assumptions:

1. The water and ice stratify into two distinct layers at each time step.
2. Temperature gradients within the water and ice layers can be neglected (Trinkl et al., 2009).
3. Sub-cooling of the ice layer can be neglected, with the ice temperature T_{ice} thus assumed to be constant at 0°C throughout the simulations. Ice compaction is also assumed have a negligible impact on tank performance in an overall system context (Trinkl et al., 2009).
4. The top and bottom of the ice tank are well insulated and, as such, heat exchange with the environment through these sections is negligible. Heat losses from the ice layer to the air in the top of the tank are also assumed to be negligible.
5. Incoming fluid from the heat pump and solar collectors is introduced as a uniformly distributed spray over the top of the storage tank.
6. Density and porosity are uniform throughout the ice layer. Ice thickness is assumed to be constant throughout the layer.

3.2 Mathematical Model

The ice tank can be separated into two distinct control volumes: an ice layer and a water layer, as shown in Figure 3-1.

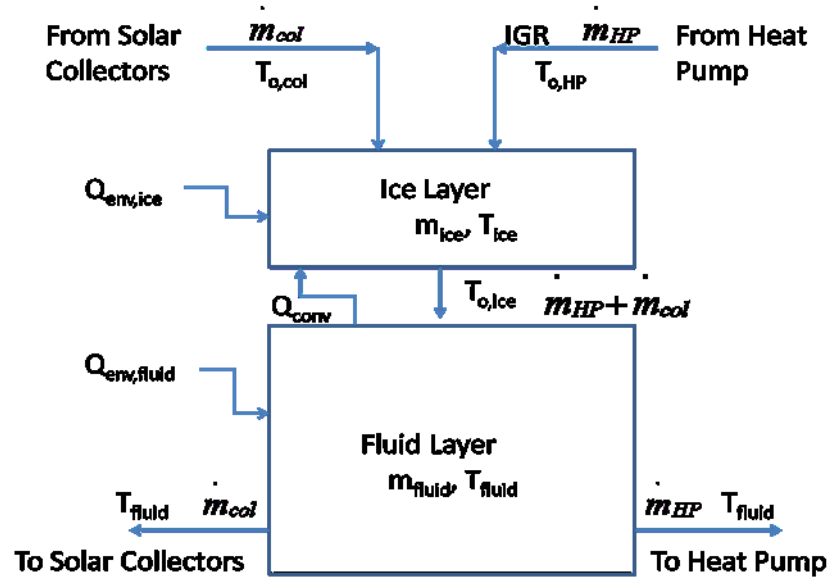


Figure 3-1: Ice and Water Layer Control Volumes

3.2.1 Energy Balances

The mathematical model is based on energy balances developed in this study for the ice and water layers shown in Figure 3-1. The energy balance for the ice layer is written as:

$$\begin{aligned}
 -L \frac{dm_{ice}}{dt} = & \dot{m}_{col} c_p (T_{o,col} - T_{o,ice}) + \dot{m}_{HP} c_p (T_{o,HP} - T_{o,ice}) - IGR \cdot L \\
 & + UA_{s,ice} (T_{env} - T_{ice}) + hA_c (T_{fluid} - T_{ice})
 \end{aligned} \tag{3-1}$$

where:

L is the latent heat of ice (333 kJ/kg)

m_{ice} is the mass of ice in the ice tank (kg)

\dot{m}_{col} is the mass flow rate of fluid from the solar collectors (kg/h)

\dot{m}_{HP} is the mass flow rate of fluid from the heat pump (kg/h)

c_p is the specific heat of the fluid (kJ/kg·°C)

IGR is the ice generation rate (kg/h)

$T_{o,col}$ is the fluid temperature exiting the solar collectors (°C)

$T_{o,ice}$ is the fluid temperature exiting the ice layer (°C)

$T_{o,HP}$ is the fluid temperature exiting the heat pump evaporator (°C)

T_{env} is the temperature of the ambient air surrounding the tank (°C)

T_{ice} is the temperature of the ice layer (0°C)

T_{fluid} is the fluid temperature in the ice tank (°C)

U is the tank loss coefficient (kJ/h·m²·°C)

h is the convective heat transfer coefficient between the ice and water layers (kJ/h·m²·°C)

$A_{s,ice}$ is the surface area of ice in contact with the sides of the storage tank (m²)

A_c is the contact area between the ice and water layers (m²)

The energy balance on the water layer is written as:

$$m_{fluid} c_p \frac{dT_{fluid}}{dt} = \left(\dot{m}_{HP} + \dot{m}_{col} \right) c_p (T_{o,ice} - T_{fluid}) + UA_{s,fluid} (T_{env} - T_{fluid}) - hA_c (T_{fluid} - T_{ice}) \quad (3-2)$$

where:

m_{fluid} is the mass of fluid in the ice tank (kg)

$A_{s,fluid}$ is the surface area of fluid in contact with the sides of the storage tank (m²)

3.2.2 Effectiveness Coefficient Approach

The water temperature exiting the ice layer ($T_{o,ice}$) is calculated based on the heat transfer between the incoming fluid stream (at $T_{o,col}$ and $T_{o,HP}$ respectively) and the ice in the tank (at T_{ice}).

Heat transfer is defined using an effectiveness coefficient ε (Behschnitt, 1996) which relates actual heat transfer between the incoming fluid and the ice layer to a theoretical maximum heat transfer in which the exiting fluid temperature equals the ice temperature ($T_{ice}=0^\circ\text{C}$):

$$\varepsilon = \frac{\dot{m}_{HP} c_p (T_{o,HP} - T_{o,ice}) + \dot{m}_{col} c_p (T_{o,col} - T_{o,ice})}{\dot{m}_{HP} c_p (T_{o,HP} - T_{ice}) + \dot{m}_{col} c_p (T_{o,col} - T_{ice})} \quad (3-3)$$

where:

ε is the effectiveness coefficient (-)

$T_{o,ice}$ is then defined as:

$$T_{o,ice} = \frac{\dot{m}_{col} T_{o,col} + \dot{m}_{HP} T_{o,HP} - \varepsilon \left(\dot{m}_{HP} (T_{o,HP} - T_{ice}) + \dot{m}_{col} (T_{o,col} - T_{ice}) \right)}{\dot{m}_{col} + \dot{m}_{HP}} \quad (3-4)$$

Behschnitt (1996) originally proposed a linear function for ϵ (Figure 3-2), in which the heat transfer effectiveness varied with the ratio of the actual ice mass to the maximum ice mass capacity of the tank.

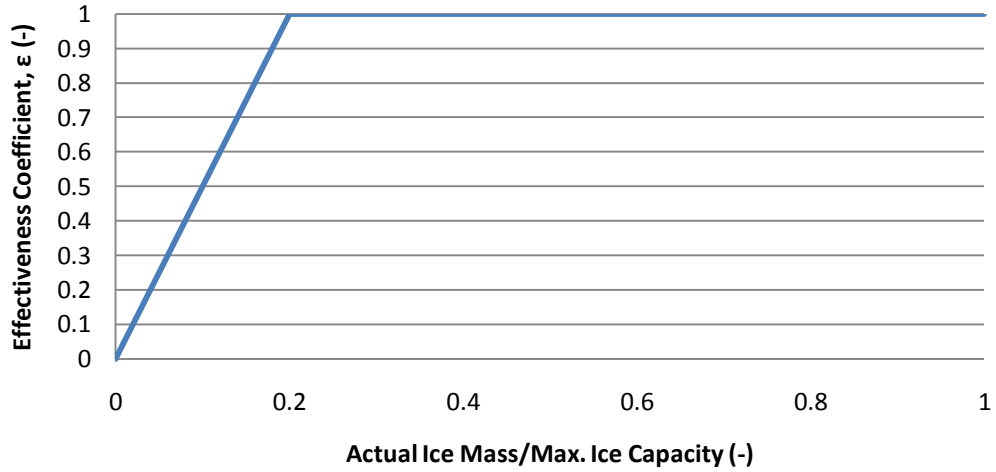


Figure 3-2: Effectiveness Function Proposed by Behschnitt (1996)

In this study, experimental data from ASHRAE Report RP707 (ASHRAE, 1993) was used to calculate ϵ as a function of the fraction of ice mass in the storage tank (γ). For calculation purposes, γ is defined as:

$$\gamma = \frac{m_{ice}}{m_{tank}} \quad (3-5)$$

where m_{tank} refers to the total mass storage capacity of the tank, equal to the sum of m_{ice} and m_{fluid} (kg).

Three experimental cases were selected for function development, with a summary of test parameters provided in Table 3-1. Each case was selected due to the uniform distribution of inlet water over the top of the ice layer as assumed by Type 213. It was assumed that all inlet fluid entered from the collector loop so that $\dot{m}_{HP}=0$.

Table 3-1: Experimental Parameters for Effectiveness Function Development (ASHRAE, 1993)

Test Parameters	Run		
	5	6	10
Initial Ice Mass, m_{ice}^0 (kg)	1107	1522	1388
Initial Fluid Temperature, T_{fluid}^0 (°C)	0	0	0
Inlet Fluid Flow Rate, \dot{m}_{col} (kg/h)	2730	2730	2730
Inlet Fluid Flow Temperature, $T_{o,col}$ (°C)	6.7	19.2	7.2

Test data was available in the form of graphs depicting the remaining ice fraction and tank outlet fluid temperature as a function of time. Experimental fluid temperatures corresponded to the average reading of twelve thermocouples arranged along the perimeter outlet at the bottom of the test tank. Each graph was digitized using the FindGraph computer program (UNIPHIZ Lab, 2011) to determine numerical values of the remaining ice fraction and fluid outlet temperature at points in time. The effectiveness at each digitized point was then calculated based on the assumption that the measured outlet fluid temperature was the same as the fluid temperature exiting the ice layer ($T_{o,ice}=T_{fluid}$):

$$\varepsilon = \frac{(T_{o,col} - T_{o,ice})}{(T_{o,col} - T_{ice})} = \frac{(T_{o,col} - T_{fluid})}{(T_{o,col} - T_{ice})} \quad (3-6)$$

where T_{ice} was assumed to be 0°C.

Figure 3-3 shows a graph of ε for all three test runs as a function of the total ice fraction in the tank. Calculated effectiveness data was limited to a range $0.02 \leq \gamma \leq 0.44$. The lower limit was selected due to accuracy issues resulting from the low resolution of the graphs in ASHRAE RP707. The upper limit for γ was based on the maximum ice mass tested in ASHRAE RP707.

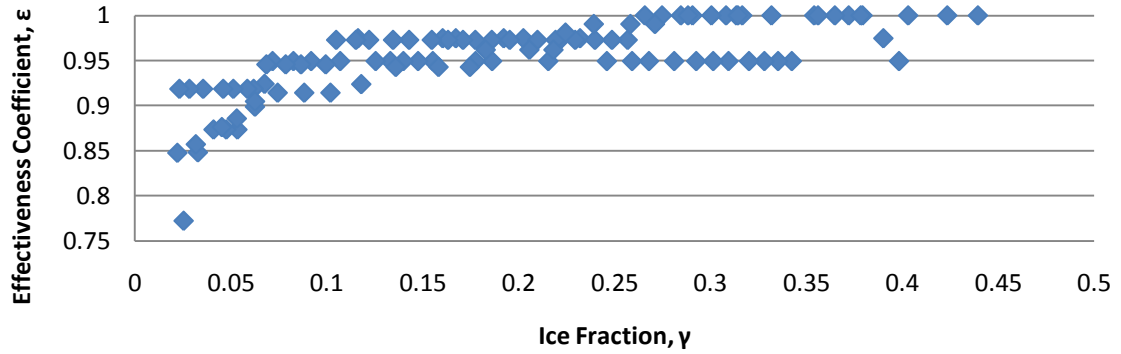


Figure 3-3: Calculated Effectiveness Coefficient as a Function of Ice Fraction

A piecewise effectiveness coefficient function is presented in eqn. (3-7), while a visual depiction is presented in Figure 3-4. The equation for the data range $0.02 \leq \gamma \leq 0.44$ was based on a fifth order polynomial regression performed on a data set comprising all three test runs summarized in Table 3-1. The resulting coefficient of determination for this region was 0.715. It was assumed that effectiveness reduced linearly from a value of $\epsilon=0.847$ at $\gamma=0.02$ to $\epsilon=0$ at $\gamma=0$ (Behschnitt, 1996). Above $\gamma=0.44$ the effectiveness coefficient was set to its maximum potential value of 1.

$$\epsilon = \begin{cases} 42.35\gamma & | 0 \leq \gamma < 0.02 \\ 121.5\gamma^5 - 165.9\gamma^4 + 88.77\gamma^3 - 23.31\gamma^2 + 3.12\gamma + .7928 & | 0.02 \leq \gamma \leq 0.44 \\ 1 & | 0.44 < \gamma \leq 1 \end{cases} \quad (3-7)$$

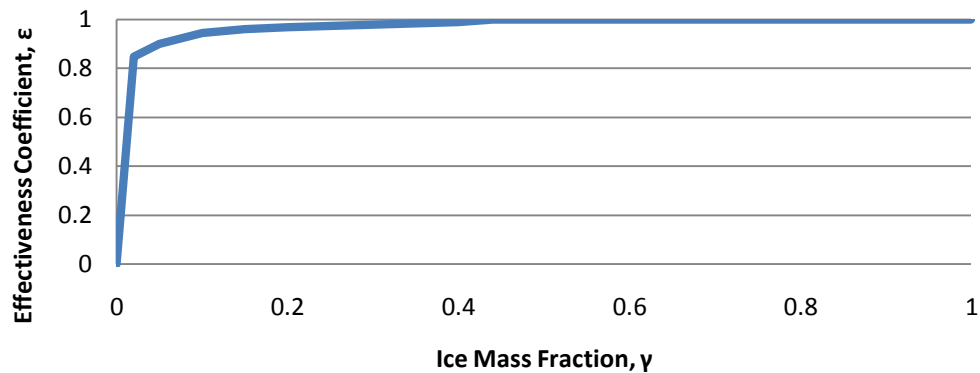


Figure 3-4: Effectiveness Function for Type 213

3.2.3 Discretization of Energy Balance Equations

The energy balance equations for the ice and water nodes are discretized to allow for the numerical solution of the tank fluid temperature (T_{fluid}^t) and ice mass (m_{ice}^t) at the end of time step t . The discretized equation for the ice layer is:

$$-L \frac{(m_{ice}^t - m_{ice}^{t-1})}{\Delta t} = \left(\begin{aligned} &\dot{m}_{HP}^t c_p (T_{o,HP}^t - T_{o,ice}^t) + \dot{m}_{col}^t c_p (T_{o,col}^t - T_{o,ice}^t) - IGR^t \cdot L \\ &+ UA_{s,ice}^t (T_{env}^t - T_{ice}^t) + hA_c^t (T_{fluid}^{t-1} - T_{ice}^t) \end{aligned} \right) \quad (3-8)$$

where:

Δt refers to the time step (h)

For the water layer the energy balance becomes:

$$m_{fluid}^t c_p \frac{(T_{fluid}^t - T_{fluid}^{t-1})}{\Delta t} = \left(\begin{aligned} &\left(\dot{m}_{HP}^t + \dot{m}_{col}^t \right) c_p (T_{o,ice}^t - T_{fluid}^{t-1}) \\ &+ UA_{s,fluid}^t (T_{env}^t - T_{fluid}^{t-1}) - hA_c^t (T_{fluid}^{t-1} - T_{ice}^t) \end{aligned} \right) \quad (3-9)$$

3.2.4 Calculation Assumptions

The model incorporates the following calculation assumptions:

1. Variables $A_{s,ice}^t$, $A_{s,fluid}^t$, A_c^t , and $T_{o,ice}^t$ are all dependant on the amount of ice inside the tank. The model evaluates these variables based on the amount of ice at the end of the previous time step $t-1$. If m_{ice}^{t-1} is 0 kg, the contact area between the ice and water layers (A_c^t) is set to 0 m².
2. Density and specific heat values are based on the tank fluid temperature at the end of time step $t-1$.
3. Heat transfer to and from the water layer is based on the fluid temperature at the end of time step $t-1$.

3.3 TRNSYS Integration

The TRNSYS energy simulation program is used to develop a new component model of the ice storage tank (Type 213). TRNSYS offers users an open and modular software architecture in which to simulate a variety of building systems. Of particular importance is the way that TRNSYS structures the solution process at each time step. Unlike many programs, which follow a Loads-System-Plant order of system simulations, TRNSYS does not require a hierarchy to be placed on the order in which components (called Types) are solved in the simulation. This means that developers of new Types do not need to edit the kernel of the program, or decide where the new component best fits in the predefined solving structure. Instead, new Types in TRNSYS are created as external .dll files, which are loaded by the TRNSYS kernel as required at the start of each simulation. This approach simplifies the component development process and prevents undesired modifications to the simulation program itself.

3.3.1 TRNSYS Component Development

Development Procedure

Development of new TRNSYS Types is simplified through the New Component module available in the TRNSYS Simulation Studio. Using this feature involves a series of steps:

1. Development of a Proforma. Each TRNSYS component is essentially a black box: At each time step t a series of defined inputs, parameters, and derivatives are combined according to a mathematical model to calculate a set number of component outputs (Figure 3-5).

Each variable input during the calculations or output by the Type must first be defined in the Proforma. The Proforma acts as the visual interface for the new Type, providing a bridge between the Simulation Studio and the mathematical model defining the

component. Creating a Proforma involves defining the following characteristics of the model:

- a. Inputs (Variables input to the Type that change with time)
- b. Parameters (Values input to the Type that are constant throughout the simulations)
- c. Derivatives (Initial values of variables used in the governing partial differential equations of the mathematical model)
- d. Outputs (Variables which are calculated by the Type at each time step)

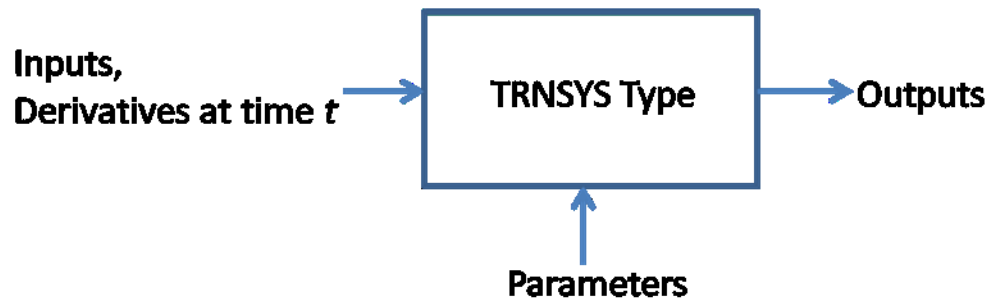


Figure 3-5: TRNSYS Component Approach

2. Creation of template source code and project files. This step is performed through the use of an Export command within the component creation module. While TRNSYS components can be developed using any common programming language, the component creation module only allows template source and project files to be created in C++ or Fortran. Due to compiler compatibility issues all development work for Type 213 has been performed using Microsoft Visual C++ (Microsoft Corp., 1998).

The template source code contains a skeleton component file based on the required TRNSYS structure and the defined Proforma. The created project file contains all the

necessary coding to properly link with the TRNSYS kernel once the mathematical modeling of the component has been added to the source file.

3. Integration of mathematical model within component. This step involves adding the necessary mathematical equations and solving algorithm to the source code file. All coding for Type 213 was performed using Microsoft Visual C++ (Microsoft Corp., 1998).
4. Compilation of the component. This involves using the Build command in Visual C++ once all required coding has been completed. The Build command creates a new external .dll file which is placed into a folder in the main TRNSYS directory dedicated to user developed components.
5. Use of the component. Once Steps 1-4 have been completed, the new component is displayed in the component library within the TRNSYS Simulation Studio. The new component can be then added to the simulation file as with any standard component.

Time Considerations

One of the main coding challenges encountered in the development of Type 213 was the storage of data across time steps. At each time step t , Type 213 calculates m_{ice}^t and T_{fluid}^t using conditions at the end of time step $t-1$. This approach requires that the Type 213 has a knowledge of m_{ice}^{t-1} and T_{fluid}^{t-1} calculated at the end of the previous time step. To facilitate this, two global storage variables are created in the C++ coding: SIce (Size 2x1) and STemp (Size 2x1). The data reading and storage procedure is as follows:

1. At each iteration at time t , the ice mass (m_{ice}^{t-1}) and tank fluid temperature (T_{fluid}^{t-1}) at the end of the previous time step are read from the storage variables. These values serve as initial conditions for calculations at time t .

$$m_{ice}^{t-1} = SIce(1,1) \quad (3-10)$$

$$T_{fluid}^{t-1} = STemp(1,1) \quad (3-11)$$

The calculated ice mass and tank fluid temperature at each TRNSYS iteration at time t are then stored in the second position of the storage arrays:

$$SIce(2,1) = m_{ice}^t \quad (3-12)$$

$$STemp(2,1) = T_{fluid}^t \quad (3-13)$$

2. Once TRNSYS has completed its calculation iterations and converged on a system solution at a particular time step t , the after-convergence portion of the Type source code is called. This section of the code allows for the modification of any storage arrays before they are read again at the next time step $t+1$. In Type 213, this section is used to place the final calculated values of m_{ice}^t and T_{fluid}^t in the first position in each storage array in preparation for when the arrays are next read at time $t+1$.

$$SIce(1,1) = m_{ice}^t \quad (3-14)$$

$$STemp(1,1) = T_{fluid}^t \quad (3-15)$$

3.3.2 Description of TRNSYS Proforma

Type 213 Parameters

Table 3-2 contains a summary of parameters for the ice storage tank. These values remain constant throughout the simulations.

Table 3-2: Summary of Parameters for Type 213

Parameter	Unit	Description
V_{tank}	m^3	Maximum storage volume of tank
rd_{tank}	m	Radius of tank
U	$kJ/(hr \cdot m^2 \cdot ^\circ C)$	Heat loss coefficient of tank

The total mass storage capacity of the ice tank is subsequently calculated based on the assumption that V_{tank} is reached at a maximum ice mass fraction of 0.40 (Poirier, 2011a):

$$m_{tank} = \frac{V_{tank} \rho_{ice} \rho_{fluid}}{(0.4 \rho_{fluid} + 0.6 \rho_{ice})} \quad (3-16)$$

where:

m_{tank} is the total mass storage capacity of the ice tank (kg)

V_{tank} is the maximum storage volume of the ice tank (m^3)

ρ_{ice} is the density of ice (916.7 kg/m^3)

ρ_{fluid} is the density of water (999.9 kg/m^3)

Type 213 Derivatives

Table 3-3 contains a summary of derivatives for Type 213. Derivatives in TRNSYS can be viewed as the initial conditions to the governing partial differential equations of the mathematical model.

Table 3-3: Summary of Derivatives for Type 213

Derivative	Unit	Description
T_{fluid}^0	°C	Tank fluid temperature at time $t=0$
m_{ice}^0	kg	Ice mass at time $t=0$

Type 213 Inputs

Table 3-4 contains a summary of input values provided by TRNSYS to TYPE 213 at each time step of the simulations.

Table 3-4: Summary of Inputs for Type 213

Input	Unit	Description
$T_{o,HP}^t$	°C	Fluid temperature into tank from heat pump
\dot{m}_{HP}^t	kg/h	Flow rate into tank from heat pump
$T_{o,col}^t$	°C	Fluid temperature into tank from solar collectors
\dot{m}_{col}^t	kg/h	Flow rate into tank from solar collectors
IGR^t	kg/h	Ice generation rate
T_{env}^t	°C	Temperature of ambient air outside tank

During simulations the value of T_{env}^t was set to the air temperature on the first floor of the home.

Type 213 Outputs

Table 3-5 contains a summary of outputs for Type 213.

Table 3-5: Summary of Outputs for Type 213

Output	Unit	Description
T_{fluid}^t	°C	Tank fluid temperature at end of time step t
m_{ice}^t	kg	Ice mass at end of time step t
\dot{m}_{HP}^t	kg/h	Flow rate to heat pump loop
\dot{m}_{col}^t	kg/h	Flow rate to solar collector loop

3.3.3 Description of Iterative Approach

Obtaining T_{fluid}^t and m_{ice}^t involves successively solving equations (3-8) and (3-9). However, obtaining a solution to equation (3-9) requires an estimate of the fluid mass at time step t (m_{fluid}^t), which cannot be known until m_{ice}^t has been calculated. As such, an iterative solving approach is implemented to allow for the calculation of the required outputs.

TRNSYS may call Type 213 several times during a time step until a convergent solution for the overall system is obtained. For each call to Type 213 during a time step, the iterative approach described below is used.

At the first iteration $n=0$:

1. The mass of fluid at time step t is assumed equal to the mass of fluid at time $t-1$:

$$m_{fluid,0}^t = m_{fluid}^{t-1} \quad (3-17)$$

2. Equation (3-9) is first solved to determine the tank fluid temperature $T_{fluid,0}^t$. This value is then used along with eqn. (3-8) to determine the ice mass $m_{ice,0}^t$.

At iterations $n \geq 1$,

1. The mass of fluid at time step t is recalculated based on the final ice mass determined during the previous iteration ($m_{ice,n-1}^t$):

$$m_{fluid,n}^t = m_{tank} - m_{ice,n-1}^t \quad (3-18)$$

2. Equation (3-9) is solved to determine the new tank fluid temperature $T_{fluid,n}^t$. This value is then used in conjunction with eqn. (3-8) to determine the new final ice mass $m_{ice,n}^t$.
3. The tank fluid temperature ($T_{fluid,n}^t$) and ice mass ($m_{ice,n}^t$) at iteration n are compared with values calculated at the previous iteration $n-1$. Iterations are terminated when:

$$\left| T_{fluid,n}^t - T_{fluid,n-1}^t \right| \leq 0.01^\circ C \quad (3-19)$$

$$\text{and } \frac{\left| m_{ice,n}^t - m_{ice,n-1}^t \right|}{m_{ice,n-1}^t} \leq 0.01 \quad (3-20)$$

Steps 1 and 2 are repeated if the two conditions defined in eqn. (3-19) and eqn. (3-20) are not met.

3.4 Validation of Simulation Results

Type 213 is validated with experimental results to ensure that the component model provides acceptable estimates of the ice mass and tank fluid temperature over time. The validation process is divided into two subsections:

1. Validation of the charging (ice building) process.
2. Validation of the discharge (ice melting) process.

3.4.1 Validation of the Charging (Ice Building) Process

Simulated results from the charging (ice building) process were compared with experimental data obtained from an ice slurry test tank at CanmetENERGY, Varennes, Canada (Poirier, 2011b). The experimental tank had a total fluid capacity of 632 kg, and a maximum ice mass of approximately 250 kg. The tank had an inner radius of 0.96 m and a height of 1.23 m. Tests were performed using a 5% (by mass) ethylene glycol solution and an ice generation rate of 1.96 kg/min.

The ethylene glycol solution was extracted from the bottom of the ice tank and directed to the evaporator of an ice slurry generator. Ice slurry exiting the evaporator was reintroduced to the top of the tank via an opening created in the side of the storage container. Fluid temperatures at the bottom of the ice tank were recorded and used to determine the experimental ice fraction. The fluid temperature was recorded at 15 s intervals, with the corresponding ice fraction (γ) then calculated using the formula (Poirier, 2011b):

$$\gamma = -2.16 - 2.385T_{fluid} - 0.789T_{fluid}^2 - 0.096T_{fluid}^3 \quad (3-21)$$

Type 213 was modified to include the change in concentration of ethylene glycol in the tank. It was assumed that the ice tank was initially filled with a 5% ethylene glycol solution. The total mass of glycol in the tank during the charging process was then:

$$m_{glycol} = 0.05 \cdot (m_{tank}) \quad (3-22)$$

where:

m_{glycol} is the mass of glycol in the tank (kg)

Assuming that the ice layer consisted of pure water, the glycol mass concentration at any point in the simulation was then:

$$\lambda_{glycol}^t = \frac{m_{glycol}}{m_{fluid}^t} \quad (3-23)$$

where:

λ_{glycol}^t is the glycol mass concentration at time t (-)

It was assumed that all inlet flows to Type 213 entered from the heat pump loop. The outlet fluid temperature from the heat pump evaporator was then varied according to the freeze point of the solution at the current ethylene glycol concentration. Calculation of the current freeze point was based on data obtained from 1st Choice Portable Chillers (2011), which provided freeze point temperatures at ethylene glycol mass concentrations ranging from 0-60%. Fitting a third order polynomial to the given data set ($R^2=0.999$), the freeze point temperature T_{glycol} at a certain glycol mass concentration λ_{glycol} was then:

$$T_{glycol} = -72.683\lambda_{glycol}^3 - 58.769\lambda_{glycol}^2 - 23.634\lambda_{glycol} - 0.2738 \quad (3-24)$$

where:

T_{glycol} is the glycol freeze point temperature (°C)

Figure 3-6 compares the simulated and experimentally determined ice fractions in the tank. The maximum difference between the simulated and experimental results is 7% of the tank storage capacity. Temperature stratification within the tank is a possible reason for the larger discrepancies between the simulated and experimental ice fractions after $t=40$ minutes. Experimental ice fractions were calculated using eqn. (3-21), which assumes that the tank is well

mixed. The lack of mechanical agitation during the test may have led to this equation providing less accurate estimates of the ice mass in the tank.

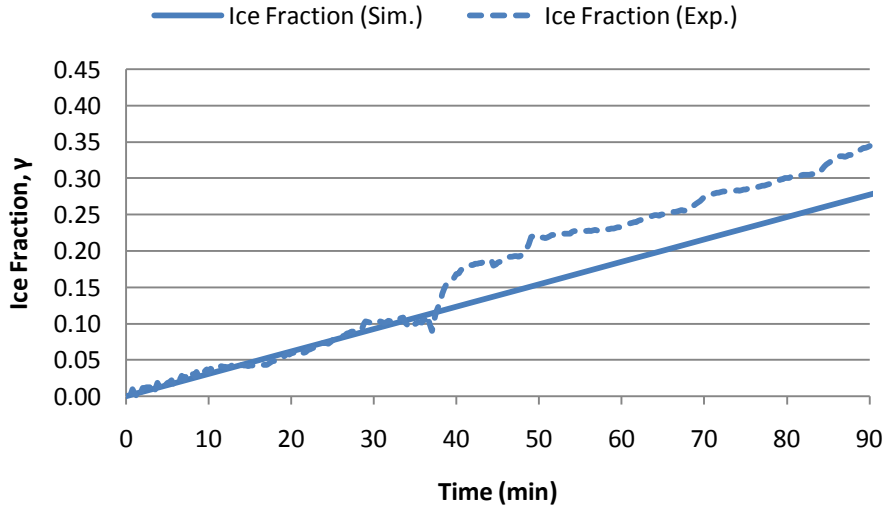


Figure 3-6: Comparison of Simulated and Experimental Ice Fraction During Charging Process
 (IGR=1.96 kg/min, $T_{fluid}^0=-1.5^{\circ}\text{C}$, $m_{ice}^0=0$ kg)

A comparison of the tank fluid temperatures is shown in Figure 3-7. Simulated and measured results show good agreement with a maximum discrepancy of 0.30°C.

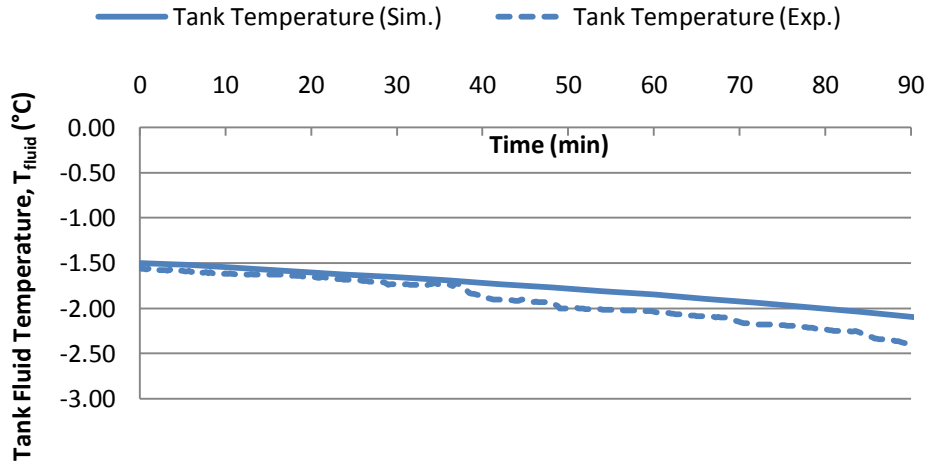


Figure 3-7: Comparison of Simulated and Experimental Tank Fluid Temperatures During Charging Process (IGR=1.96 kg/min, $T_{fluid}^0=-1.5^{\circ}\text{C}$, $m_{ice}^0=0$ kg)

3.4.2 Validation of the Discharge (Ice Melting) Process

In addition to the three test cases used to develop the effectiveness function (Run#5, Run#6, Run #10), two separate test cases (Run #4, Run#8) were selected from ASHRAE RP707 (ASHRAE, 1993) to validate the performance of the component model during ice melting operations. These test cases were selected due to the uniform distribution of inlet fluid across the top of the ice tank as assumed by Type 213. Test data in the report was given for a rectangular tank (2.44 m by 1.22 m, with a height of 1.22 m) operating in conjunction with an ice harvester system using pure water as a working fluid.

Water extracted from the bottom of the ice tank was first directed to a heating vessel consisting of six electrical heating elements. A nozzle was then used to uniformly distribute the inlet fluid over the top of the ice storage tank. Thermocouples were used to measure the fluid temperature at the tank inlet and outlet, while a control unit turned the heating elements on/off in order to maintain a defined inlet water temperature. Fluid flow rates were controlled using a gate valve at the pump outlet.

Key test parameters are provided below in Table 3-6. It was assumed that all fluid flow entered directly from the solar collector loop, with the flow rate from the heat pump (\dot{m}_{HP}) fixed at 0 kg/h.

Table 3-6: Key Discharge Test Parameters (ASHRAE, 1993)

Test Parameters	Run	
	4	8
Initial Ice Mass, m_{ice}^0 (kg)	1205	1499
Initial Fluid Temperature, T_{fluid}^0 (°C)	0	0
Inlet Fluid Flow Rate, \dot{m}_{col} (kg/h)	2730	2730
Inlet Fluid Flow Temperature, $T_{o,col}$ (°C)	7.8	19.4

Figure 3-8 shows a comparison of the simulated and experimental ice fractions during the discharge process for Run #4, while Figure 3-9 shows the same information for Run #8.

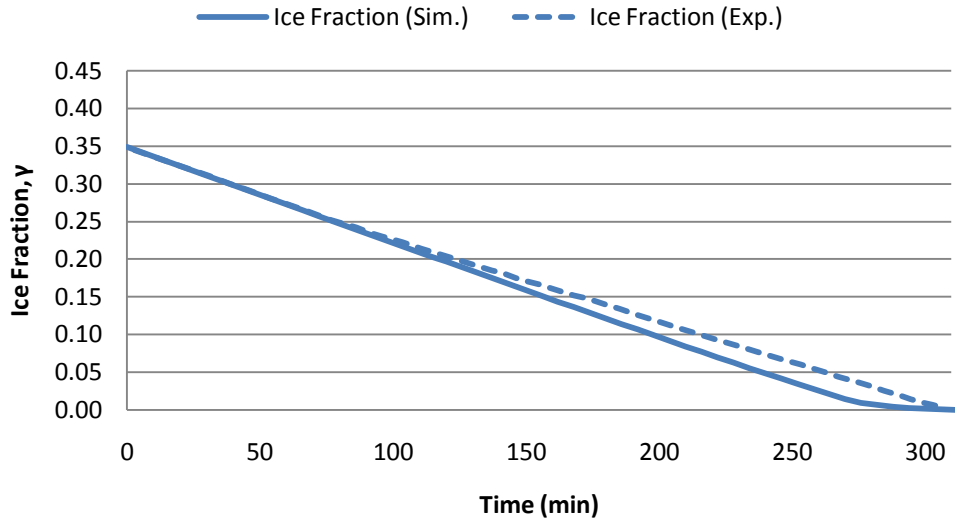


Figure 3-8: Comparison of Simulated and Experimental Ice Fraction During Discharge Process for Run#4 ($T_{o,col}=7.8^{\circ}\text{C}$, $\dot{m}_{col}=2730\text{ kg/h}$, $T_{fluid}^0=0^{\circ}\text{C}$, $m_{ice}^0=1205\text{ kg}$)

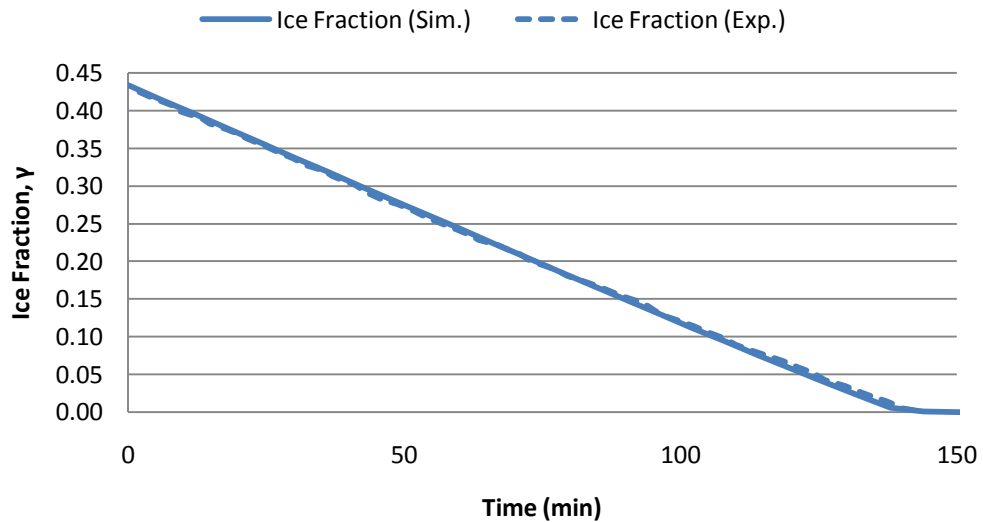


Figure 3-9: Comparison of Simulated and Experimental Ice Fraction During Discharge Process for Run #8 ($T_{o,col}=19.4^{\circ}\text{C}$, $\dot{m}_{col}=2730\text{ kg/h}$, $T_{fluid}^0=0^{\circ}\text{C}$, $m_{ice}^0=1499\text{ kg}$)

An examination of the simulated and experimentally determined ice fractions in the tank shows good agreement for both Run #4 and Run #8. The maximum difference between the two data sets is approximately 3% of the tank storage capacity for Run #4 (Figure 3-8), and 1% of the tank storage capacity for Run #8 (Figure 3-9).

Figure 3-10 contains a comparison of tank fluid temperatures over the ice melting period for Run #4, while Figure 3-11 shows the same data for Run #8.

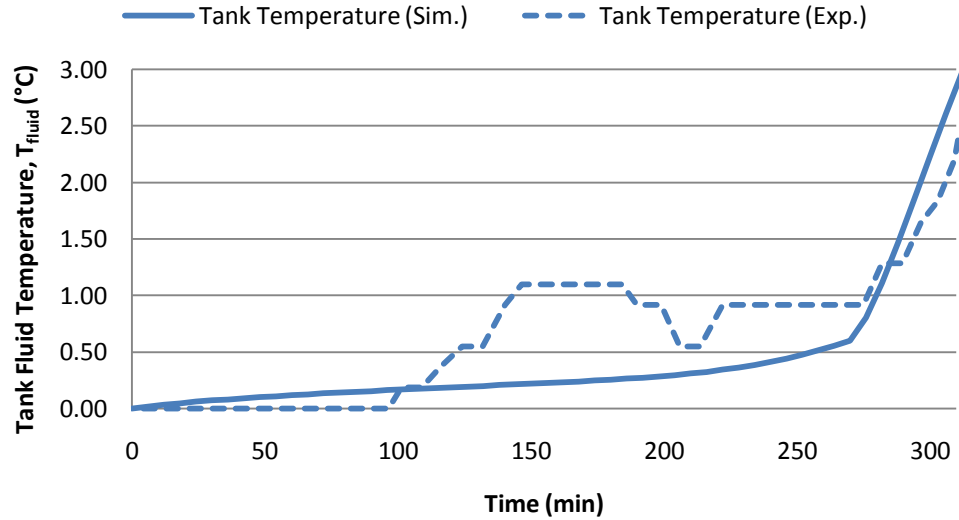


Figure 3-10: Comparison of Simulated and Experimental Fluid Temperature During Discharge Process for Run #4 ($T_{o,col}=7.8^{\circ}\text{C}$, $\dot{m}_{col}=2730\text{ kg/h}$, $T_{fluid}^0=0^{\circ}\text{C}$, $m_{ice}^0=1205\text{ kg}$)

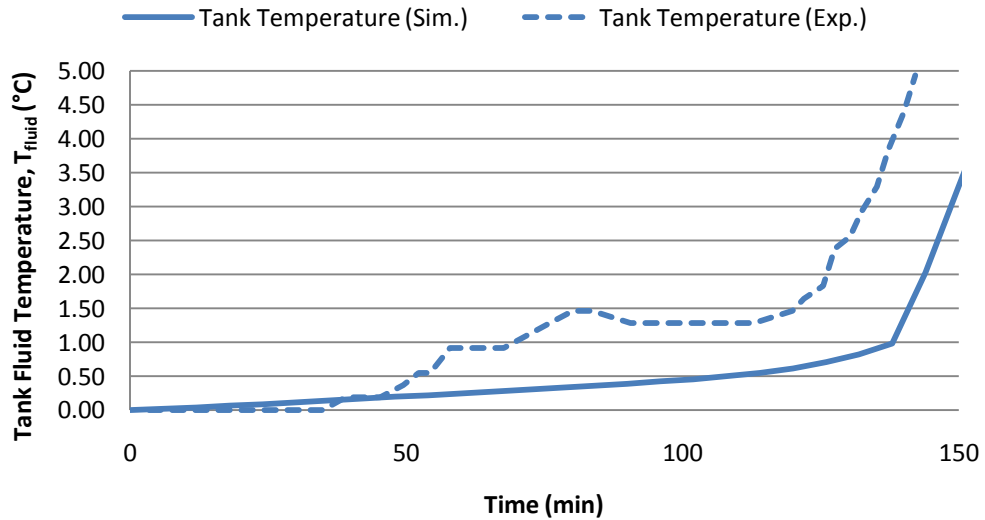


Figure 3-11: Comparison of Simulated and Experimental Fluid Temperature During Discharge Process for Run #8 ($T_{o,col}=19.4^{\circ}\text{C}$, $\dot{m}_{col}=2730\text{ kg/h}$, $T_{fluid}^0=0^{\circ}\text{C}$, $m_{ice}^0=1499\text{ kg}$)

A review of Figure 3-10 and Figure 3-11 shows that Type 213 is able to match the general trend of a slow tank fluid temperature increase at high ice fractions, followed by a steeper rise in fluid temperatures as the ice fraction approaches zero. The maximum discrepancy between the simulated and experimental results is approximately 0.75°C for Run #4, and 3°C for Run #8. A possible reason for these discrepancies is the fact that measured tank temperatures were obtained from water outlets at the bottom of the storage tank, and thus may not represent the average fluid storage temperature as output by Type 213. Furthermore, the accuracy of the thermocouples used for temperature readings is typically +/- 0.5°C (Tong, 2001), which could also contribute to the discrepancy between the simulated and experimental values.

3.5 Summary

A new mathematical model has been developed to simulate a non-agitated ice slurry storage tank. The model, based on energy balances for the ice and water layers, has been integrated into TRNSYS as Type 213. Verification of the new model with experimental data shows that it is able to accurately predict performance in all modes of operation.

4. Modeling of a Solar Assisted Heat Pump Using Ice Slurry

This chapter presents the modeling of a solar assisted heat pump using ice slurry. The concept and operations of the system are first discussed. The modeling approach using the TRNSYS energy simulation program is then presented in terms of the components and control strategies used.

4.1 TRNSYS Overview

TRNSYS (TraNsient SYstem Simulation program) is used to develop a computer model of the solar assisted heat pump system (Klein et al, 2004). This program offers a number of features, including:

- a. Component based approach to simulations.

TRNSYS provides users with a large library of standard components (called Types) including solar collectors, storage tanks, controllers, and HVAC and hydronic devices. Systems are defined by linking individual components together through mass and energy balances. This approach offers flexibility in defining the layout and operations of novel systems such as the solar assisted heat pump examined in this study.

- b. Ability to define new components.

TRNSYS permits users to create new Types if a desired component is not available in the standard library. This feature allows the user to tailor the simulated system to their exact specifications, and is used in this study to model the ice storage tank.

- c. Links with other analysis programs

TRNSYS can also be linked with other analysis programs such as Microsoft Excel (Microsoft, 2007) and MATLAB (Mathworks, 2008). This study combines TRNSYS and

GenOPT (Wetter, 2009) to perform an optimization study using a user selected set of variables, constraints, and optimization algorithm.

TRNSYS consists of a number of modules, including:

Simulation Studio

The Simulation Studio is the visual interface for system simulations. Within this module, users add iconic representations of each of the components in the system. These icons are then connected together using a linking tool, which allows for a visual depiction of the relationship between individual components. Parameters including the simulation start time, end time, and time step are defined in the Control Cards menu. A Build command creates a text based input file once the system layout has been fully defined.

TRNBUILD

The TRNBUILD module allows users to develop single and multi-zone building models. Designers can define a number of building parameters including the orientation, envelope construction, glazing and infiltration rate. Once the building has been fully defined it can be imported into the Simulation Studio to be linked with the weather file and HVAC system.

TRNEXE and TRNEDIT

TRNEXE is used to run the input text file created in the Simulation Studio and control the printed output of system variables. TRNEDIT allows users to perform parametric runs on the system and create a distributable file for the project.

4.2 System Description

A new solar assisted heat pump system is proposed in which solar thermal collectors are able to operate in series with an ice storage tank. A heat pump is used to link the ice tank with a stratified storage tank acting as a heat distribution point for the home.

Operating the solar collectors in series with an ice storage tank allows for an improvement in collector efficiencies due to the lower temperature fluid entering the collector. Figure 4-1 illustrates the theoretical collector efficiencies during the winter (Outside temperature -5°C) when (1) the collector are operating against an ice storage tank and (2) the collectors are operating against a warm water storage tank. Using a direct configuration (collectors in series with a warm water storage tank) offers the benefit that no additional energy input is required to operate a heat pump. However, solar collector efficiencies in the direct configuration are significantly lower than for an ice storage system. The reduced collector efficiency in the direct configuration leads to shorter periods of time when useful collector gains can be obtained. Using ice storage has the potential to increase the collector utilization period, resulting in larger thermal energy inputs into the system.

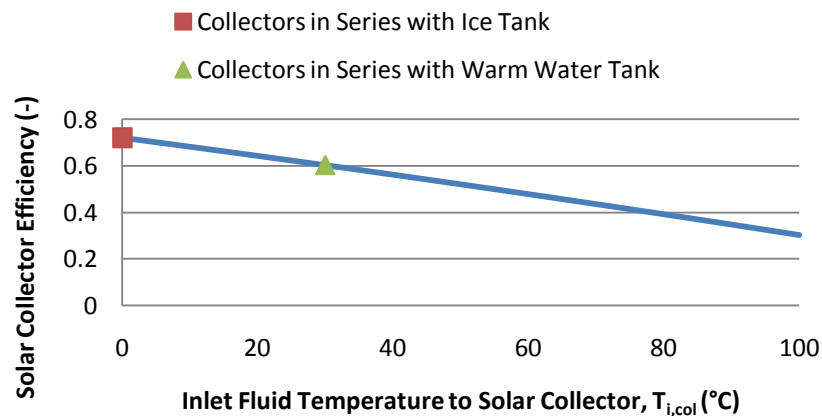


Figure 4-1: Impact of System Layout on Solar Collector Performance

A diagram of the proposed system is shown in Figure 4-2. To allow the system to operate in its most energy efficient configuration, two distinct solar loops are proposed:

a. Solar Loop A.

In this configuration, the collectors (I in Figure 4-2) operate in series with the ice storage tank (II). The heat pump (III) is operated to transfer thermal energy from the ice storage tank to the Warm Water Storage Tank (WWST, IV).

Solar Loop A improves solar collector efficiencies by circulating a low temperature fluid in the collector loop. This increase in efficiency allows useful thermal gains to be obtained from the collector array during times of lower solar radiation when a direct configuration would not be able to operate effectively.

b. Solar Loop B.

In this configuration, the collectors operate directly against the WWST (IV), bypassing the heat pump (III).

Solar Loop B allows the system to avoid operating the heat pump when the solar collector outlet temperature is high enough to provide direct heating and DHW preparation.

The ventilation loop is comprised of a heat recovery ventilator and a heating coil (VIII). Incoming ventilation air from the outdoors is preheated by exhaust air from the home, with additional heating up to the setpoint temperature of 20°C provided by the heating coil. A constant speed pump (VI_f) circulates water from the top of the WWST to the heating coil.

A radiant floor loop (VII) is selected to heat the first floor and basement levels of the home, as these systems provide higher exergetic efficiencies (Zmeureanu and Wu, 2007) and improved thermal comfort (Boerstra et al, 2000) in comparison to electrical baseboard or high temperature radiator heating. A variable speed pump (VI_e) circulates fluid through the radiant floor loop to maintain a constant operative temperature of 20°C on the first floor of the home. The supply temperature to the radiant floor is varied using a tempering valve (IX).

4.3 Modeling of Solar Assisted Heat Pump in TRNSYS

TRNSYS is selected to develop a model of the proposed system, which involves taking a component based approach to system simulations.

4.3.1 Summary of TRNSYS Components Used

A summary of the TRNSYS components used is provided in Tables 4-1 to 4-7.

Table 4-1: TRNSYS Storage Components

Component	Type	Name
Ice Storage Tank	213	Ice Tank
Warm Water Storage Tank	534	WWST

Table 4-2: TRNSYS Hydronic Components

Component	Type	Name
Tee Piece	11h	Tee Piece
Tempering Valve	11b	Temp Valve
Fluid Diverter	647	FD Col, FD Loop, FD RF
Fluid Mixer	649	FM Col, FM Loop, FM RF
Constant Speed Pumps	654	Loop A Pump, Loop B Pump, Evap Pump, Cond Pump, Vent Pump
Variable Speed Pump	656	RF Pump
Tankless Water Heater	659	WH RF, WH Vent, WH DHW
Piping	709	Inlet Piping, Outlet Piping

Table 4-3: TRNSYS System Control Components

Component	Type	Name
Differential Controller	2b	TmaxTankIce, TmaxTankStrat, TmaxTankStratB TempContStrat, TempContIce, IceCont, Humidon-Base, Humidon-1st, Shadingon,Lightson
PID Controller	23	PID RF
Time Step Delay	93	CD Strat, CD Ice, CD IceMass

Table 4-4: TRNSYS HVAC Components

Component	Type	Name
Air Diverter	646	AD
Air Mixer	648	AM
Heating Coil	753	Heating Coil
Heat Recovery Unit (HRU)	760	HRU

Table 4-5: TRNSYS Data Input/Output and Calculation Components

Component	Type	Name
Equations	EQN	hc, RHSet, Light+Shading, Eff, Eff-2, Eff-3 ColCnt, HPEvap, HPCond, IceGen, Vent Coeff, Q-Vent, Rad Floor, Tsetheat, DHW, RH, Pump, Aux, HP, HP Out,
Data File Reader	9	DHW Data
Simulation Summary	28	Pumps Sum, Aux Sum, Vent Sum, Lights Sum, HP Sum, RH Sum, HP to load
Online Printer with File	65a	Warm Water Tank Printer, Ice Tank Printer
Heating Season Indicator	515	HeatSeason
Forcing Function	516	Occupancy
Scheduler	518	Ground Refl

Table 4-6: TRNSYS Weather and Temperature Components

Component	Type	Name
Radiation Processor	16g	RD
Psychometrics	33	Psych
Sky Temperature	69b	Sky Temp
Weather File Reader	89b	Weather File

Table 4-7: TRNSYS Miscellaneous Components

Component	Type	Name
Multi-zone Building	56b	Home
Solar Collectors	537	AR1, AR2, AR3, AR4, AR5, AR6, AR7, AR8, ColCalcA, ColCalcB
Heat Pump	668	Heat Pump/Ice Generator
Ground Coupling	701	Ground

Modeling Approach

The home (Type 56b) represents the central portion of the TRNSYS model. The house exchanges data at each time step with the basement heat loss model (Type 701). A data reader (Type 89b) is used to obtain weather information from an external file, while a radiation processor (Type 16g) is used to determine the incident radiation on each surface of the home. Monthly ground reflection values are supplied to the radiation processor using a scheduler component (Type 518). Sky temperatures (Type 69b) and psychometric properties (Type 33) are also calculated and input to the home. The component *hc* (Equation Type) is used to calculate the convective heat transfer coefficient as a function of the wind velocity.

Control Strategy

Two forcing function components are used to define the occupancy level (Type 516) and heating season (Type 515) for the simulations. Differential controllers (Type 2b) are used to control the humidity, lighting, and shading inside the home. *Humidon-1st* and *Humidon-base* are used to maintain a relative humidity of 25% on the first floor and basement levels. *LightsOn* and *ShadingOn* are used to set the internal lighting and shading devices based on exterior solar radiation levels. A detailed description of each of the control strategies is provided in Hugo (2008).

Description of TRNSYS Components

Home: Type 56b

TRNSYS Type 56b is used to simulate a multi-zone home based on the work of Hugo (2008). The proposed building consists of a single above grade floor and a finished basement, and represents a typical single family home built in Montreal during the 1990s. A wood frame

construction is used, with a brick veneer and a gable roof. The heated living space is divided into two thermal zones: Main floor, and Basement. Occupancy is simulated based on a family of four, and is varied depending on the time of day and period during the week (weekday or weekend). A summary of key physical parameters for the study home is provided in Table 4-8.

Table 4-8: Description of Physical Parameters of Home

Total Floor Area (m ²)	210
Heated Floor Area (m ²)	186
Heated Volume (m ³)	483.6
Orientation (°)	0
Roof Angle (°)	45
Roof Area (m ²)	148.5
Infiltration Rate (ach ₅₀)	1.5

All windows in the home are double glazed with a low emissivity coating and an Argon filled cavity. A summary of the window area for each face of the home is provided in Table 4-9.

Table 4-9: Summary of Window Area for Home

Face	Area (m ²)
North	9.1
East	1.5
South	9.1
West	0.0

Table 4-10 summarizes the thermal performance of the building envelope. The thermal resistances of all main building envelope components meet or exceed the values required by Quebec law (Government of Quebec, 2011) and the Model National Energy Code of Canada for Homes (Canadian Commission on Building and Fire Codes, 1997).

Table 4-10: Summary of Thermal Performance of Key Building Materials

Component	Thermal Resistance (m²·°C/W)
Ceiling/Roof	7.61
Exterior Walls	6.49
Foundation Walls	4.74
Basement Floor	2.82

The U-Value for the double glazed window is 1.26 W/m²·°C.

The above described home is first simulated with electric baseboard heaters located on the first floor and basement in order to determine the base case energy consumption. DHW preparation is obtained through two immersed electrical heating elements inside the DHW storage tank. Daily DHW consumption is set at 266 L/day (Aguilar, 2005) while the hourly profile is based on the work of Jordan and Vajen (2001). Table 4-11 contains a summary of energy consumption for this base case system over a heating season from Oct. 1st to May 15th.

Table 4-11: Energy Consumption of Base Case Home

Consumption Classification	Energy Consumption (kW·h)
Total Energy Consumption (Heating, DHW, Ventilation, Lighting, Humidity Control)	12878
Mechanical System Energy Consumption (Heating, DHW, Ventilation)	11434

Ground Coupling: Type 701

TESS Type 701 (TESS, 2007) is used to model heat transfer between the basement of the home and the surrounding ground. This involves dividing the soil around the home into two distinct regions:

a. Near Field Zone.

This represents the soil region closest to the basement surfaces. Soil temperatures in this region are dependent on soil depth, time of year, and heat transfer from the boundary walls of the home.

b. Far Field Zone.

This represents the soil region beyond the near field zone. Soil temperatures in this region are a function of time of year and soil depth only. It is assumed that the far field region acts as an infinite sink/source of energy. As such, any conductive heat transfer between the near and far field regions has no impact on the soil temperature in the far field region.

Type 701 works by first dividing the near field soil region into a number of user defined 3-D control volumes. Energy balances are then solved on each control volume at each simulation time step using an iterative solving approach. The model assumes that heat transfer between all internal soil control volumes occurs entirely via conduction. Energy balances for surface soil nodes take into account the thermal gains and losses from convection and radiation. Moisture migration effects are neglected.

Soil properties used during energy balance calculations are summarized in Table 4-12 (Hugo, 2008).

Table 4-12: Soil Properties Input to Type 701

Soil Property	Value
Conductivity (W/m·°C)	2.42
Density (kg/m ³)	3200
Specific Heat (kJ/kg°C)	0.84
Surface Emissivity (-)	0.9
Surface Absorptance (-)	0.75

Initial soil temperature profiles are calculated using the Kasuda Correlation (Kasuda and Archenbach, 1965), which requires that the user supply the annual mean surface temperature, annual surface temperature amplitude, and the day of year when the lowest surface temperature occurs. A summary of these properties is provided in Table 4-13 (Hugo, 2008).

Table 4-13: Kasuda Correlation Properties

Property	Value
Mean Surface Temperature (°C)	6.3
Surface Temperature Amplitude (°C)	30.3
Minimum Surface Temperature Occurrence (days)	11

Integrating Type 56b with Type 701 involves first defining the five boundary surfaces which are in contact with the ground (Four below grade walls and a slab on grade floor). The zone side surface temperature for each of the five surfaces is then input into Type 701. Using this data, in combination with the U value for each boundary surface, Type 701 calculates the temperature at the interface between the boundary wall and soil. These values are then used as an input for Type 56b to allow for an analysis of heat transfer in the basement zone.

Ground Reflectance: Type 518 and 16g

Ground reflectance is an important consideration when calculating the solar radiation incident on a surface, as the reflectance of solar radiation due to snow cover can result in improved solar collector performance. The radiation processor (Type 16g) is limited in that it only contains one

input for the ground reflectance (i.e ground reflectance cannot be defined within Type 16g for each month). To facilitate monthly ground reflectance values, the radiation processor is connected with a scheduler Type 518 (TESS, 2007), which contains the ground reflectance for each month. A summary of the input ground reflectance values is summarized in Table 4-14 (Hugo, 2008).

Table 4-14: Ground Reflectance Values

Month	Ground Reflectance
January	0.36
February	0.36
March	0.31
April	0.22
May	0.20
June	0.20
July	0.20
August	0.20
September	0.20
October	0.20
November	0.22
December	0.31

4.3.2.2 Development of TRNSYS Solar Collector Loop Model

Figure 4-4 contains a diagram of the solar loop section of the TRNSYS model. Fluid flows are represented by solid bold lines. Control connections are denoted by dashed lines, while connections required for heat transfer and weather-dependant calculations appear as thin solid lines. Only three parallel solar collector arrays are shown in Figure 4-4 in order to provide a clear depiction of loop operations (During system simulations a maximum of eight parallel arrays are used).

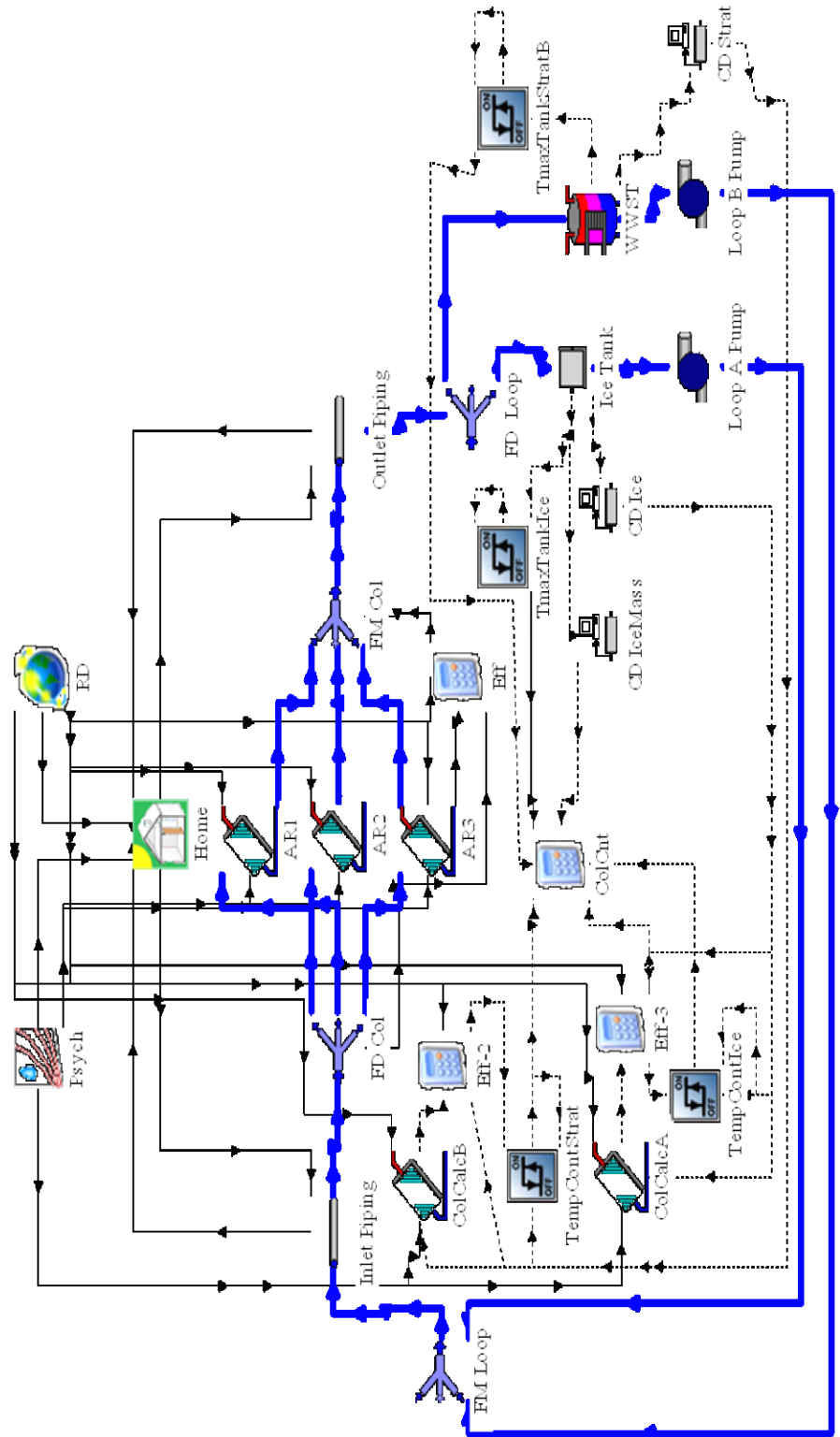


Figure 4-4: Solar Loop Portion of the TRNSYS Simulation Model

Modeling Approach

Flat plate solar collectors (Type 537) are used to provide thermal energy to the system. Flow diverter components (Type 647) are used to:

- i. Split the fluid flow between the parallel collector arrays (*FD Col*)
- ii. Direct outlet flow to the appropriate storage tank (*FD Loop*).

Two flow mixer components (Type 649) are used to:

- i. Combine flow from the parallel collector arrays (*FM Col*)
- ii. Direct incoming flow from the storage tanks to the solar collectors (*FM Loop*).

Constant speed pumps (Type 654) are used to circulate water from the ice tank (Type 213) or WWST (Type 534) to the solar collectors. The component *Eff* (Equation Type) is used to prevent calculation errors which lead to collector efficiencies greater than 100%.

Solar Loop Control Strategy

Selection of Solar Loop

The solar loop has two operational modes:

- a. Solar Loop A, with the solar collectors operating against ice tank.
- b. Solar Loop B, with the solar collectors operating against the WWST.

Selection of the appropriate solar loop is based on the anticipated solar collector outlet temperature when operating in the Loop B configuration ($T_{o,col,LoopB}$). This temperature is calculated by a controller at each time step based on the ambient air temperature, incident

solar radiation, collector specific flow rate, and water temperature at the bottom of the WWST. Loop B does not have to operate for these calculations to be completed.

Loop A is used when:

$$T_{o,col,LoopB} < T_{set} \quad (4-1)$$

where:

$T_{o,col,LoopB}$ is the anticipated outlet collector temperature in the Loop B configuration (°C)

T_{set} is a user defined setpoint temperature (°C)

When eqn. (4-1) is satisfied the Loop B configuration is unable to produce water at a high enough temperature to use directly in heating and DHW applications. During these periods Loop A is operated to increase the solar collector efficiency, resulting in higher thermal gains and longer collector utilization periods.

Loop B is then used when:

$$T_{o,col,LoopB} \geq T_{set} \quad (4-2)$$

When eqn. (4-2) is satisfied Loop B is capable of producing water at a high enough temperature to meet heating and DHW needs directly. The heat pump is not required to heat water in the WWST.

Circulation Pump Control

Two constant speed pumps (Loop A Pump, Loop B Pump) are used to circulate fluid in the collector loops. The pump flow rate is set proportional to the total solar collector area. On/Off operations for each solar circulation pump are defined using the component *ColCnt* (Equation Type), which analyzes four different control parameters:

a. Mode Selection

Selection of the appropriate solar loop is achieved using the component *ColCnt*. This component receives the anticipated Loop B outlet collector temperature ($T_{o,col,LoopB}$) as an input. Equations (4-1) and (4-2) are then analyzed to determine the correct operational mode.

Anticipated collector performance in Loop A and Loop B is continuously calculated using two test arrays: *ColCalcA* (Loop A, Type 537), and *ColCalcB* (Loop B, Type 537). The collector area for each test component is set equal to the size of one of the arrays used in the operational collector loop. Inlet temperatures are based on the fluid temperatures at the bottom of the ice tank (*ColCalcA*) or WWST (*ColCalcB*), while the fluid flow rate is held constant throughout the simulations at a rate proportional to the solar collector area. These arrays are used only for control purposes, and have no impact on system energy consumption.

A time delay is incorporated into the solar mode selection process to avoid solution convergence issues. Two input delay components (Type 93) hold the WWST and ice tank fluid temperatures before passing this data to the collector test arrays.

b. Tank Temperature Control

Two differential controllers (Type 2b) are used to limit fluid temperatures in the ice tank and WWST. The controller *TmaxTankIce* allows the Loop A circulation pump to operate only when the fluid temperature in the ice tank (T_{fluid}) is below 13°C, as this represents the maximum inlet fluid temperature to the heat pump evaporator. The controller *TmaxTankStratB* allows the Loop B pump to operate only when the temperature at the top of the WWST (T_{WWST}) is below 60°C.

c. Useful Energy Gain From Solar Collectors

To avoid unnecessary pump operations, the solar collector loops should only operate when useful thermal gains can be obtained. The differential controllers *TempContIce* (Type 2b) and *TempContStrat* (Type 2b) are used to monitor the anticipated fluid temperature rise across the solar collectors in the Loop A ($\Delta T_{\text{col,LoopA}}$) and Loop B ($\Delta T_{\text{col,LoopB}}$) configurations respectively. Anticipated fluid temperature increases are calculated using the two test arrays *ColCalcA* and *ColCalcB*. Each circulation pump is allowed to operate when its associated solar loop is able to produce a fluid temperature rise of greater than 3°C.

d. Ice Mass in Ice Storage Tank

The component *ColCnt* is used to monitor the amount of ice (m_{ice}) in the ice storage tank. If this value rises above 90% of the maximum ice storage capacity of the tank ($m_{\text{ice,max}}$), the system will always operate in the Loop A configuration. This control feature is added to limit the amount of time that the ice mass is at its maximum in the tank. Operating at the maximum ice capacity results in the heat pump being unable to

extract thermal energy from the ice tank, with heating and DHW requirements then met through auxiliary heating elements.

An input delay component (*CD IceMass*, Type 93) is used to avoid possible solution convergence issues by holding the value of ice mass in the tank before passing it to *ColCnt*.

All four control aspects are examined simultaneously at each time step to determine the appropriate operating signal to the each of the solar circulation pumps. The Loop A pump is allowed to operate when one of the following three conditions is met:

1. $T_{o,col,LoopB} < T_{set}, T_{fluid} < 13^{\circ}\text{C}, \Delta T_{col,LoopA} > 3^{\circ}\text{C}$ or
2. $T_{o,col,LoopB} \geq T_{set}, T_{fluid} < 13^{\circ}\text{C}, \Delta T_{col,LoopA} > 3^{\circ}\text{C}, T_{WWST} < 60^{\circ}\text{C}, m_{ice} > 0.9m_{ice,max}$ or
3. $T_{o,col,LoopB} \geq T_{set}, T_{fluid} < 13^{\circ}\text{C}, \Delta T_{col,LoopA} > 3^{\circ}\text{C}, T_{WWST} \geq 60^{\circ}\text{C}$

The Loop B pump is allowed to operate when one of the following two conditions is met:

1. $T_{o,col,LoopB} \geq T_{set}, T_{WWST} < 60^{\circ}\text{C}, \Delta T_{col,LoopB} > 3^{\circ}\text{C}, m_{ice} \leq 0.9m_{ice,max}$ or
2. $T_{o,col,LoopB} < T_{set}, T_{WWST} < 60^{\circ}\text{C}, \Delta T_{col,LoopB} > 3^{\circ}\text{C}, T_{fluid} \geq 13^{\circ}\text{C}$

The control conditions for each solar loop pump are mutually exclusive: Operating Loop A precludes using Loop B, and vice versa. If none of pump control conditions are met the solar loop pumps will not operate.

Practical Implementation of Control Strategy

Practical implementation of the control strategy requires the use of several devices. Firstly, a pyranometer and a temperature sensor are needed on the south facing roof to measure the solar irradiance and ambient air temperature. Thermocouples must be installed at the bottom

of the ice tank and WWST to determine the potential inlet collector temperatures for both solar loops.

As the ice fraction in the ice tank rises, the volume of the stored material also increases. Sensors are needed in the ice tank to detect when the height of the air/ice interface reaches a value corresponding to the maximum storage volume of the tank.

A computer controller is needed to calculate the potential collector performance in both solar loops based on the measured data, and manufacturer supplied collector properties. These controllers would then determine the appropriate control signal to each circulation pump based on the conditions described above.

Description of TRNSYS Components

Solar Collectors: Type 537

Solar collectors located on the south facing roof are used to provide thermal energy to the heat pump system. Flat plate collectors are selected due to their high performance at the low inlet fluid temperatures expected in this system (ASHRAE, 2006). Collectors are arranged into parallel arrays along the roof of the home, with each array containing three panels in series (Area 1.99 m²/panel).

TESS Type 537 (TESS, 2007) is chosen to model each collector array, with collector performance evaluated based on the thermal efficiency equation (Duffie and Beckman, 2006):

$$\eta_{col} = F_R(\tau\alpha)K_{\theta} - F_R U_L \frac{(T_{i,col} - T_{amb})}{G_T} - F_R U_{L/T} \frac{(T_{i,col} - T_{amb})^2}{G_T} \quad (4-3)$$

where:

η is the collector efficiency (-)

F_R is the heat removal factor (-)

$(\tau\alpha)$ is the combined transmittance/absorptance product (-)

K_θ is the incidence angle modifier (-)

U_L is the collector heat loss coefficient ($W/m^2 \cdot ^\circ C$)

$U_{L/T}$ is the temperature dependency of collector heat loss coefficient ($W/m^2 \cdot ^\circ C^2$)

$T_{i,col}$ is the inlet fluid temperature into the collector ($^\circ C$)

T_{amb} is the ambient air temperature ($^\circ C$)

G_T is the total incident radiation on the surface (W/m^2)

The optical efficiency of the solar collector ($F_R(\tau\alpha)_n$) varies with the incidence angle (θ). To model this phenomenon $F_R(\tau\alpha)_n$ is corrected using an incidence angle modifier K_θ . Type 537 divides the overall incidence angle modifier into three components: Beam, Diffuse, and Ground Reflected.

For beam radiation the incidence angle modifier becomes:

$$K_{\theta,beam} = 1 - b_0 \left[\frac{1}{\cos \theta} - 1 \right] - b_1 \left[\frac{1}{\cos \theta} - 1 \right]^2 \quad (4-4)$$

where:

$K_{\theta,beam}$ is the incidence angle modifier for beam radiation (-)

b_0 is the first order incidence angle modifier (-)

b_1 is the second order incidence angle modifier (-)

θ is the incidence angle (°)

For diffuse radiation the incidence angle modifier becomes:

$$K_{\theta,dif} = 1 - b_0 \left[\frac{1}{\cos \theta_{dif}} - 1 \right] - b_1 \left[\frac{1}{\cos \theta_{dif}} - 1 \right]^2 \quad (4-5)$$

where:

$K_{\theta,dif}$ is the incidence angle modifier for diffuse radiation (-)

θ_{dif} is the effective incidence angle for diffuse radiation on the collector (°)

The effective incidence angle for diffuse radiation is calculated as:

$$\theta_{dif} = 59.68 - 0.1388\beta + 0.001497\beta^2 \quad (4-6)$$

where:

β is the collector tilt angle (°)

For ground reflected radiation this becomes:

$$K_{\theta,gnd} = 1 - b_0 \left[\frac{1}{\cos \theta_{gnd}} - 1 \right] - b_1 \left[\frac{1}{\cos \theta_{gnd}} - 1 \right]^2 \quad (4-7)$$

where:

$K_{\theta,gnd}$ is the incidence angle modifier for ground reflected radiation (-)

θ_{gnd} is the effective incidence angle for ground reflected radiation on the collector (°)

The effective incident angle for ground reflected radiation is calculated as:

$$\theta_{gnd} = 90.0 - 0.5788\beta - 0.002693\beta^2 \quad (4-8)$$

The overall incidence angle modifier can then be calculated as:

$$K_{\theta} = \frac{K_{\theta,beam}G_{beam} + K_{\theta,dif}G_{dif}\left(\frac{1+\cos\beta}{2}\right) + K_{\theta,gnd}G_{gnd}\omega_{gnd}\left(\frac{1-\cos\beta}{2}\right)}{G_T} \quad (4-9)$$

where:

G_{beam} is the beam radiation incident on the collector (W/m^2)

G_{dif} is the diffuse radiation incident on the collector (W/m^2)

G_{gnd} is the ground reflected radiation incident on the collector (W/m^2)

ω_{gnd} is the ground reflectance (-)

Certain parameters in the collector efficiency equation ($F_R(\tau\alpha)_n$, F_RU_L , $F_RU_{L/T}$) are provided by the manufacturer for a single collector operating at a specified test flow rate. To accurately model collector performance, corrections must be made for the actual operating flow rate and number of collectors in series. As these correction factors are based on linear collector efficiency curves, eqn. (4-3) must be redefined as:

$$\eta_{col} = R_1R_2\left(K_{\theta}F_R(\tau\alpha) - F_RU_L' \frac{(T_{i,col} - T_{amb})}{G_T}\right) \quad (4-10)$$

where:

U_L' is the modified first order collector efficiency coefficient ($W/m^2 \cdot ^\circ C$)

R_1 is the flow correction factor (-)

R_2 is the series correction factor (-)

The product $F_R U_L'$ can be calculated using the expression:

$$F_R U_L' = F_R U_L + F_R U_{L/T} (T_{i,col} - T_{amb}) \quad (4-11)$$

Corrections due to non-test flow rates are achieved by multiplying by a flow modification factor

R_1 :

$$R_1 = \frac{N_{series} \dot{m}_{col} c_p}{A_{col}} \left(\frac{1 - e^{\left(\frac{(-F' U_L A_{col}) / (N_{series} \dot{m}_{col} c_p)}{R_{test}} \right)}}{R_{test}} \right) \quad (4-12)$$

where:

N_{series} is the number of collectors in series (-)

\dot{m}_{col} is the collector flow rate (kg/h)

c_p is the specific heat of the circulating fluid (kJ/kg·°C)

A_{col} is the collector area (m²)

R_{test} is the test correction factor (-)

F' is a collector efficiency parameter (-)

Equation (4-12) requires the estimation of two additional parameters: R_{test} and $F' U_L$

The parameter $F'U_L$ is calculated using the expression:

$$F'U_L = \begin{cases} F_R U_L' & \text{if } \frac{F_R U_L'}{\dot{m}_{test} c_p} \geq 1 \\ \dot{m}_{test} c_p \ln \left(1 - \frac{F_R U_L'}{\dot{m}_{test} c_p} \right) & \text{if } \frac{F_R U_L'}{\dot{m}_{test} c_p} < 1 \end{cases} \quad (4-13)$$

where:

\dot{m}_{test} is the fluid mass flow rate at test conditions (kg/h)

The test correction factor R_{test} is defined as:

$$R_{test} = \dot{m}_{test} c_p \left(1 - e^{\left(\frac{-F'U_L}{\dot{m}_{test} c_p} \right)} \right) \quad (4-14)$$

The efficiency expression is corrected for a series panel arrangement by multiplying by the series correction factor R_2 :

$$R_2 = \frac{1 - \left(1 - \frac{R_1 A_{col} F_R U_L'}{\dot{m}_{col} c_p N_{series}} \right)^{N_{series}}}{N_{series} \left(\frac{R_1 A_{col} F_R U_L'}{\dot{m}_{col} c_p N_{series}} \right)} \quad (4-15)$$

A summary of collector properties at test conditions is summarized in Table 4-15. Performance data is based on the use of a TitanPowerPlus SU-2 Flat Plate Solar Collector (SunMaxx Solar, 2010). Pure water from the ice tank (Loop A) or WWST (Loop B) is used directly at the solar collectors. The use of heat exchangers in the collector loop is avoided to reduce the amount of

thermal losses. It is assumed that a drainback feature is implemented to prevent water from freezing in the collectors and piping when the solar circulation pumps are not in use.

Table 4-15: Summary of Collector Array Properties

$F_R(\tau\alpha)$ (-)	0.740
$F_R U_L$ (W/m ² ·K)	3.79260
$F_R U_{L/T}$ (W/m ² ·K ²)	0.00356
$F_R U_L'$ (W/m ² ·K)	4.09
b_0 (-)	0.05
b_1 (-)	0.111
A_{col} (m ²)	1.99
\dot{m}_{test} (kg/h·m ²)	80.40
Working Fluid	Water
Collector Azimuth (°)	0

Solar Loop Pumps: Type 654

Two TESS Type 654 (TESS, 2007) components are used to model the Loop A and Loop B circulation pumps. Pump performance is based on a Wilo Star 25/4 (Wilo, 2010) operating using pure water as a working fluid.

The required pump head was calculated to be 14.9 kPa based on data obtained from The Engineering Toolbox (2010), ASHRAE (2005) and SunMaxx Solar (2010). Pressure drop calculations were performed assuming a maximum collector area of 47.76 m² (eight collector arrays), with a manufacturer recommended specific collector flow rate of 50 kg/h·m² (SunMaxx Solar, 2010).

Type 709: Piping

TESS Type 709 (TESS, 2007) is used to model the piping connecting the water storage tanks with the solar collectors. Each pipe is divided into three nodes to allow for thermal interactions between the component and the basement, first floor, and attic of the home. The air temperature in each of these zones is supplied to Type 709 as an input. The resulting thermal gains/losses are then returned to Type 56b for load calculation purposes. Table 4-16 contains a summary of piping parameters.

Table 4-16: Piping Parameters

Material	Copper
Length (m)	10
Number of Nodes (-)	3
Insulation Level (W/m ² ·°C)	0.04

Warm Water Storage Tank: Type 534

TESS Type 534 (TESS, 2007) is selected to develop a multi-node model of the Warm Water Storage Tank (WWST). The tank is divided into four isothermal nodes to achieve a balance between simulation accuracy and computational speed (Arias et al, 2008). Heat transfer between each node occurs through fluid conduction and convection. Effects are also included for heat gains or losses from the ambient, which are calculated based on the air temperature on the first floor of the home.

All connections to the WWST operate in a Fixed Outlet/Variable Inlet mode. The outlet node for each connection is specified and remains constant throughout the simulations. Inlet fluid is then matched with the tank node closest in temperature through the use of a stratifier device. Table 4-17 contains a summary of the outlet connection nodes for each loop served by the WWST. Node 1 corresponds to the top of the tank, while Node 4 represents the bottom fluid layer.

Table 4-17: Outlet Loop Connections to WWST

Loop	Outlet Connection Node
Solar Loop B	4
Heat Pump Condenser	4
Ventilation/Heating Coil	1
Radiant Floor	1

The tank geometry is based on the use of a Viessmann V-300 storage vessel (Viessmann, 2010). A vertical coiled heat exchanger is located internal to the tank and is used for DHW preparation, with heat exchanger parameters summarized in Table 4-18.

Table 4-18: Heat Exchanger Properties

Tube Inner Diameter (m)	0.032
Tube Outer Diameter (m)	0.044
Wall Conductivity (kJ/h·m·K)	58.32
Coil Diameter (m)	0.65
Coil Pitch (m)	0.07

Ice Tank: Type 213

A custom ice tank model (Type 213) is developed by the author as described in Chapter 3 of this study. The maximum ice mass fraction is set at 0.40 (Poirier, 2011a).

4.3.2.3 Development of TRNSYS Heat Pump Loop

Figure 4-5 shows the TRNSYS model of the heat pump loop. Fluid loops are represented by solid bold lines. Control connections are denoted by dashed lines, while connections required for additional calculations appear as thin solid lines.

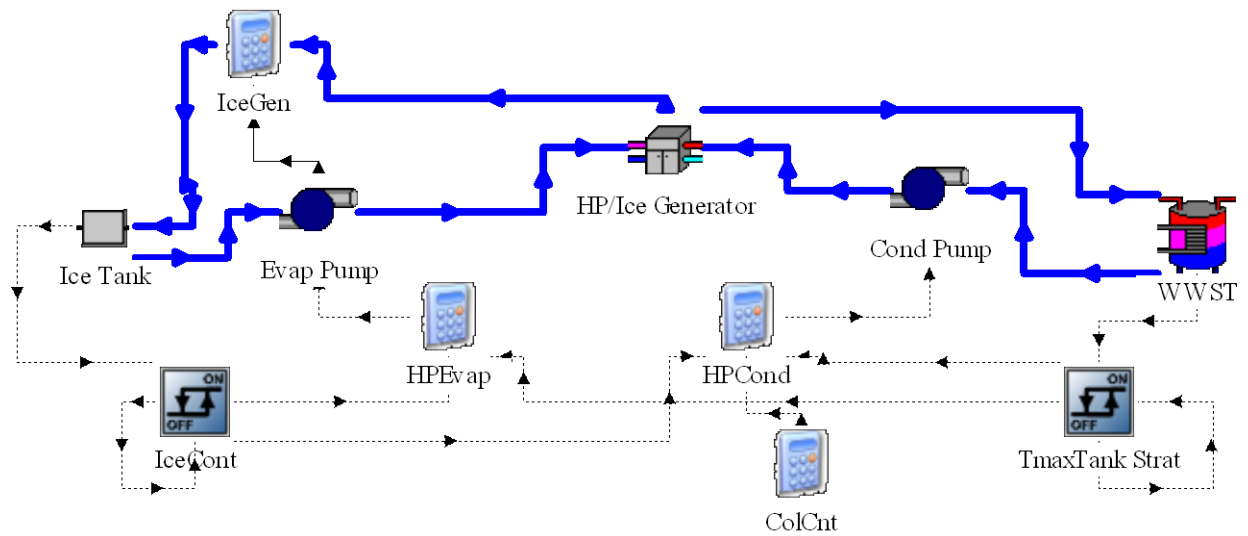


Figure 4-5: Heat Pump Portion of TRNSYS Simulation Model

Modeling Approach

A constant speed pump (Type 654) is used to circulate fluid from the bottom of the ice storage tank (Type 213) to the evaporator of the heat pump (Type 668). The component *IceGen* (Equation Type) is used to calculate the ice slurry fraction at the outlet of the heat pump evaporator. A second constant speed pump (Type 654) is used to circulate water from the bottom of the WWST (Type 534) to the heat pump condenser.

Heat Pump Loop Control Strategy

The evaporator and condenser pumps operate simultaneously, and are turned on and off based on three different control signals. The differential controller *TmaxTankStrat* (Type 2b) turns on when the temperature at the top of the WWST falls below 35°C (the maximum temperature required by the radiant floor system). This controller turns off when the temperature at the top of the WWST rises above 37°C. The differential controller *IceCont* (Type 2b) prevents the ice inventory in the ice tank from exceeding a mass fraction of 0.40. The component *ColCnt* (Equation Type) is used to prevent the heat pump from operating during Loop B operations.

The control signals are amalgamated using two TRNSYS equation types (*HPEvap*, *HPCond*) which allow the pumps to operate only when all control conditions are met. The heat pump itself does not operate unless there is a fluid flow through the evaporator and the condenser.

Description of TRNSYS Components

Heat Pump/ Ice Generator: Type 668

TESS Type 668 (TESS, 2007) is used to model the heat pump/ice generator. Component performance is calculated based on a user provided data file containing the power input and heating capacity as a function of the inlet fluid temperatures to the evaporator and condenser. A summary of the data file is provided in Appendix A1 of this thesis.

The heat pump is modeled on an Emerson ZB38KCE-TF5 compressor operating with R-507 refrigerant (Poirier, 2010). It is assumed that the temperature difference between the refrigerant and inlet fluid is 6°C at the evaporator and 10°C at the condenser (Dincer and Kanoglu, 2010). The device has a COP of 4.03 at a design point defined by an inlet evaporator fluid temperature of 0°C and an inlet condenser fluid temperature of 20°C.

The heat pump also acts as the ice generator for the system. Ice crystals begin to form when the refrigeration capacity of the heat pump is high enough to cool the fluid exiting the evaporator to 0°C. An orbital rod located inside the evaporator agitates the flow and prevents ice crystals from agglomerating and sticking to the walls.

As a stand-alone model, Type 668 is not capable of calculating the outlet ice fraction from the evaporator. As such, the component *IceGen* (Equation Type) is used to simulate this element of the system. *IceGen* receives the inlet and outlet fluid temperatures from the heat pump in addition to the heating capacity at the current operational point. Any outlet temperature (from

Type 668) below 0°C indicates that the refrigeration capacity of the heat pump is sufficient to generate ice at the current operational point. If this is the case, *IceGen* first resets the exiting fluid temperature from the heat pump to 0°C. Assuming that the inlet fluid contains no ice, the outlet ice fraction can be determined using the expression (IIR, 2005):

$$X_o = \frac{1}{L} \left(\frac{\Phi}{\dot{m}_{HP}} + c_p (T_{o,HP} - T_{i,HP}) \right) \quad (4-16)$$

where:

X_o is the outlet ice fraction (-)

L is the latent heat of ice (333.6 kJ/kg)

$T_{o,HP}$ is the outlet fluid temperature from the heat pump (°C)

$T_{i,HP}$ is the inlet fluid temperature to the heat pump (°C)

Φ is the refrigeration capacity of the heat pump (kJ/h)

\dot{m}_{HP} is the flow rate through the heat pump evaporator (kg/h)

The Ice Generation Rate (IGR) is then:

$$IGR = \dot{m}_{HP} (X_o) \quad (4-17)$$

where:

IGR is the Ice Generation Rate (kg/h)

Evaporator and Condenser Circulation Pumps: Type 654

Two TESS Type 654 (TESS, 2007) components are used to model the constant speed evaporator and condenser pumps. Evaporator pump performance is based on a Wilo TOP D-30, while the condenser pump performance is based on a Wilo Star-RS 25/2 (Wilo, 2010).

A summary of pump parameters is provided in Table 4-19. The evaporator and condenser flow rates have been selected based on a design point defined by an inlet evaporator fluid temperature of 0°C and an inlet condenser fluid temperature of 20°C. The evaporator pump flow rate is set to achieve a 5% ice fraction at the design point, while the condenser pump flow rate is selected based on a maximum 15°C temperature rise across the condenser. Pressure drop calculations are based on information provided in The Engineering Toolbox (2010) and ASHRAE (2005).

Table 4-19: Circulation Pump Properties for Heat Pump Loop

	Evaporator Pump	Condenser Pump
Model	Wilo TOP-D 30	Wilo Star-RS 25/2
Rated Flow Rate (kg/h)	3420	1250
Power Consumption (W)	64.9	14.8
Pump Head (kPa)	3.29	4.26

4.3.2.4 Development of TRNSYS Radiant Floor Loop

Figure 4-6 shows TRNSYS model of the radiant floor loop. Fluid loops are represented by solid bold lines. Control connections are denoted by dashed lines, while connections required for additional calculations appear as thin solid lines.

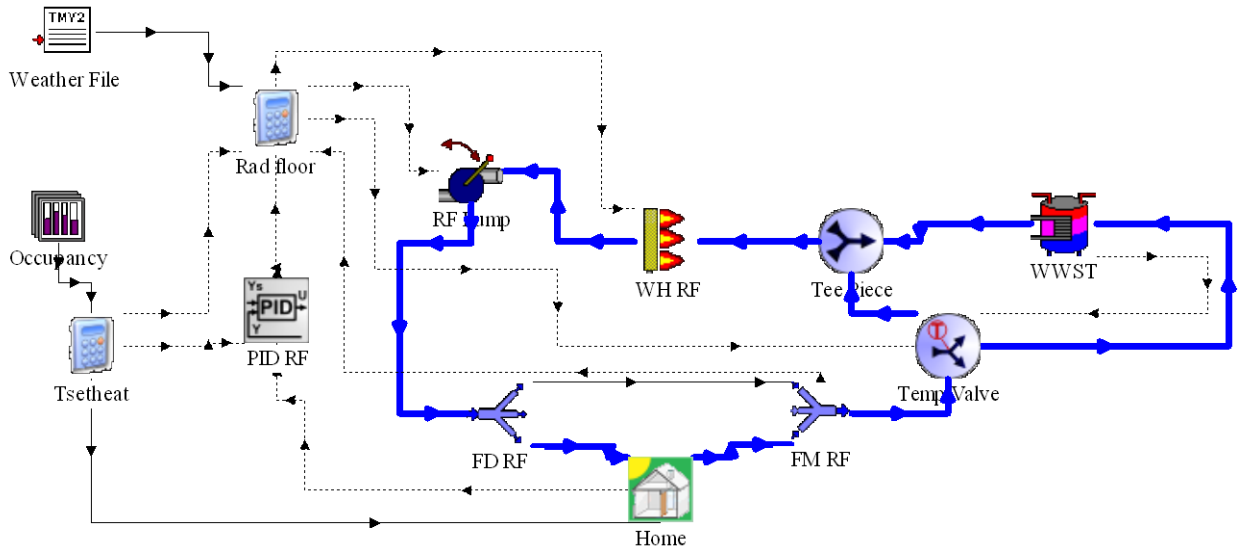


Figure 4-6: Radiant Floor Loop Portion of TRNSYS Simulation Model

Modeling Approach

A variable speed pump (Type 656) is used to circulate fluid in the radiant floor loop. Fluid extracted from the WWST (Type 534) is split between the first floor and basement of the home using a flow diverter (Type 647). Return flow from each thermal zone is recombined using a flow mixer (Type 649). A tee piece (Type 11h) and tempering valve (Type 11b) are used to control the temperature of fluid supplied to the radiant floor loop. A tankless hot water heater (Type 659) is also used to provide additional heating (if necessary) up to the radiant floor supply temperature.

Radiant Floor Loop Control Strategy

The radiant floor loop contains mechanisms to control both the supply temperature and flow rate of the circulating fluid.

Temperature Control

The supply water temperature to the radiant floor loop is varied depending on the outdoor air temperature (Figure 4-7). The supply temperature ranges from a maximum of 35°C at outdoor design conditions (-23°C) to a minimum of 25°C at an outdoor air temperature of 18°C.

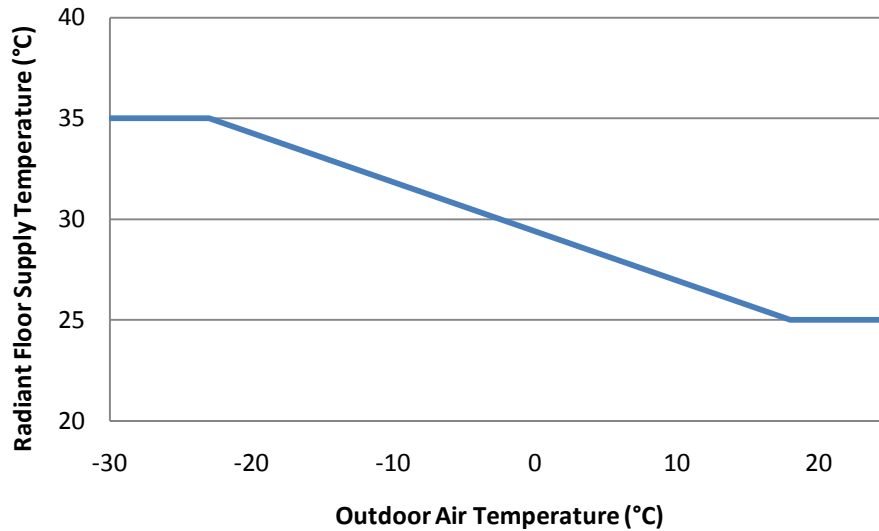


Figure 4-7: Supply Fluid Temperature to Radiant Floor Loop

The linear variation of the supply temperature is then:

$$T_{\text{sup}} = -0.2439T_{\text{amb}} + 29.39 \quad | -23^{\circ}\text{C} \leq T_{\text{amb}} \leq 18^{\circ}\text{C} \quad (4-18)$$

where:

T_{sup} is the radiant floor supply temperature (°C)

The component *RadFloor* (Equation Type) calculates T_{sup} and inputs this temperature to the tempering valve component. The tempering valve then bypasses a certain fraction of fluid around the WWST to obtain the desired floor supply temperature at the outlet of the tee piece.

Flow Rate Control

A PID Controller (Type 23) modulates the flow rate of the variable speed pump to maintain a constant operative temperature of 20°C on the first floor of the home. Control of the operative temperature is selected as this value is viewed as an important indicator of thermal comfort (Kuchen and Fisch, 2008). Given the current operative temperature, Type 23 calculates the pump flow rate based on the controller parameters provided in Table 4-20 (Hugo, 2008).

Table 4-20: PID Controller Parameters

Gain Constant	744
Integral Time (h)	8
Derivative Time (h)	0.5
Maximum Flow Rate (kg/h)	2500
Minimum Flow Rate (kg/h)	186

RadFloor takes the calculated flow rate as an input and determines the control signal to the pump using the expression:

$$CS = \frac{\dot{m}_{calc}}{\dot{m}_{rated}} \quad (4-19)$$

where:

CS is the control signal to the pump (-)

\dot{m}_{calc} is the calculated mass flow rate from the PID controller (kg/h)

\dot{m}_{rated} is the rated flow rate of the pump (2500 kg/h)

Description of TRNSYS Components

Radiant Floor Integration with Type 56b

The radiant floor system is modeled by adding an ‘Active Layer’ to the floor description in Type 56. This active layer contains the piping used to heat each of the thermal zones being served by the new system. A process called ‘Autosegmentation’ is used to divide the first floor and basement into a number of smaller segments to comply with the minimum non-zero flow rate constraints imposed by TRNSYS. For this case study, a minimum non-zero flow rate of 1 kg/h·m² is selected to limit the simulation time (Hugo, 2008).

The pipe length for each zone is calculated using the expression:

$$S_{Pipe} = \frac{A_{floor}}{N_{Loops} Y_{pipe}} \quad (4-20)$$

where:

S_{Pipe} is the length of the piping segment (m)

A_{floor} is the floor area (m²)

N_{Loops} is the number of piping loops in the zone (-)

Y_{Pipe} is the pipe spacing (m)

A summary of floor properties is provided in Table 4-21 (Hugo, 2008).

Table 4-21: Radiant Floor Piping Properties

Pipe Material	PEX
Pipe Spacing (m)	0.10
Pipe Outside Diameter (m)	0.02
Pipe Wall Thickness (m)	0.002
Pipe Wall Conductivity (W/m·°C)	0.35
Number of Pipe Loops in Zone (-)	10
Pipe Length, 1 st floor (m)	105
Pipe Length, Basement (m)	86

Variable Speed Pump: Type 656

TESS Type 656 (TESS, 2007) is used to model the variable speed circulation pump. Pump performance is based on a Wilo Stratos ECO-ST with a rated power of 40 W (Hugo, 2008). The power consumption at a particular mass flow rate can be calculated using the expression (Hugo, 2008):

$$\dot{P} = \dot{P}_{rated} \left(0.30 + 6.38(CS) - 19.87(CS)^2 + 31.12(CS)^3 - 18.88(CS)^4 + 1.95(CS)^5 \right) \quad (4-21)$$

where:

\dot{P} is the power consumption of the pump at a certain mass flow rate (W)

\dot{P}_{rated} is the rated power consumption of the pump (W)

Tankless Hot Water Heater: Type 659

TESS Type 659 (TESS, 2007) is used to model the tankless electric hot water heater. Performance is based on a 15 kW Eemax Series Two device (Eemax, 2010). It is assumed that the heating element has an efficiency of 100%.

4.3.2.5 Development of TRNSYS Ventilation Loop

Figure 4-8 shows the TRNSYS model of the ventilation loop. Fluid flows are represented by solid bold lines. Air flows are denoted by dashed lines, while connections required for performance and weather calculations appear as thin solid lines.

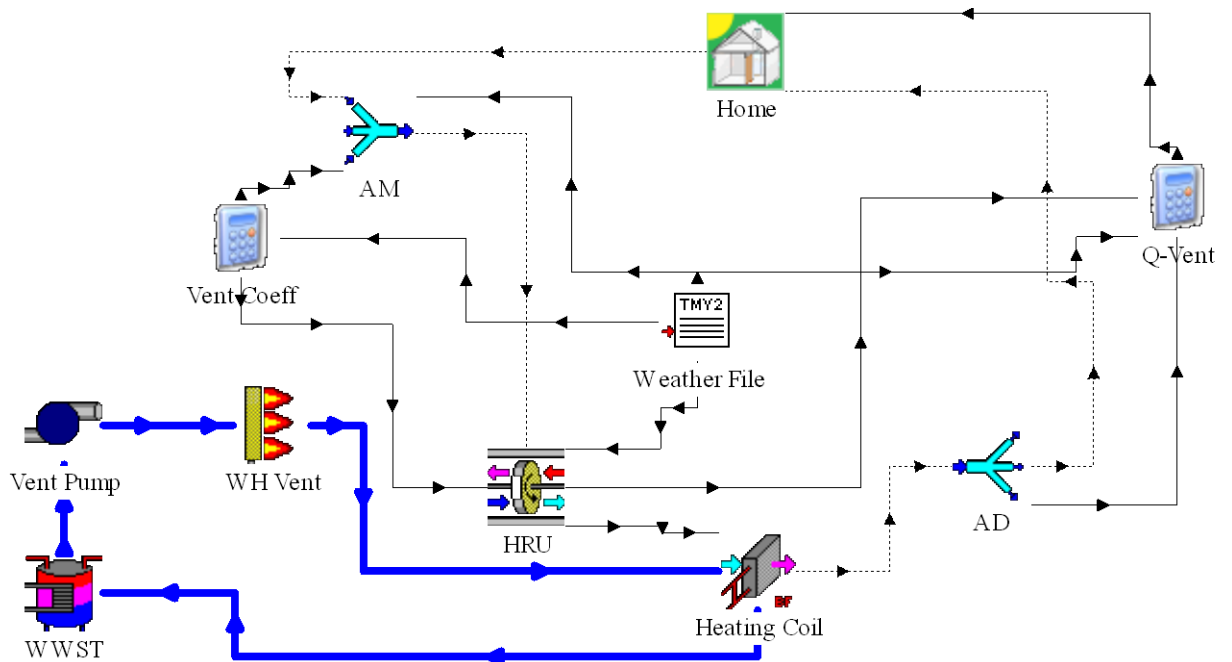


Figure 4-8: Ventilation Loop Portion of TRNSYS Simulation Model

Modeling Approach

The ventilation system consists of separate air and water loops. A constant speed pump (Type 654) circulates fluid in the water loop, while a tankless hot water heater (Type 659) ensures that the fluid temperature entering the heating coil (Type 753) is at least 30°C

A Heat Recovery Unit (HRU, Type 760) is used in the air loop to recover thermal energy from the exhaust air. A flow diverter (Type 646) is used to split fresh ventilation air between the first floor and basement levels. Similarly, a flow mixer (Type 648) is used to combine exhaust air from the two levels of the home before entering the HRU. The Equation Type *Vent Coeff* is used to define the ventilation air flow rate and efficiency of the HRU. The component *Q-Vent* (Equation Type) is used to convert flow rates calculated by TRNSYS (in kg/h) into air changes per hour (ach).

The ventilation rate is set at 0.35 ach and consists entirely of outdoor air. The temperature of air entering the home is controlled using a bypass valve at the heating coil, with warm water diverted as necessary to maintain a constant setpoint temperature of 20°C.

Description of TRNSYS Components

Heat Recovery Unit: Type 760

TESS Type 760 (TESS, 2007) is used to simulate the Heat Recovery Unit (HRU). The component operates in an uncontrolled mode in which the outlet temperatures of the exhaust and ventilation flows are not held constant. Moisture transfer between the two air streams is neglected.

Component performance is based on the use of a Venmar HRU (Venmar, 2007). The heat recovery efficiency and power consumption are summarized in Table 4-22.

Table 4-22: HRU Properties

Sensible Heat Recovery Efficiency	0.64 if $T_{amb} > -13^{\circ}$ 0.62 if $T_{amb} \leq -13^{\circ}\text{C}$
Power Consumption	110 W if $T_{amb} > -13^{\circ}\text{C}$ 114 W if $T_{amb} \leq -13^{\circ}\text{C}$

Circulation Pump: Type 654

TESS Type 654 (TESS, 2007) is used to model the constant speed circulation pump. Pump performance is based on the use of a Wilo STRATOS 25/1-4 (Wilo, 2010). The ventilation air flow rate is set at 150 kg/h in order to achieve a 15°C fluid temperature drop across the heating coil at outdoor design conditions. A summary of pump parameters is shown below in Table 4-23.

Table 4-23: Summary of Ventilation Pump Parameters

Rated Flow Rate (kg/h)	150
Power Consumption (W)	4.85
Pump Head (kPa)	4.45

Tankless Hot Water Heater

TESS Type 659 (TESS, 2007) is used to model the tankless hot water heater. Component performance is as described in Section 4.3.2.4 of this thesis.

4.3.2.6 Development of TRNSYS DHW Loop

Figure 4-9 shows the TRNSYS layout of the DHW loop.

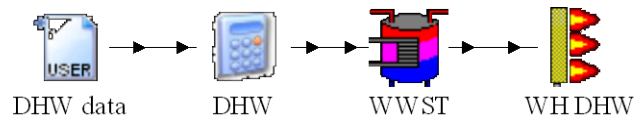


Figure 4-9: TRNSYS Modeling of DHW Simulation Loop

Modeling Approach

A data file reader (Type 9) obtains DHW flow rate from an external file at each time step of the simulation. The temperature of inlet water from the city main is calculated by the component *DHW* (Equation Type) based on the day of the year. Water from the city main is heated using a vertical coiled heat exchanger located internal to the WWST (Type 534). Additional heating up to the DHW setpoint of 45°C is obtained by using an electrical tankless hot water heater (Type 659).

Description of TRNSYS Components Used

DHW Data File Reader: Type 9

Type 9 is used to obtain the DHW flow rate from an external text file. The daily average water consumption is set at 266 L/day (Aguilar, 2005). The DHW demand profile is based on the work of Jordan and Vajen (2004), which provided DHW flow rates for a single family European home at various time intervals (1min, 6min, 1 hour). All system simulations are performed in TRNSYS using a 6 minute time step.

The DHW flow profile for January 2nd is shown in Figure 4-10.

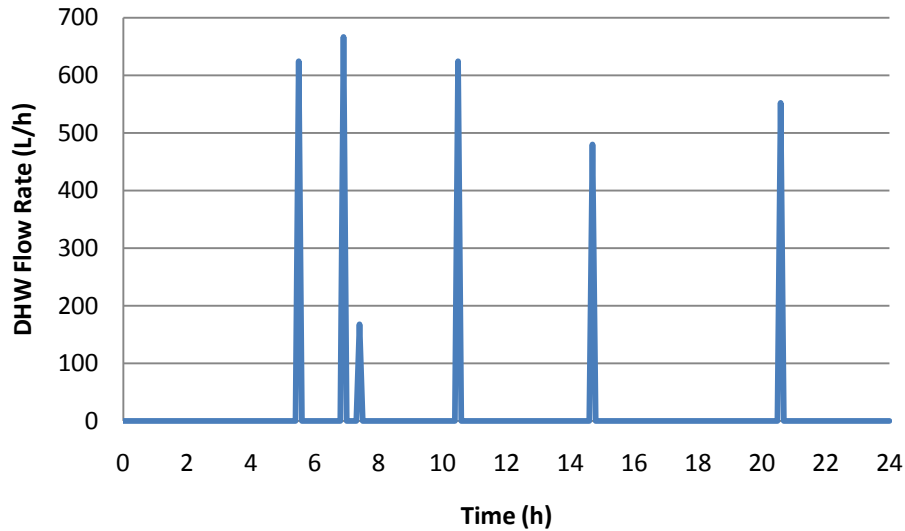


Figure 4-10: Simulated DHW Flow Profile for Jan. 2nd

DHW: Equation Type

The component *DHW* (Equation Type) calculates the temperature of water entering from the city main. The temperature is calculated using a best fit equation based on measured data for an aqueduct in Montreal, QC (Dumas and Marcoux, 2004). The equation, using a Fourier series with seventeen harmonics, can be written as (Hugo, 2008):

$$T_{city} = a + v_1 \cos(zN) + w_1 \sin(zN) + v_2 \cos(2zN) + w_2 \sin(2zN) + \dots \quad (4-22)$$

Where:

T_{city} is the temperature of water from the city main (°C)

N is the day of year (-)

a is a correlation coefficient

z is a correlation coefficient

$v_1..v_{17}$ are harmonic coefficients (-)

$w_1..w_{17}$ are harmonic coefficients (-)

A table defining the value of each coefficient is provided in Appendix A2.

Tankless Hot Water Heater: Type 659

TESS Type 659 (TESS, 2007) is used to model the tankless hot water heater. Component performance is as described in Section 4.3.2.4 of this thesis.

4.4 Summary

This chapter has presented the control strategy and TRNSYS modeling approach for a proposed solar assisted heat pump system using ice slurry. The results of an optimization process are provided in Chapter 5 of this thesis, while a detailed analysis of system performance is presented in Chapter 6.

5. Optimization of a Solar Assisted Heat Pump using Ice Slurry

This chapter presents the methodology and results of a mathematical optimization performed on the proposed ice slurry system. The set of selected design variables is first introduced, followed by a discussion of the optimization objective function. The optimization algorithm is then described in detail, focusing on the search process and parameters used. The chapter concludes with the results of several optimizations performed on the system.

5.1 Optimization Variables

The optimization process centers on design variables defining the solar collectors and thermal storage capacity of the proposed ice slurry system. The set of independent design variables is presented first, followed by the set of variables dependent on the optimization process.

5.1.1 Independent Design Variables

The selected set of independent design variables defines the performance and operations of the solar collector loop, and the thermal storage capacity of the system. Each design variable is listed below:

1. Solar collector area (A_{col})
2. Solar collector tilt angle (β)
3. Solar collector specific flow rate ($\dot{m}_{col,s}$)
4. Ice storage tank volume (V_{ice})
5. Warm water storage tank volume (V_{wwst})
6. Solar loop selection control temperature (T_{set})

All design variables are assumed to be continuous. Using a mix of continuous and discrete variables has been avoided as it would require the use of a complex optimization algorithm

(Wetter, 2009) which could potentially require a large number of simulations to reach the optimal point (Wetter and Wright, 2004).

In reality, the solar collector area and warm water storage tank volume are discrete variables. The optimized values for these two variables will be converted to discrete values through a sensitivity analysis performed around the determined optimal point.

Design Variable Range

Table 5-1 presents the bounds of each design variable in the study.

Table 5-1: Study Range of Independent Design Variables

Parameter	Lower Bound	Upper Bound
A_{col} (m ²)	5.97	65.67
β (°)	35	90
$\dot{m}_{col,s}$ (kg/h·m ²)	20	70
V_{Ice} (m ³)	0.3	32.3
V_{WWST} (m ³)	0.3	1.5
T_{set} (°C)	10	40

The upper bound for the solar collector area is selected based on the collectors taking up the maximum possible area on the south facing roof at the roof angle of 45°. This consists of 11 parallel arrays, with each array made up of three panels connected in series (5.97 m² per array). The lower limit is set based on the minimum typical collector area seen in European solar combi-systems (Vogelsanger and Laipple, 2006).

The upper and lower bounds for the collector tilt angle and specific collector flow rate are based on the operating ranges suggested by the solar collector manufacturer (SunMaxx Solar, 2011).

The upper bound for the ice tank volume is limited by the physical size of the ice tank within the home. The lower limit is set based on the minimum typical storage tank volume found in a solar combi-system (Lund, 2005).

The upper and lower bounds for the warm water storage tank volume are selected based on the typical range of storage tank volumes found in solar combi-systems (Lund, 2005).

The lower bound for the solar loop control temperature has been selected as it gives priority to Loop B operations. The upper bound has been selected as it directs the system to give the Loop A configuration priority.

5.1.2 Dependant Design Variables

Two system parameters are dependent on the design variables.

Pipe Diameter

The diameter of piping linking the solar collectors with the home is dependent on the collector area and specific collector flow rate. This diameter is reselected so as to maintain a velocity V_{pipe} of 0.6 m/s (Viessmann, 2011):

$$d_{pipe} = 2 \left(\frac{A_{col} \dot{m}_{col,s}}{\pi \rho_{fluid} V_{pipe}} \right)^{1/2} = 2 \left(\frac{\dot{m}_{col}}{\pi \rho_{fluid} V_{pipe}} \right)^{1/2} \quad (5-1)$$

where:

d_{pipe} is the diameter of the pipe used (m)

$\dot{m}_{col,s}$ is the specific solar collector flow rate (kg/s·m²)

\dot{m}_{col} is the total solar collector flow rate (kg/s)

ρ_{fluid} is the density of the collector working fluid (kg/m^3)

V_{pipe} is the fluid velocity in the pipe (m/s)

Solar Loop Pump Rated Power

The power input to the solar loop pumps also changes with the collector area and specific collector flow rate. It is assumed that the pump head is constant at the value presented in Chapter 4. The pump power is then recalculated during each optimization run according to the following formula:

$$\dot{P} = \frac{Q_{\text{col}} \Delta P}{\eta_{\text{pump}}} \quad (5-2)$$

where:

\dot{P} is the pump power input (W)

Q_{col} is the volumetric flow rate through the pump (m^3/s)

ΔP is the pump head (Pa)

η_{pump} is the combined electrical and mechanical pump efficiency (-)

5.2 Optimization Objective Function

The purpose of this optimization study is to minimize the heating operating energy use for the home over a single heating season (Oct. 1st to May 15th). The heating operating energy use is defined as:

$$E_{Op} = E_{A,RF} + E_{A,DHW} + E_{A,Vent} + E_{i,HP} + E_{i,Pump} \quad (5-3)$$

where:

E_{Op} is the heating operating energy use over the heating season (kW·h)

$E_{A,RF}$ is the auxiliary energy input to the radiant floor (kW·h)

$E_{A,DHW}$ is the auxiliary energy input to meet DHW demand (kW·h)

$E_{A,Vent}$ is the auxiliary energy input to the water in ventilation loop (kW·h)

$E_{i,HP}$ is the energy input to the heat pump (kW·h)

$E_{i,pump}$ is the energy input to the circulation pumps (kW·h)

5.3 Optimization Algorithm

A Hooke-Jeeves algorithm is applied to minimize the objective function. This algorithm is chosen due to its ability to handle the discontinuous cost functions found in building optimization (Wetter, 2009), while also requiring a smaller amount of simulations in comparison to a particle swarm or hybrid algorithm (Wetter and Wright, 2004).

5.3.1 Description of Algorithm

The Hooke-Jeeves optimization procedure can be defined as follows (Wetter, 2009):

1. Evaluate objective function at vector x_k . The vector x_k of design variables represents the point corresponding to the lowest value of the objective function determined during the optimization process. In the case of the first iteration ($k=1$), a vector of user defined initial values is used.
2. Perform a global search around x_k . This involves individually increasing and decreasing the value of each optimization variable based on a user defined step size s to determine if a reduction in the objective function can be obtained.

Any new value reducing the objective function is recorded in the exploration vector x' before the algorithm moves on to modulating the next optimization variable. If no reduction in the objective function is found for an optimization variable, the value at the start of the search iteration (x_k) is recorded in x' .

Mathematically this process can be defined as:

$$M \triangleq \{x \in X \mid x' = x_k \pm \Delta_k s^i e_i, i \in \{1, \dots, n\}\} \quad (5-4)$$

where:

X is the set of constraints defined by the upper and lower optimization variable bounds

x' is an exploration vector

x_k is the vector corresponding to the lowest value of the objective function

Δ is the mesh size factor

s is the step size for optimization variable i

e is the search direction for optimization variable i

n is the number of optimization variables being examined.

3. Evaluate the objective function at the vector x' .

$$\underline{\text{If } f(x') < f(x_k),}$$

- a. Increase the iteration counter to $k+1$.
- b. Designate the vector x' as the point corresponding to the lowest value of the objective function.

$$x_k = x' \tag{5-5}$$

Maintain the previous values of the mesh size factor and mesh size exponent:

$$\Delta_k = \Delta_{k-1} \tag{5-6}$$

$$y_k = y_{k-1} \tag{5-7}$$

where:

y is the mesh size exponent

- c. Perform an exploratory move. This involves shifting the base point for the optimization process according to the formula:

$$x_b = x_k + (x_k - x_{k-1}) \tag{5-8}$$

where:

x_b is a new base point for the search algorithm

- d. Evaluate the objective function at x_b .

If $f(x_b) < f(x_k)$, designate x_b as the point corresponding the lowest value of the objective function:

$$x_k = x_b \tag{5-9}$$

e. Perform a global search around the point x_b . The search set is defined as:

$$M \triangleq \{x \in X \mid x' = x_b \pm \Delta_k s^i e_i, i \in \{1, \dots, n\}\} \quad (5-10)$$

If $f(x') < f(x_k)$, the vector x' is designated as the new minimum point:

$$x_k = x' \quad (5-11)$$

f. Perform a local search around the point x_k . The search set is defined as:

$$M \triangleq \{x \in X \mid x' = x_k \pm \Delta_k s^i e_i, i \in \{1, \dots, n\}\} \quad (5-12)$$

If $f(x') < f(x_k)$, the vector x' is designated as the new minimum point:

$$x_k = x' \quad (5-13)$$

g. Evaluate the results of the exploratory move.

- i. If step (d), step (e) or step (f) has led to a reduction in the objective function, repeat steps (a)-(f).
- ii. If step (d), step (e), or step (f) does not reduce the objective function, follow the steps below.

If $f(x') \geq f(x_k)$,

- a. Increase the iteration counter to $k+1$.
- b. Maintain the base search point:

$$x_k = x_{k-1} \quad (5-14)$$

- c. Reduce the mesh exponent and mesh size factors. The mesh exponent is recalculated as:

$$y_k \triangleq y_{k-1} + c \quad (5-15)$$

where:

c is the mesh exponent increment.

The mesh size factor is then calculated as:

$$\Delta_k \triangleq \frac{1}{r^{y_k}} \quad (5-16)$$

where:

r is the mesh size divider

- d. Repeat steps 1-3.

4. Repeat steps (1) to (3) until the termination conditions are met.

$$\Delta_k < \Delta_{\min} \quad (5-17)$$

Or:

$$k > k_{\max} \quad (5-18)$$

5.3.2 Demonstration of Optimization Algorithm

A sample optimization is performed to demonstrate the use of the Hooke-Jeeves algorithm. The selected objective function to minimize is:

$$z(v, w) = v^2 + (w - 4)^2 \quad (5-19)$$

Table 5-2 contains a summary of the optimization parameters for this sample problem.

Table 5-2: Optimization Parameters for Sample Function

Parameter	Value
Mesh size divider (r)	2
Initial Mesh Exponent (γ_1)	0
Mesh Exponent Increment (c)	1
Minimum Mesh Size Factor (Δ_{min})	0.25

The initial point for the algorithm, x_1 , is selected as (3,7), while the step sizes are selected as $s_v=1, s_w=1$.

A visual representation of the optimization process is provided in Figure 5-1. The algorithm requires three successful search moves to find the lowest value of the objective function. A detailed description of the sample optimization is provided in Appendix A3.

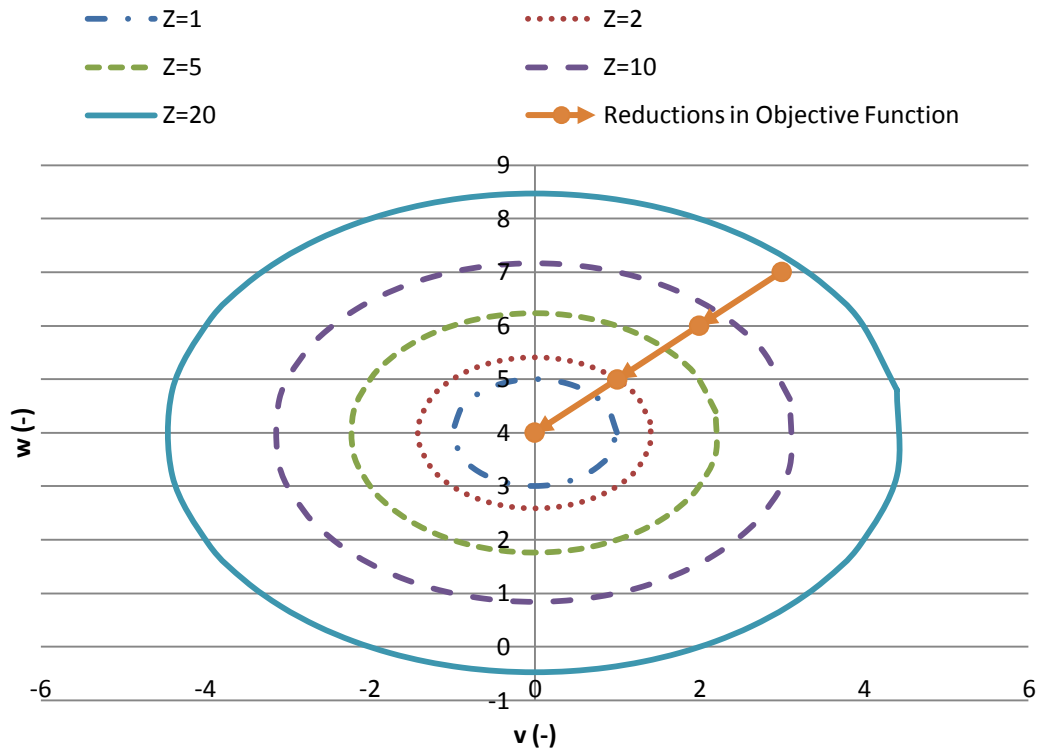


Figure 5-1: Search Path of Sample Optimization

5.3.3 Optimization Parameters

Table 5-3 defines the algorithm parameters as used in the optimization study of the proposed ice slurry system (Wetter and Wright, 2004).

Table 5-3: Algorithm Parameters for Ice Slurry Study

Parameter	Value
Mesh Size Divider (r)	2
Initial Mesh Exponent (y_1)	0
Mesh Exponent Increment (c)	1
Minimum Mesh Size Factor (Δ_{\min})	0.0625
Maximum Iterations (k_{\max})	100

The initial values and step sizes for each optimization variable are provided in Table 5-4.

Table 5-4: Initial Values of Optimization Variables

Parameter	Initial	Step Size, s
A_{col} (m ²)	35.67	10
β (°)	45	5
$\dot{m}_{\text{col},s}$ (kg/h·m ²)	50	10
V_{ice} (m ³)	16.3	4
V_{WWST} (m ³)	0.9	0.2
T_{set} (°C)	30	5

5.4 Optimization using GenOPT and TRNSYS

The GenOPT computer program (Wetter, 2009) is a generic optimization tool which can be linked with TRNSYS to search for the optimum set of building design variables that minimize a defined objective function.

Each TRNSYS simulation is based on the information provided in a text based input file (.dck file). This file contains the numerical values of the design parameters and defines the interrelationship between various components in the system. Depending on the complexity of

the simulation model, the input file may also point to additional external files providing information such as the geometry of a storage tank or the performance of a heat pump.

GenOPT makes use of this text based simulation approach to link with TRNSYS. Before the optimization process begins, the user provides GenOPT with templates of any files containing the numerical value of a design variable (e.g the .dck file and an external file defining tank performance). These templates are edited such that the numerical value of the design variable is replaced by a symbolic representation, allowing GenOPT to quickly identify the location of all variables to be optimized. The template files provide GenOPT with a base representation of the system which is subsequently used to explore the solution space.

At the start of each simulation:

1. GenOPT replaces the symbolic variable representation in the template files with numerical values corresponding to a selected search point. These files are then provided as inputs to TRNSYS.
2. TRNSYS uses the input files provided by GenOPT to run a simulation.

At the end of each simulation:

1. TRNSYS calculates and saves the value of the objective function in an external file.
2. GenOPT reads the value of the objective function. The program then decides what further action is required based on the value of the objective function and the optimization algorithm being employed.

A visual depiction of the relationship between GenOPT and TRNSYS is provided in Figure 5-2.

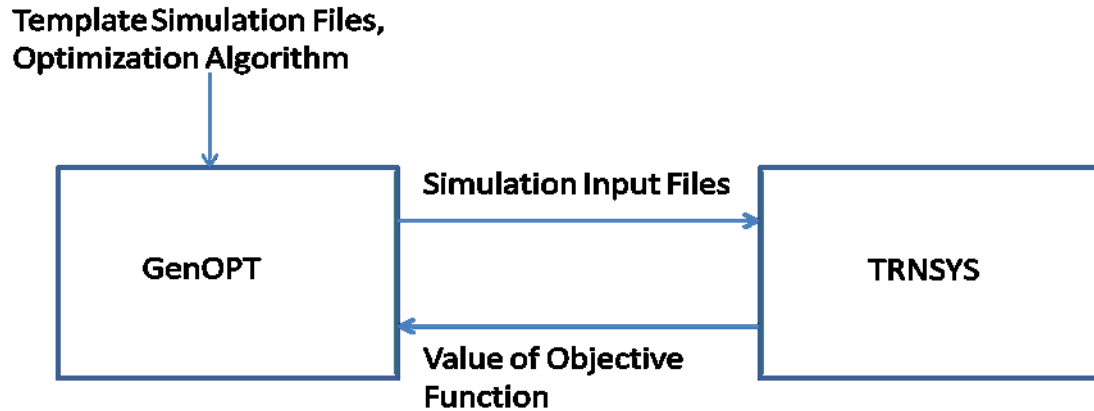


Figure 5-2: Information Exchange between GenOPT and TRNSYS

5.5 Optimization Results

TRNSYS and GenOPT are linked to perform a series of optimizations on a solar assisted heat pump operating using ice slurry. Optimizations are first performed to examine the impact of different control strategies. A sensitivity analysis is then presented to determine an acceptable operating range for each optimization variable.

5.5.1 Comparison of Optimization Results using Different Control Strategies

Optimizations are performed using two different solar loop control strategies:

1. Strategy #1. This proposed control strategy (Chapter 4) is based on monitoring the potential collector outlet temperature during Loop B operations. All variable constraints and initial conditions are as outlined in Table 5-1 and Table 5-4.
2. Strategy #2. This control strategy is based on the work of Trinkl et al. (2009) as presented in Chapter 2 of this thesis. The value of T_{set} is examined between a range $0^{\circ}\text{C} \leq T_{set} \leq 15^{\circ}\text{C}$, with an initial starting point of 10°C and step size s of 2.5°C . All other variable constraints and initial conditions are as outlined in Table 5-1 and Table 5-4.

Optimizations are performed with the objective of minimizing the heating operating energy use over a heating season from Oct. 1st to May 15th. Each simulation is performed including a 30 day pre-simulation period to reduce the effects of initial estimates of the ice mass and fluid temperatures in the storage tanks. All simulations are performed using an Intel Core™2 6300 processor at 1.86 GHz and 1.00 GB of RAM, with each TRNSYS simulation taking approximately 1.25 h.

Table 5-5 contains a comparison of the optimization results for the two control strategies.

Table 5-5: Optimization Results for Two Control Strategies

	Control Strategy	
	#1	#2
Total Optimization Time (h)	125	107.5
Minimum Heating Operating Energy Use (kW·h)	1495	2807
<i>Optimization Variables</i>		
A_{col} (m ²)	65.67	65.67
β (°)	67.5	60
$\dot{m}_{col,s}$ (kg/h·m ²)	20	25
V_{ice} (m ³)	32.05	32.3
V_{WWST} (m ³)	1.5	1.5
T_{set} (°C)	29.375	5

The optimization process produces a similar set of design variables for each control strategy. The minimum heating operating energy use occurs near the upper bounds of the solar collector area, ice tank volume, and WWST volume, when thermal gains and storage capacities are highest. Both optimization runs highlight the need to have the solar collectors in a more vertical orientation to maximize the capture of solar radiation during the winter months. The optimal

values for the specific collector flow rate are near the lower limit suggested by the collector manufacturer, resulting in the solar collectors producing higher outlet fluid temperatures.

Although the design solution is similar for both control strategies, the heating operating energy use is significantly lower when using Strategy #1. This result suggests that, in the case of the proposed system layout and climate, using a control strategy based on the solar collector outlet temperature represents a more effective approach in reducing the auxiliary energy use. Strategy #1 will thus be used for all further analysis.

Since the control strategy may play an important role, a sensitivity analysis is performed to determine the impact of modifying the solar loop control temperature T_{set} on the heating operating energy use. T_{set} is varied from 10°C to 40°C, with all remaining design variables held constant as defined in Table 5-5. The heating operating energy over the heating season for different values of T_{set} is shown in Figure 5-3.

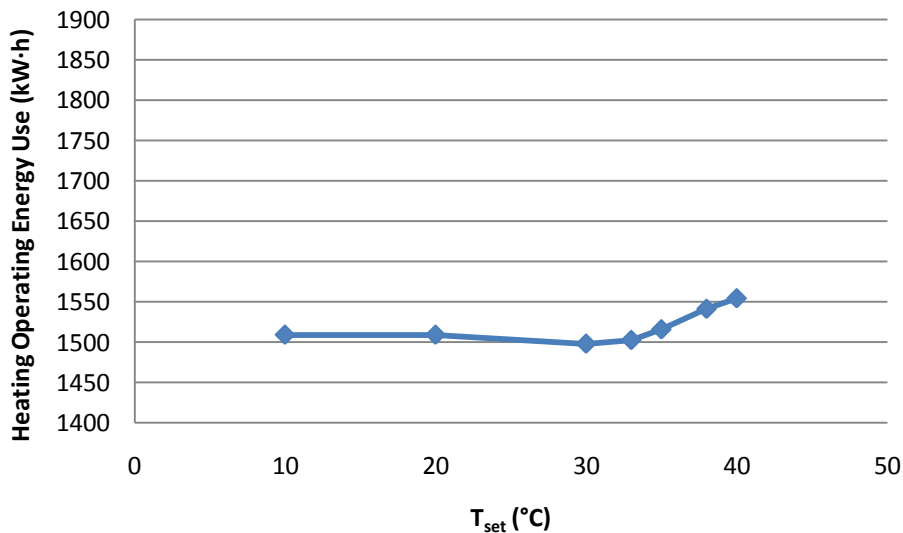


Figure 5-3: Impact of T_{set} on Heating Operating Energy Use

Varying T_{set} over the complete operating range results in a maximum 3.8% change in the objective function (when all other variables remain at their optimal values). As such, the control

strategy can be simplified by removing the dependence on T_{set} . This simplification reduces the number of optimization variables, thus resulting in fewer required simulations to reach the optimal point.

Using the new control sequence, Loop A is allowed to operate when one of the following conditions is met:

1. $T_{fluid} < 13^{\circ}\text{C}$, $T_{WWST} < 60^{\circ}\text{C}$, $\Delta T_{col, LoopA} > 3^{\circ}\text{C}$, $m_{ice} > 0.9m_{ice,max}$ or
2. $T_{fluid} < 13^{\circ}\text{C}$, $T_{WWST} \geq 60^{\circ}\text{C}$, $\Delta T_{col, LoopA} > 3^{\circ}\text{C}$

Loop B is then allowed to operate when:

1. $T_{WWST} < 60^{\circ}\text{C}$, $\Delta T_{col, LoopB} > 3^{\circ}\text{C}$, $m_{ice} \leq 0.9m_{ice,max}$

A third optimization is performed to examine the energy performance of the ice slurry system with the new control strategy, with the results summarized in Table 5-6. All variable constraints and initial conditions remain the same as previously defined in Table 5-1 and Table 5-4.

Table 5-6: Optimization Results for Modified Control Strategy

Parameter	Value
Total Optimization Time (h)	102.5
Minimum Heating Operating Energy Use (kW·h)	1504
<i>Optimization Variables</i>	
A_{col} (m ²)	65.67
β (°)	65.625
$\dot{m}_{col,s}$ (kg/h·m ²)	20.625
V_{ice} (m ³)	32.05
V_{WWST} (m ³)	1.50

The optimized results for the new control strategy compare well with previous results for Strategy #1 shown in Table 5-5. The new control strategy is able to obtain similar reductions in

the objective function while reducing the total optimization time by 22.5 hours. The results of this third optimization will form the basis for all further analysis in this thesis.

5.5.2 Sensitivity Analysis

A sensitivity analysis is performed with two objectives:

1. Convert the optimized results for A_{col} and V_{WWST} to discrete values by examining the heating operating energy use at available equipment sizes.
2. Determine possible operating ranges for continuous design variables β , $\dot{m}_{col,s}$, and V_{ice} .

The sensitivity analysis is performed by examining each optimization variable separately. During each analysis all other design variables are held constant at the optimized values summarized in Table 5-6.

Solar Collector Area

The solar collector area is a discrete variable: The total area must be a multiple of the collector area for a single panel. To convert the continuous value for A_{col} in Table 5-6 to a discrete value, the heating operating energy use is calculated using 8, 9, 10 and 11 parallel collector arrays (Each array consists of three panels in series, with a total area of 5.97 m²). The impact of the solar collector area on the heating operating energy use is shown in Figure 5-4.

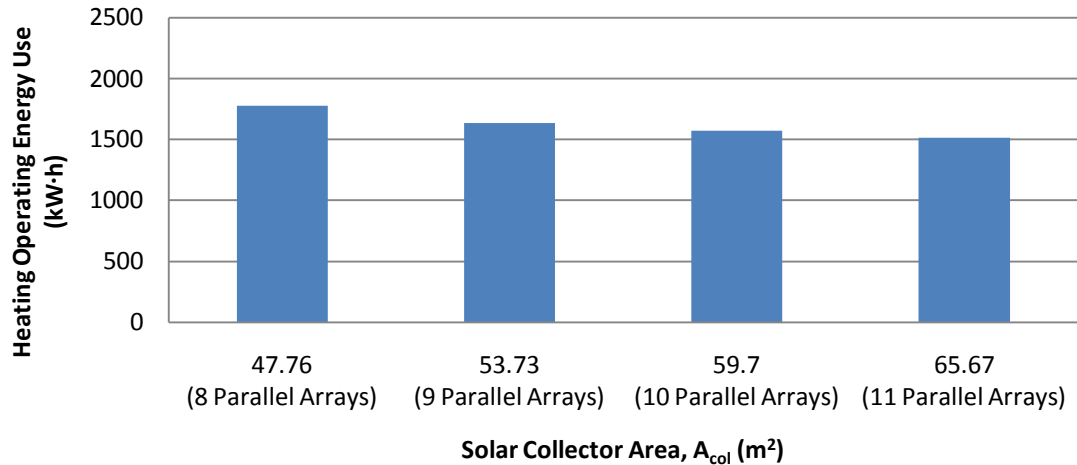


Figure 5-4: Impact of A_{col} on Heating Operating Energy Use

Reducing the solar collector area from 11 parallel arrays (the determined optimal) to 10 parallel arrays results in a 3.8% increase in the heating operating energy use of the system. Smaller collector areas reduce the amount of thermal energy supplied to the system, leading to increased use of the heat pump and auxiliary heaters. A collector area of 65.67 m² (11 parallel arrays) will be used for further study as this corresponds to the lowest value for the heating operating energy use.

Warm Water Tank Volume

The warm water tank volume is a discrete variable: The storage tank volume must match a tank size available in the marketplace. V_{WWST} is converted to a discrete value by examining the heating operating energy use at tank volumes of 0.75 m³, 1.00 m³, 1.28 m³, and 1.50 m³ ((Jenni Energietechnik AG, 2011), (SUNSYSTEM, 2011)). The impact of varying the WWST volume is shown in Figure 5-5.

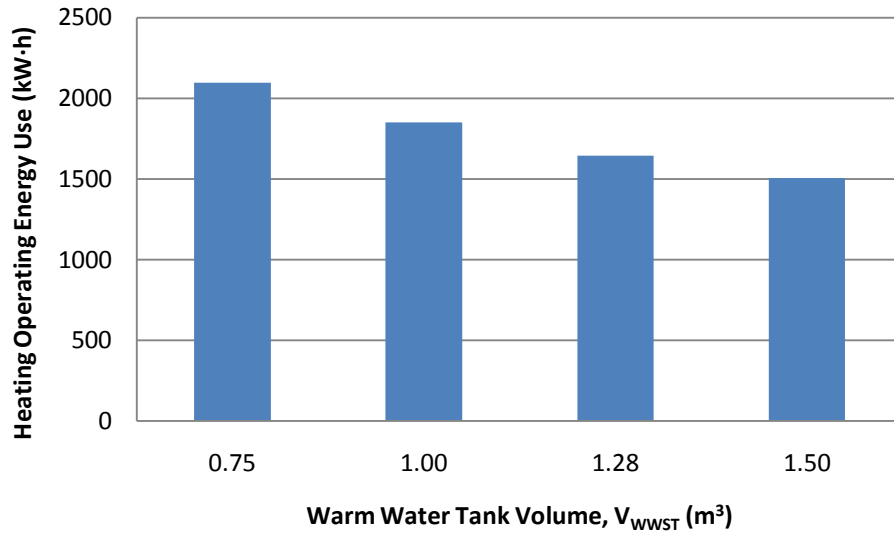


Figure 5-5: Impact of V_{WWST} on Heating Operating Energy Use

Decreasing the tank volume from 1.50 m³ (the determined optimal) to the next available tank size of 1.28 m³ results in a 9.3% increase in the heating operating energy use. Reducing the volume of the WWST limits the amount of fluid available at the required temperature for heating and DHW. Smaller tank volumes also limit the amount of time that the system can operate in the Loop B configuration before the maximum storage temperature of 60°C is reached. The solar collectors therefore provide less thermal energy to the WWST, resulting in increased use of the heat pump and auxiliary heaters. A tank volume of 1.50 m³ will be used for all further analysis due to the significant increase in the heating operating energy use at the next available tank size.

Solar Collector Tilt Angle

The solar collector tilt angle is a continuous variable, with the designer defining this parameter during the installation of the collector array. The impact of the tilt angle is examined by varying β in the manufacturer suggested region of 35° to 90° (SumMaxx Solar, 2011). The resulting impact on the operating energy is shown in Figure 5-6.

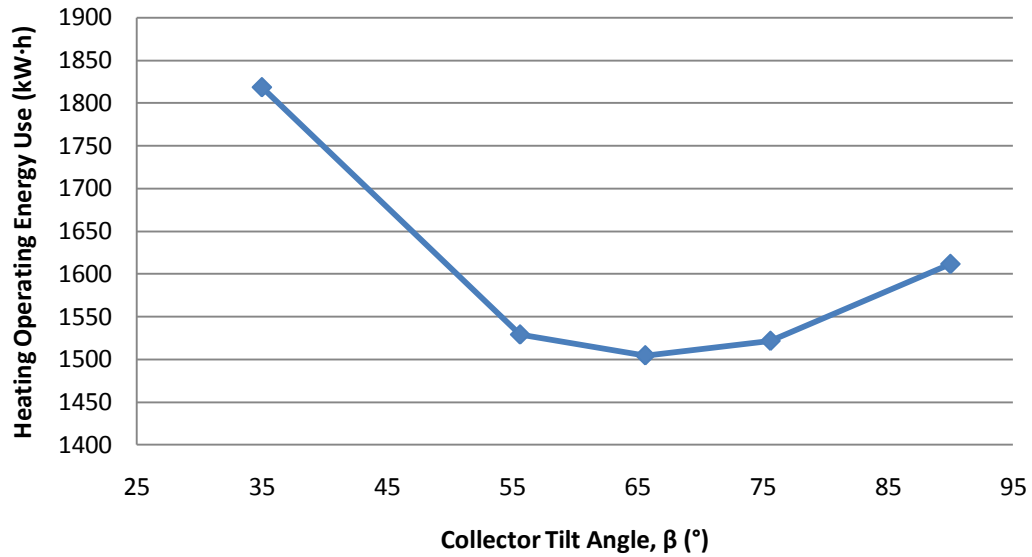


Figure 5-6: Impact of β on Heating Operating Energy Use

Varying the collector tilt angle from its optimal value (65.625°) reduces the thermal gains obtained from the solar collectors, resulting in an increase in the heating operating energy use of the home. The heating operating energy use remains within 5% of the optimal provided that the tilt angle remains in the range $52^\circ \leq \beta \leq 85^\circ$.

Specific Collector Flow Rate

The specific collector flow rate is a continuous parameter selected by the designer. The value of $\dot{m}_{col,s}$ is varied in the manufacturer suggested operating range of $20 \text{ kg/h}\cdot\text{m}^2$ to $70 \text{ kg/h}\cdot\text{m}^2$ (SunMaxx Solar, 2011) in order to determine the effect on the heating operating energy use. Results are shown in Figure 5-7.

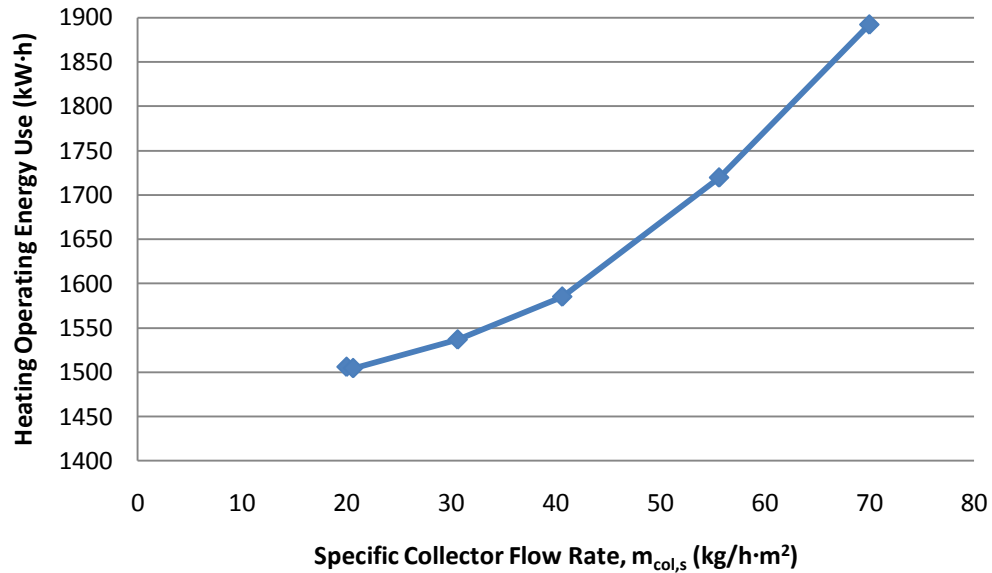


Figure 5-7: Impact of $\dot{m}_{col,s}$ on Heating Operating Energy Use

An increase in the specific collector flow rate coincides with a rise in the heating operating energy use of the home. Higher flow rates result in lower collector outlet temperatures, thus requiring additional use of the heat pump and auxiliary heaters. The heating operating energy use can be maintained within 5% of the optimal provided that the designer selects a specific flow rate within the range $20 \text{ kg/h}\cdot\text{m}^2 \leq \dot{m}_{col,s} \leq 40 \text{ kg/h}\cdot\text{m}^2$.

Ice Tank Volume

Due to the potentially large volume of the ice tank, it is assumed that the tank is built on-site. As such, V_{ice} is treated as a continuous variable, with the tank built to match the volume required. The impact of varying the ice tank volume is examined by reducing V_{ice} by 10%, 20%, 30% and 50%, with the maximum allowable tank volume ($V_{ice}=32.3 \text{ m}^3$) also tested. The resulting impact on the heating operating energy use is shown in Figure 5-8.

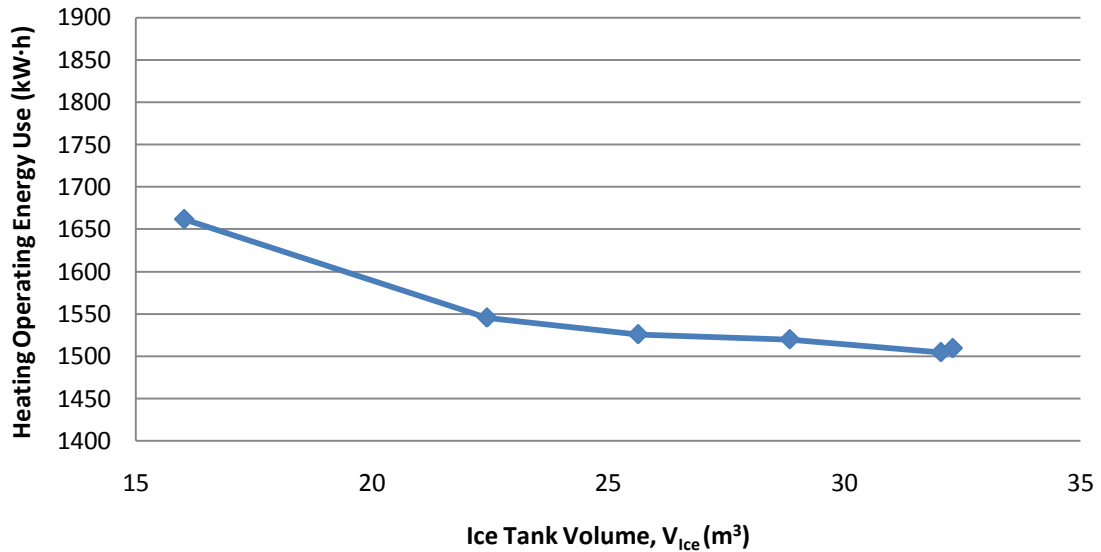


Figure 5-8: Impact of V_{ice} on Heating Operating Energy Use

Varying the ice tank volume has a minimal impact on system performance. Although a reduction in V_{ice} results in a smaller thermal storage capacity, the heating operating energy use remains within 10.4% of the optimal point throughout the range of tank volumes examined. Furthermore, the operating energy use remains within 5% of the optimal provided that the designer selects a tank volume in the range $20.5\text{ m}^3 \leq V_{ice} \leq 32.2\text{ m}^3$.

Conclusions of Sensitivity Analysis

The system is most sensitive to reductions in the WWST volume. Examining system performance at the next smallest available tank size showed that the heating operating energy use increased by 9.3%. Reducing this tank volume decreases the amount of hot water immediately available for heating and DHW purposes, while also limiting the amount of time that the solar collectors can operate in the Loop B configuration. The highly sensitive nature of this design variable means that the system designer should take care to ensure that a sufficiently large tank volume is used.

System performance is moderately sensitive to variables defining the solar collectors. Reducing the amount of parallel collector arrays from 11 to 10 resulted in a 3.8% increase in the heating operating energy use. An examination of the solar collector specific flow rate and tilt angle showed that the heating operating energy use of the system remained within 5% of the optimal for a significant portion of the manufacturer specified operating ranges. It can be concluded that, although solar collectors are an important provider of thermal energy to the system, the designer has a degree of flexibility in selecting the collector area and operating conditions.

System performance is relatively insensitive to changes in the ice tank volume. Reducing the tank size by a factor of 2 resulted in a 10.4% increase in the heating operating energy use. The heating operating energy use also remained within 5% of the optimal for a significant range of the tank volumes examined. The relatively insensitive nature of this design variable suggests that the ice tank does not act as the primary thermal source or storage reservoir in the system.

Based on the results of the sensitivity analysis, a set of design variables is selected for further analysis as summarized in Table 5-7.

Table 5-7: Design Variables for Further Analysis

Parameter	Value
A_{col} (m ²)	65.67
β (°)	65.625
$\dot{m}_{col,s}$ (kg/h·m ²)	20.625
V_{ice} (m ³)	32.05
V_{WWST} (m ³)	1.5

5.6 Summary

Optimizations have been performed on the proposed ice slurry system with the objective of minimizing the heating operating energy use over a single heating season. A comparison of the optimized results for two different control strategies showed that using the collector outlet temperature as a control parameter yielded a significant reduction in the heating operating energy use. This control strategy was further simplified based on the results of a sensitivity analysis. A final optimization was then performed using the new control strategy to determine a set of design variables which are used for further analysis in Chapter 6.

6. Simulated Performance of a Solar Assisted Heat Pump Using Ice Slurry

This chapter presents the TRNSYS simulation results for the proposed solar assisted heat pump using ice slurry. Performance is provided for a heating season from Oct. 1st to May 15th, as designed for the optimum variables (A_{col} , β , $\dot{m}_{col,s}$, V_{ice} , V_{WWST}) shown in Chapter 5 of this thesis. The viability of the ice slurry system is first examined through a comparison of three different heating methods. The ice slurry system is then discussed in detail, including an examination of performance on a seasonal, monthly, and daily level.

6.1 System Comparison

One of the main objectives of the proposed study is to examine the potential of using a solar assisted heat pump with ice slurry to heat a home in Montreal, QC. As such, the heating operating energy use (the electrical energy input directed towards meeting the heating and DHW loads) is compared for three different systems over a heating season from Oct. 1st to May 15th.

Case 1: A home using electrical resistance elements for heating and DHW preparation.

Case 2: A solar assisted heat pump in which the ice tank has been replaced by a sensible storage tank of the same volume.

Case 3: A solar assisted heat pump using ice slurry as defined in Chapters 4 and 5.

Each system is integrated into the house model of Hugo (2008) described in Chapter 4 of this study. A comparison of the resulting heating operating energy use is shown in Figure 6-1.

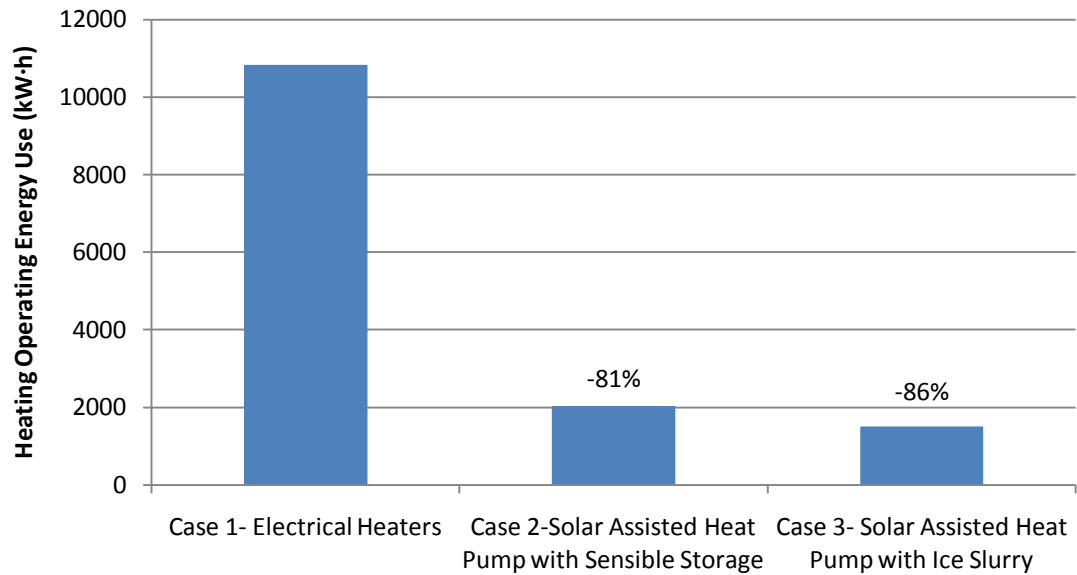


Figure 6-1: Comparison of Heating Operating Energy Use over Heating Season

Using a solar assisted heat pump with sensible storage results in a 81% reduction in the heating operating energy use in comparison to a home with electrical resistance elements (2033 kW·h vs. 10836 kW·h). Replacing the sensible storage tank with an ice slurry tank results in an additional 26% reduction in the heating operating energy use of the heat pump system (1504 kW·h vs. 2033 kW·h), and an additional 5% reduction relative to the electrical heating system (1504 kW·h vs. 10836 kW·h).

A comparison of the three systems demonstrates that solar assisted heat pumps can obtain significant reductions in the heating operating energy use of the home. In particular, the integration of ice storage with the heat pump system offers the home owner the greatest potential energy savings due to an increase in the thermal storage capacity.

6.2 Ice Slurry System Performance

The use of a solar assisted heat pump with ice slurry has been shown to significantly reduce the heating operating energy use of a high performance home in Montreal, QC. This section presents a detailed analysis of the ice slurry system and its components.

6.2.1 General Performance

The total electricity use (the electricity input to all system components in the home) over a heating season from Oct. 1st to May 15th is calculated in TRNSYS to be 3797 kW·h, or 20.4 kW·h/m² of heated floor area.

Table 6-1 shows the monthly distribution of electricity use over the heating season. Heating and DHW is defined to be the sum of the electricity input to the auxiliary heaters, heat pump, and circulation pumps. Ventilation represents the fan electricity use only.

Electricity use is highest in the months of December and January due to increased thermal loads, lower incident solar radiation, and higher demands on the humidification system. The energy consumption of the ventilation system remains relatively stable, as the speed of the fan varies marginally with the outdoor air temperature.

Table 6-1: Distribution of Electricity by End Use

Month	Electricity Use (kW·h)			
	Heating and DHW	Ventilation	Humidity Control	Lighting
October	35	82	4	124
November	225	79	52	141
December	421	82	180	144
January	461	83	228	133
February	194	75	191	108
March	123	82	128	102
April	43	79	38	88
May	2	37	1	34
Total	1504	598	821	874

Figure 6-2 shows the distribution of electricity use over the heating season. Home heating and DHW represents the single largest end use at 39%, followed by lighting (23%), humidity control (22%) and ventilation (16%).

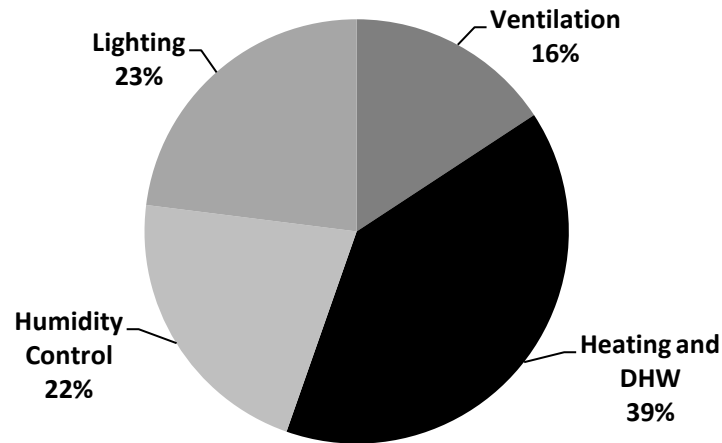


Figure 6-2: Distribution of Electricity Use over Heating Season

In addition to examining the distribution of electrical energy usage, it is also important to understand how thermal energy is supplied to the system. Table 6-2 shows the monthly contribution of thermal energy by source component. The net gain is defined to be the difference between the thermal supply and the loads imposed on the system.

Thermal energy supply is highest in December, January and February when heating and DHW loads are at their peak. Solar collectors are the largest contributors of thermal energy, with Loop B accounting for the majority of this supply. The heat pump provides a secondary source of thermal energy, operating primarily from November to February when Loop B collector operations alone are unable to maintain the fluid at top of the WWST above the minimum setpoint temperature of 35°C. The contribution of the three auxiliary heaters is minimal: The radiant floor and ventilation heaters represent less than 0.1% of the total thermal input, while

the DHW heater is used predominately in the middle of the heating season to ensure that water is supplied at the desired setpoint temperature of 45°C.

All months except December experience an overall gain in thermal energy. The extraction of thermal energy in December is due to a combination of higher heating loads and the reduced intensity and duration of solar radiation on the collectors.

It should be noted that the sum of the thermal energy input by the heat pump and auxiliary heaters (1384 kW·h) is less than the overall electricity input for heating and DHW purposes (1504 kW·h). This is because the overall value also includes the electricity inputs for the circulation pumps.

Table 6-2: Monthly Thermal Energy Input

Month	Thermal Energy Input (kW·h)							
	Solar Collectors- Loop A	Solar Collectors- Loop B	Heat Pump	Auxiliary Heater- Radiant Floor	Auxiliary Heater- DHW	Auxiliary Heater- Ventilation	Heating and DHW Load	Net (% of Supply)
October	70	692	15	0	12	0	760	29(4)
November	651	605	158	1	49	0	1455	9(1)
December	633	877	297	2	98	0	2435	-528(-28)
January	1527	1203	371	2	62	0	2669	495(16)
February	760	1369	134	1	41	0	2141	164(7)
March	265	1340	65	1	43	0	1712	2(0)
April	99	884	21	0	12	0	975	41(4)
May	0	250	0	0	0	0	219	31(12)
Total	4004	7221	1060	7	317	0	12367	242(2)

System Solar Fraction

The solar fraction is an important measure of system performance, defining the percentage of the heating and DHW load met using solar energy. The solar fraction of the system is calculated to be:

$$F_{solar} = 1 - \frac{(E_{i,aux} + E_{i,Pump} + E_{i,HP})}{\int_{Heating\ Season} (Q_{load}) dt} = 0.88 \quad (6-1)$$

where:

F_{solar} is the solar fraction (-)

$E_{i,aux}$ is the energy input to the auxiliary heaters (kW·h)

$E_{i,pump}$ the energy input to the circulation pumps (kW·h)

$E_{i,HP}$ is the energy input to the heat pump (kW·h)

Q_{load} is the combined heating and DHW load of the home (kW)

System Coefficient of Performance

The coefficient of performance (COP_{sys}) relates the thermal energy obtained from the system to the electrical energy required to operate the system. COP_{sys} is calculated to be:

$$COP_{sys} = \frac{\int_{Heating\ Season} (Q_{load}) dt}{(E_{i,aux} + E_{i,Pump} + E_{i,HP})} = 8.22 \quad (6-2)$$

where:

COP_{sys} is the system coefficient of performance (-)

6.2.2 Component Performance

To develop a full understanding of system operations it is important to examine the individual performance of key components. This section examines four main pieces of equipment:

1. Ice Tank
2. Warm Water Storage Tank (WWST)
3. Heat Pump
4. Solar Collectors

Ice Tank

Figure 6-3 shows the change in ice mass in the tank over the heating season. The ice inventory in the tank remains near zero until the start of January, when increased use of the heat pump and reduced use of the Loop A collector configuration leads to an overall extraction of energy. A peak ice mass of 7090 kg is achieved on January 19th, with this corresponding to 57% of the maximum ice storage capacity of the tank ($m_{ice,max}=12369$ kg). Towards the end of January, increased gains from the Loop A mode outweigh the thermal demands of the heat pump. As a consequence the ice mass declines rapidly.

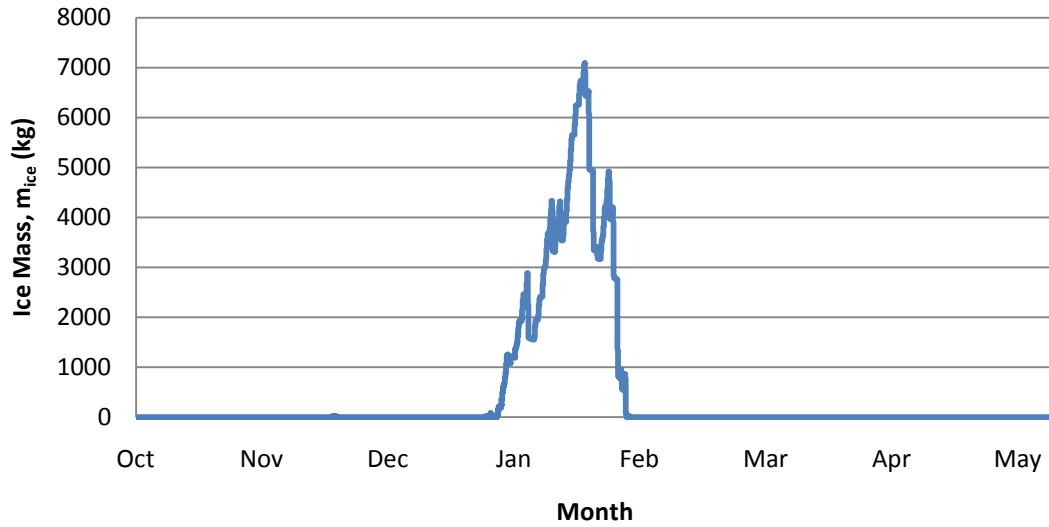


Figure 6-3: Ice Inventory in Ice Tank over Heating Season

Figure 6-4 shows the fluid temperatures in the ice tank over the heating season. Fluid temperatures remain near their maximum acceptable value of 13°C at the start and end of the heating season when thermal gains from the collectors outweigh the energy extracted by the heat pump. The fluid temperature in the tank decreases rapidly in mid-November and late December when higher heating and DHW loads result in a significant extraction of thermal energy via the heat pump. Tank temperatures remain near 0°C in January when ice is stored in the tank.

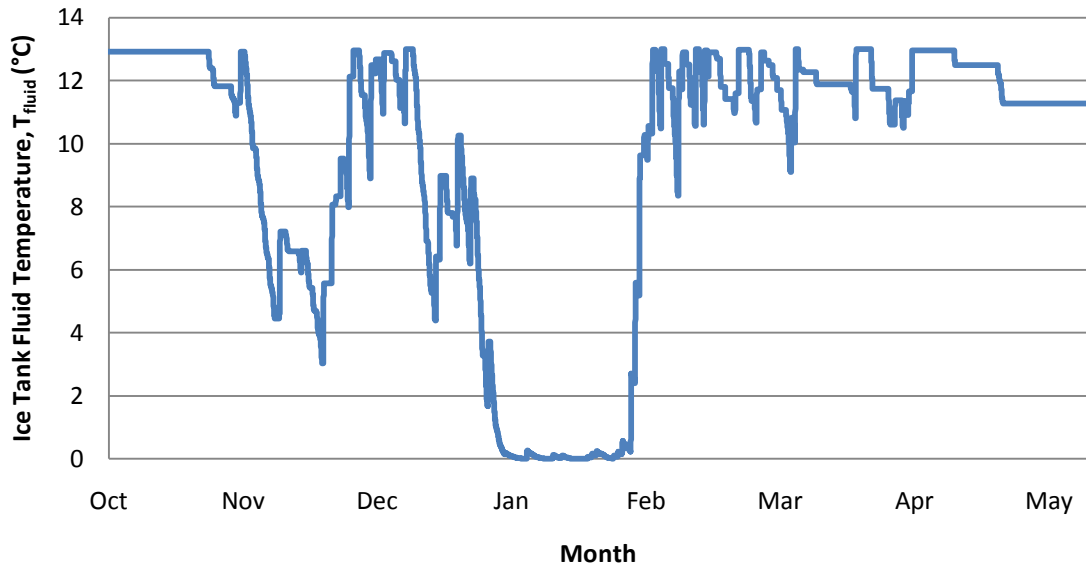


Figure 6-4: Fluid Temperature in Ice Tank over Heating Season

It can be concluded that the ice tank is sized appropriately and operates as anticipated. The latent capacity of the tank is used during the middle of the heating season when thermal demands on the system are at their peak. Although a significant amount of ice is built up, the ice mass does not approach the maximum ice storage capacity of the tank. This means that the heat pump is always able to extract thermal energy from the tank when required, while also allowing the control strategy to give priority to the Loop B collector configuration since $m_{ice} < 0.9 \cdot m_{ice,max}$.

Ice tank fluid temperatures also confirm the proper operation of the system. The performance of the solar collectors is highly dependent on the entering fluid temperature: Lower collector inlet temperatures result in reduced collector losses to the ambient, thus improving the solar collector efficiency. The colder fluid temperatures in November, December, and January maximize the performance of Solar Loop A at a time when incident radiation and ambient air temperatures are lowest. The higher fluid temperatures at the start and end of the heating season result in more desirable operating conditions for the heat pump, while having a minimal

impact on the total Loop A collector gains due to the increased intensity and duration of available solar radiation during these months.

Warm Water Storage Tank

Figure 6-5 shows the average fluid temperatures in the WWST over the heating season. Node 1 corresponds to the top of the tank, while Node 4 refers to the bottom of the tank. The overall temperature is calculated based on an average of each fluid layer in the tank.

The WWST experiences a significant degree of temperature stratification, with an average temperature difference over the heating season of 10.8°C between the Node 1 and Node 4 fluid layers. Fluid temperatures in the WWST are lowest in November and December, when the reduced intensity of incident solar radiation limits the temperature of fluid supplied to the tank by the Loop B collector configuration. Tank temperatures rise towards the start and end of the heating season as the intensity and duration of solar radiation increases.

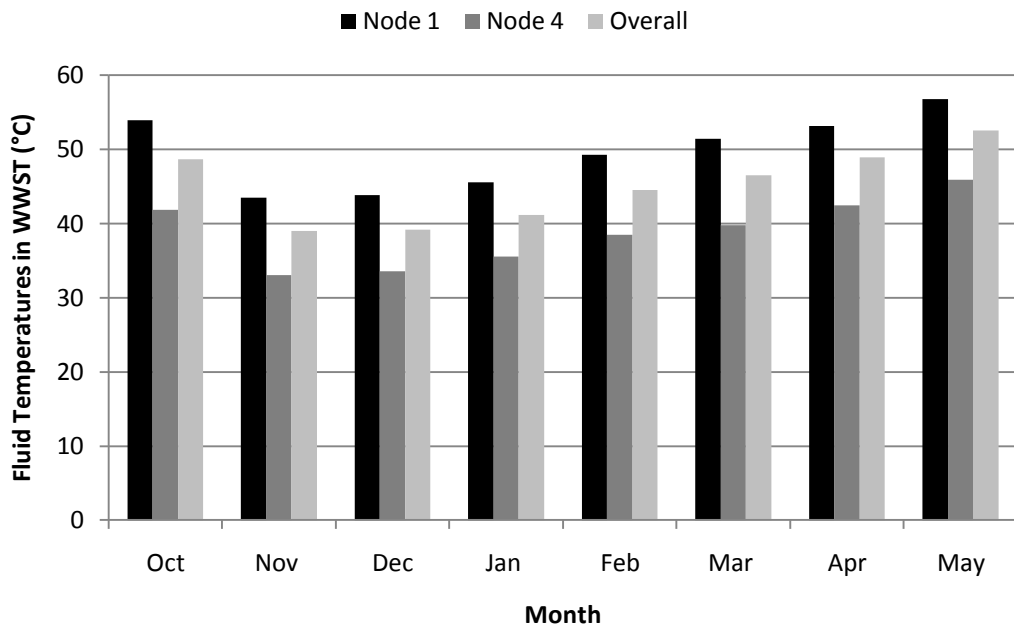


Figure 6-5: Average Fluid Temperatures in WWST over Heating Season

Table 6-3 summarizes the monthly addition and extraction of thermal energy for the WWST. The net gain is defined as the difference between thermal supply (from the heat pump and solar collectors) and thermal demand (from the radiant floor, DHW, and ventilation loads). Solar collectors are the primary contributors of thermal energy at the start and end of the heating season, while the heat pump is used predominately from November to February when Loop B operations alone are unable to maintain the fluid temperature at the top of the WWST above 35°C. The radiant floor is the primary thermal load on the tank, followed by the DHW and ventilation loops. Thermal supply is balanced each month by heating and DHW demands, with a maximum discrepancy of 3.03% of the total monthly supply.

Table 6-3: Energy Inputs/Extractions to WWST over Heating Season

Month	Total Energy Input (kW·h)					Net (% of Supply)
	Heat Pump	Solar Collectors	Radiant Floor Load	DHW Load	Ventilation Load	
October	87	654	201	422	125	-7(-0.89)
November	831	573	883	291	230	0(0.01)
December	1485	831	1541	429	365	-20(-0.86)
January	1511	1121	1744	445	417	26(1.00)
February	795	1298	1322	418	359	-6(-.27)
March	392	1283	891	482	295	6(0.39)
April	128	831	375	409	180	-4(-0.39)
May	0	226	18	153	49	7(3.03)
Total	5229	6817	6975	3048	2020	4(0.03)

An examination of the tank fluid temperatures confirms the ability of the solar collectors and heat pump to maintain the top of the WWST above 35°C throughout the heating season. The balance between thermal supply and demand suggests that the tank primarily operates as a heat distribution point rather than a long term thermal storage device.

Heat Pump

Table 6-4 summarizes the performance of the heat pump over the heating season. Energy inputs are highest in December and January when the heat pump operates frequently to maintain the top of the WWST above 35°C. COP values increases towards the start and end of the heating season, when higher fluid temperatures in the ice tank result in a smaller temperature rise across the heat pump.

Table 6-4: Summary of Heat Pump Performance

Month	Energy Input (kW·h)	Energy to Load (kW·h)	COP
October	15	88	6.0
November	158	835	5.3
December	297	1491	5.0
January	371	1518	4.1
February	134	798	6.0
March	65	394	6.1
April	21	129	6.1
May	0	0	/
Total	1060	5251	5.0

Solar Collectors

Table 6-5 summarizes the solar collector performance in both operating modes. Total collector operations peak during the middle of the heating season when thermal demands are highest. In general, Loop B accounts for the majority of the thermal energy supply owing to the increased duration of time that the system operates in this configuration. However, the lower inlet collector temperatures in the Loop A mode result in this configuration yielding a significantly higher collector heat gain per hour of operations. This is particularly evident in November and January, when Loop A provides the majority of the collector heat gains while operating for a significantly shorter period of time.

Table 6-5: Summary of Solar Loop Performance

Month	Operational Period (h)		Collector Heat Gains (kW·h)	
	Loop A	Loop B	Loop A	Loop B
October	2.1	53.3	70	692
November	24.5	47.8	651	605
December	21	64.2	633	877
January	45	82.6	1527	1203
February	23.5	95.8	760	1369
March	8.2	90.8	265	1340
April	4.1	75.4	99	884
May	0	25.2	0	250
Total	128.4	535.1	4004	7221

The solar collector efficiency is an important measure of component performance. The collector efficiency over a time period t is calculated using the equation (Duffie and Beckman, 2006):

$$\eta_{col} = \frac{\int_0^t Q_{gain,col} dt}{A_{col} \int_0^t G_T dt} \quad (6-3)$$

where:

η_{col} is the solar collector efficiency (-)

$Q_{gain,col}$ is the useful heat gain from the solar collectors (W)

A_{col} is the solar collector area (m²)

G_T is the incident radiation on the collector surface (W/m²)

Figure 6-6 presents the calculated solar collector efficiency for each month of the heating season. The overall collector efficiency is calculated based on a time-weighted average of the Loop A and Loop B efficiencies:

$$\eta_{overall} = \frac{\eta_{LoopA}t_{LoopA} + \eta_{LoopB}t_{LoopB}}{t_{LoopA} + t_{LoopB}} \quad (6-4)$$

where:

$\eta_{overall}$ is the overall solar collector efficiency (-)

η_{LoopA} is the Loop A solar collector efficiency (-)

η_{LoopB} is the Loop B solar collector efficiency (-)

t_{LoopA} is the duration of time that the system operates in the Loop A configuration (h)

t_{LoopB} is the duration of time that the system operates in the Loop B configuration (h)

Solar collector efficiencies are highest from November to January due to a smaller temperature difference between the inlet collector fluid and the ambient air. The collector efficiency for both loops decreases towards the end of the heating season as fluid temperatures in the ice tank and WWST rise. Ice storage has a significant impact on the system, with Loop A achieving a consistently higher collector efficiency due to the lower fluid temperatures available. The overall seasonal collector efficiency is calculated to be 0.43, representing a significant improvement over Hugo (2008) who calculated an annual flat plate collector efficiency of 0.21 operating in a typical solar combi-system without a heat pump or ice storage tank.

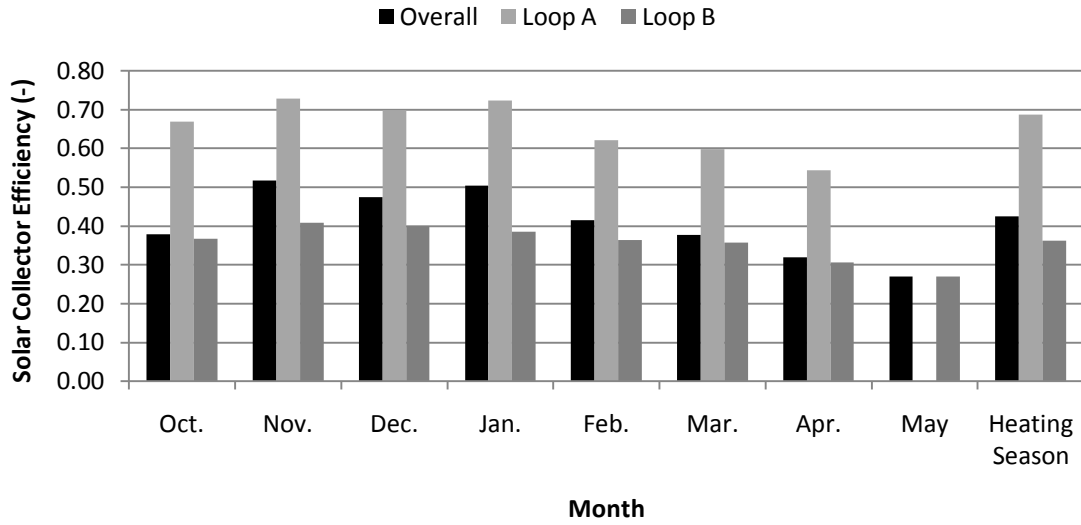


Figure 6-6: Monthly Solar Collector Efficiencies over Heating Season

Figure 6-7 shows the average outlet fluid temperature from the solar collectors for each month of the heating season. Outlet temperatures are lowest from November to January due to the reduced intensity and duration of incident solar radiation.

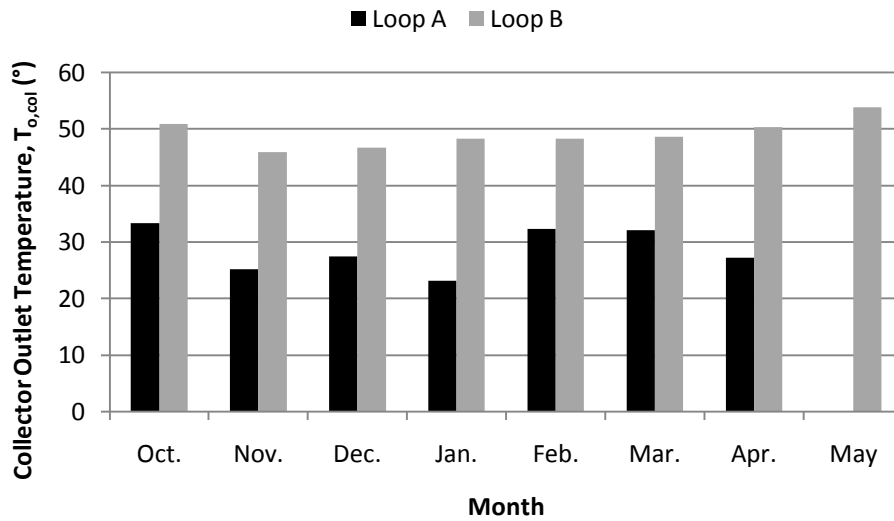


Figure 6-7: Average Monthly Solar Collector Outlet Temperatures over Heating Season

An analysis of solar collector performance highlights the benefits of using the ice slurry system. Ice storage allows for consistently high collector efficiencies in the Loop A mode. While the outlet collector temperature is lower in this configuration, the increased efficiency allows Loop A to achieve greater thermal gains per hour of utilization.

The operational period for each solar loop suggests that the control strategy is implemented properly. As expected, the system operates primarily in the Loop B configuration, producing a high temperature fluid at the collector outlet which can be used directly for heating and DHW purposes. Loop A is used predominately from November to February when Loop B operations alone are unable to satisfy the thermal demands placed on the system.

6.2.3 Daily System Performance

System performance is presented on a daily scale to further examine the implementation of the control strategy. Two study periods are selected:

1. October 25th (Start of heating season)
2. January 5th (Middle of heating season)

Study Period 1: October 25th

Figure 6-8 shows the Control Signal (CS) to the Loop A pump, Loop B pump, and heat pump. A control signal of 0 corresponds to the pump being off, while a control signal of 1 indicates that the pump is in use.

The heat pump is used from 2:00 to 10:00 to ensure that the top of the WWST is maintained above 35°C. The Loop B collector configuration is used starting at 11:00 when incident radiation is sufficient to produce a fluid temperature rise of greater than 3°C across the collectors. Loop B

operations continue intermittently until 15:00 when the collectors are no longer able to obtain useful thermal gains.

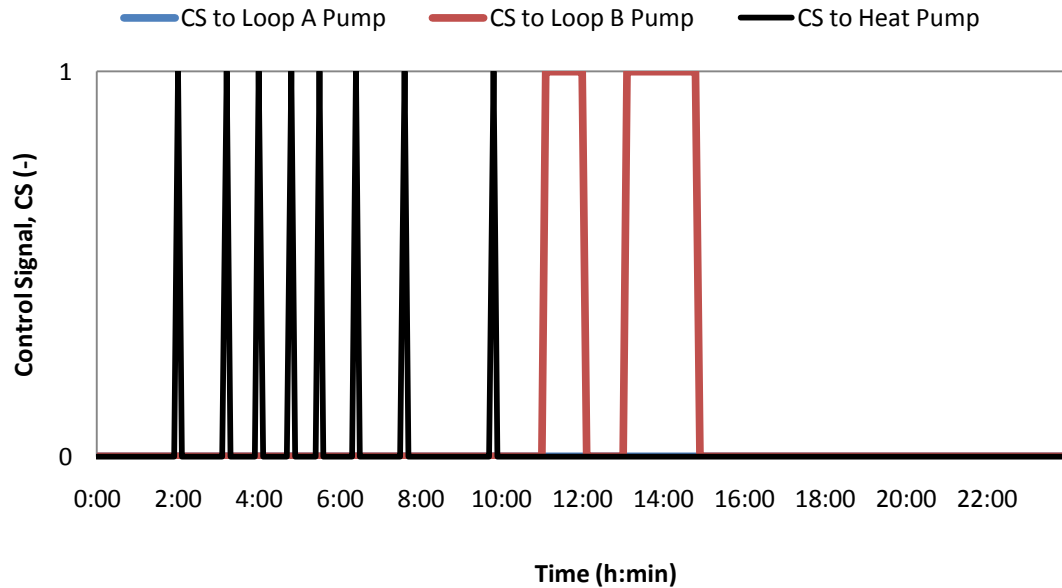


Figure 6-8: Pump and Heat Pump Control Signals for October 25th

Figure 6-9 shows the fluid temperatures in the WWST. Node 1 and Node 4 refer to the top and bottom of the WWST respectively.

Fluid temperatures decline from 0:00 to 2:00 until the Node 1 temperature reaches 35°C. At this point the heat pump turns on, heating the WWST until the Node 1 temperature rises above 37°C. This cycle is repeated until 11:00, when Loop B collector operations initiate a rise in tank temperatures. Tank temperatures decline from 15:00 onwards due to the thermal demands of the radiant floor, DHW, and ventilation loops, and the lack of thermal supply from the Loop B collector configuration.

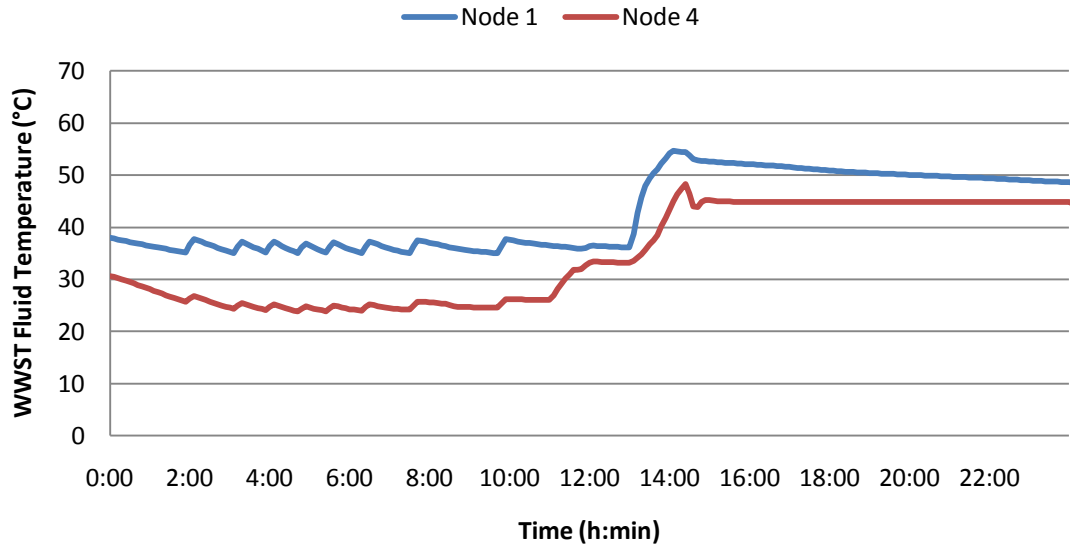


Figure 6-9: WWST Fluid Temperatures for October 25th

Figure 6-10 shows the fluid temperatures in the ice tank. Temperatures experience a slight decline from 2:00 to 10:00 when the ice tank is used as a source of thermal energy for the heat pump.

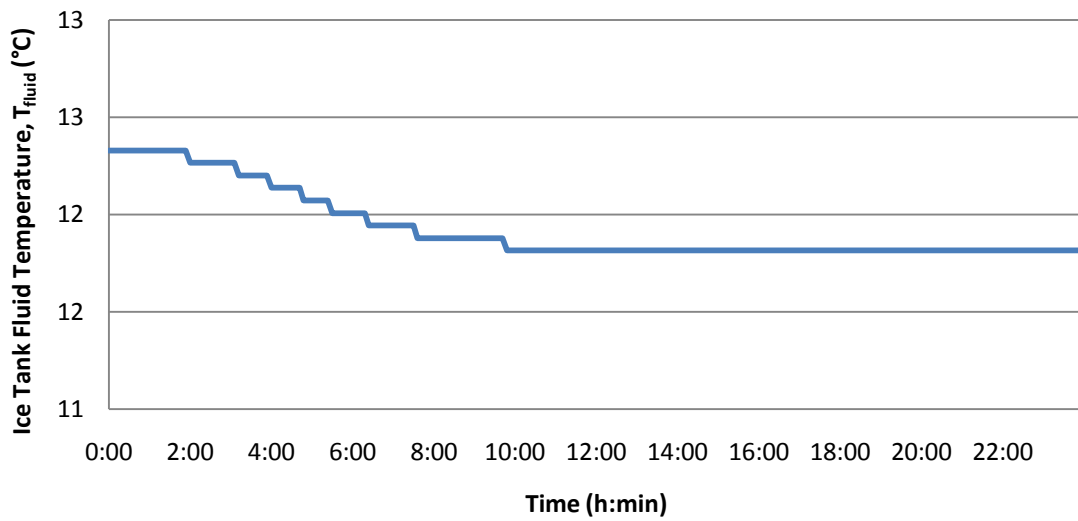


Figure 6-10: Ice Tank Fluid Temperatures for October 25th

Study Period 2: January 5th

Figure 6-11 shows the Control Signal (CS) for the Loop A pump, Loop B pump, and heat pump. A control signal of 0 corresponds to the pump being off, while a control signal of 1 indicates that the pump is in use.

The heat pump is used from 2:00 to 8:30 to ensure that the temperature at the top of the WWST remains above 35°C. Loop B operations commence at 8:30 when the collectors are able to produce the required 3°C temperature rise. Operations continue until 11:00 when the maximum temperature at the top of the WWST (60°C) is reached. At this point the system switches to the Loop A mode until the WWST temperature falls back within the acceptable range. This pattern is repeated until 15:00 when both loops are unable to obtain useful thermal gains from the collectors.

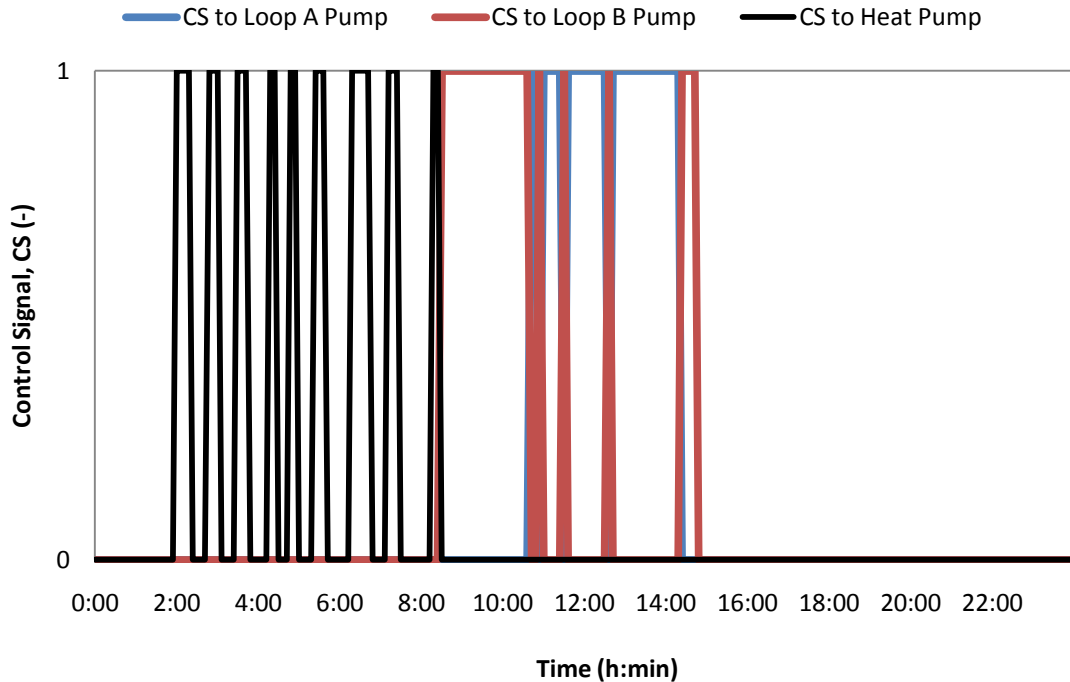


Figure 6-11: Pump and Heat Pump Control Signals for January 5th

Figure 6-12 shows the fluid temperatures in the WWST. Node 1 and Node 4 refer to the top and bottom of the WWST respectively.

Tank temperatures fall from 0:00 to 2:00 until the Node 1 temperature reaches 35°C. At this point the heat pump turns on, warming the top of the tank until it reaches 37°C. This pattern is maintained until 8:30 when the use of the Loop B configuration initiates a significant rise in tank temperatures. Loop B operations continue until 11:00 when the Node 1 temperature exceeds the maximum setpoint of 60°C. A series of shorter Loop B operations maintain the Node 1 temperature near 60°C until 15:00, after which point fluid temperatures decline due to the loads imposed by the heating, DHW, and ventilation systems.

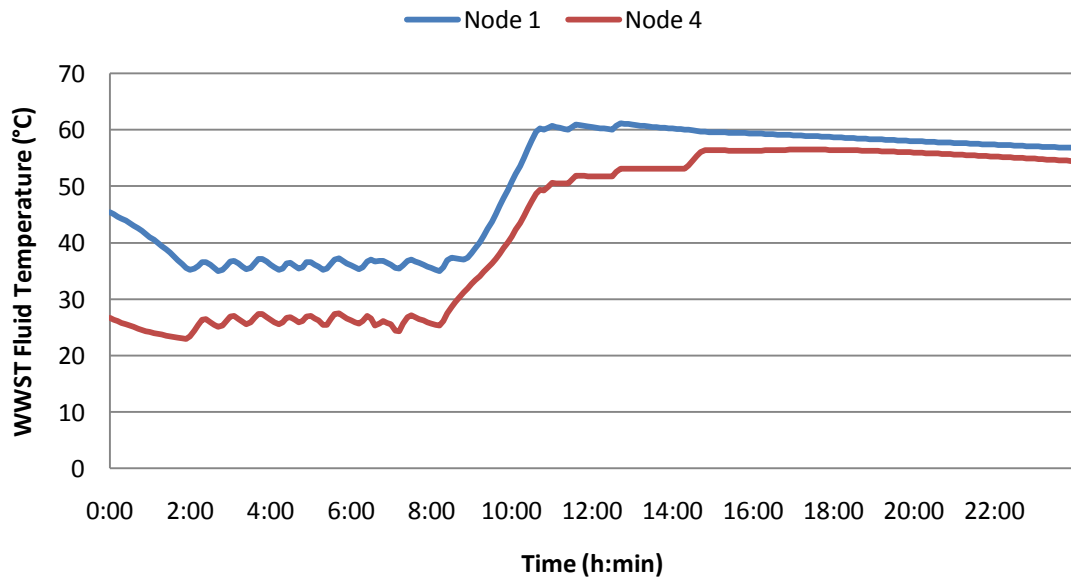


Figure 6-12: WWST Fluid Temperatures for January 5th

Figure 6-13 shows the ice mass in the ice tank. The ice inventory increases from 2:00 to 8:30 when the heat pump is used. Loop A operations then result in a steady melting of ice from 11:00 to 14:30. The ice mass continues to decline at much slower rate from 14:30 onwards due to heat losses to the fluid layer and ambient air.

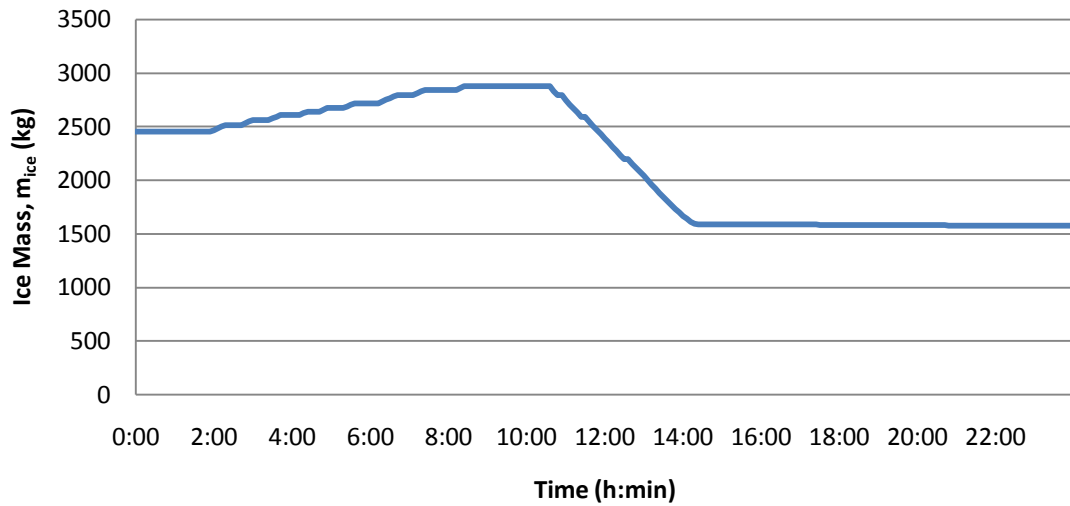


Figure 6-13: Ice Inventory in Ice Tank for January 5th

Conclusions Regarding Daily Performance

Based on the results from the two study periods, it can be concluded that the control strategy works as anticipated: Priority is given to the Loop B configuration, with the heat pump being used as a secondary source to maintain a minimum temperature of 35°C at the top of the WWST. Loop A and Loop B do not operate simultaneously at any point during the two analysis periods, while the combined use of the heat pump and Loop B configuration is also avoided.

An examination of the WWST fluid temperatures shows that the system is able to respect the defined minimum and maximum setpoint temperatures. Collector operations have a clear impact on the fluid temperatures in both the ice and WWST tanks, confirming the proper transfer of thermal energy to the system.

6.3 Summary

The performance of a solar assisted heat pump using ice slurry has been examined using the TRNSYS energy simulation program. The system demonstrated a significant potential for energy savings, achieving a solar fraction of 0.88 and a system COP of 8.22 in a high performance home in Montreal, QC. A comparison of the system with other heating methods showed that the use of ice storage resulted in an 86% reduction in the heating operating energy use relative to an electrical resistance system, and a 26% reduction relative to a solar assisted heat pump operating only using sensible storage. An analysis of system performance on a monthly and daily scale confirmed the proper implementation of the control strategy and highlighted the improvement in solar collector performance resulting from the use of ice storage.

7. Conclusions

This study has first presented the development of a mathematical model for the simulation of a non-agitated ice slurry storage tank. The model was integrated into the TRNSYS 16 simulation program and verified using available experimental data.

A computer model was then formulated to simulate a solar assisted heat pump using ice slurry. The system was integrated into a high performance home in Montreal, QC with a heating season from Oct. 1st to May 15th. Optimizations were performed on a set of design variables defining the solar collectors and the thermal storage capacity of the system, with the goal of minimizing the heating operating energy use of the home over a single heating season. The optimization results were compared for three different control strategies. A sensitivity analysis outlined the impact of each design variable on the overall performance of the system.

An analysis of the simulation results leads to the following conclusions:

1. The ice slurry tank model shows good agreement with the experimental ice mass and tank fluid temperature data during the charging and discharging modes of operation.
2. The use of a solar assisted heat pump with ice slurry has the potential to significantly reduce the heating operating energy use of a high performance home in Montreal, QC. The home had a heating operating energy use of 1504 kW·h, representing an 86% reduction relative to an electrical resistance heating system, and a 26% reduction relative to a solar assisted heat pump with sensible storage only.

The use of ice storage also resulted in an improvement in the solar collector efficiency. The system had a seasonal collector efficiency of 0.43, which represents a significant improvement over the results of Hugo (2008) who found an annual flat plate collector efficiency of 0.21 in a solar combi-system.

3. The solar collector area, ice tank volume, and warm water storage tank volume should be set near their maximum possible values to achieve the greatest reductions in heating operating energy use. The specific collector flow rate should be set near the lower bound of the manufacturer specified operating range, while the solar collectors should have a more vertical orientation to maximize the capture of solar radiation during the winter months.
4. The volume of the warm water tank needs to be selected carefully, as the heating operating energy use was found to be highly sensitive to reductions in the size of this tank. System performance was moderately sensitive to changes in the solar collector area, tilt angle, and flow rate. This allows a degree of flexibility when defining these variables. The ice tank volume exhibited a minimal impact on system performance even as the tank size was decreased by a factor of 2.
5. The solar loop control strategy should give priority to operating the solar collectors against warm water storage tank. This lowers the heating operating energy use of the home by reducing the duration of heat pump operations.

7.1 Contributions

This study presents the following components and contributions:

1. Analysis of the currently available simulation models for ice storage tanks.
2. Review of the use of ice storage for home heating, both in simulation and in practice.
3. Development of a new mathematical model for the simulation of an ice slurry storage tank.
4. Modeling of a solar assisted heat pump using ice slurry as a latent storage material.
5. Optimization of the solar assisted heat pump system using three different control strategies, with the objective of minimizing the heating operating energy use of the home.
6. A one-dimensional sensitivity analysis on the selected design variables.

7.2 Future Work

While the performance of the new ice tank model has been verified with experimental data, further improvements could be made to the modeling of the heat transfer between the ice layer and the incoming fluid stream. The current model uses an effectiveness coefficient function which was developed based on available experimental data for an ice harvester system. Further experimental work could be performed to determine an effectiveness coefficient function specific to an ice slurry system, as the smaller ice particles in this type of design may lead to small differences in the transfer of thermal energy.

The applicability of the ice tank model could also be expanded to simulate a well-mixed storage tank. Currently, it is assumed that the ice and water separate into two distinct layers at each time step. This limits the use of the tank model to situations where ice slurry remains in the tank and is not circulated to a heat transfer device. Simulating a well mixed tank would allow

designers to use the new model for a wider variety of applications, including the direct use of ice slurry at a cooling coil or solar collector.

On a system level, further research could be done to examine the impact of different types of solar collectors. Evacuated tube collectors could help to improve solar collector performance during Loop B operations, while the use of unglazed flat plate collectors could result in a decrease in the capital costs of the system. Furthermore, the possibility of circulating ice slurry directly to the solar collectors is another area of investigation. This has the potential to improve the solar collector efficiency, as the working fluid would remain at 0°C during the phase change from ice to water.

The current study focused on determining a set of design variables that minimized the heating operating energy use over a single heating season. The scope of the study could be further expanded by performing optimizations based on the lifecycle energy use or lifecycle cost. While the addition of solar collectors and thermal storage capacity results in a reduction in the energy use of the home, these devices also require an initial investment in terms of embodied energy and cost. Performing optimizations on a lifecycle basis would assist in identifying the design solutions that best balance these two competing factors.

References

1st Choice Portable Chillers. (2011). *Glycol Concentration Corresponding Freeze Point*. Retrieved Jun. 14th, 2011 from

<http://www.1stchoicechillers.com/docs/glycolconcentrationrequirements.pdf>.

Adam, C., and Andre, P. (2003). Ice Storage System (ISS): Simulation of a Typical HVAC Primary Plant with an Ice Storage Unit. *Proceedings of the Eighth International IBPSA Conference*, Eindhoven, Netherlands, 11-14 August 2003, pp 47-54. Retrieved Dec. 19th, 2009 from http://www.ibpsa.org/m_papers.asp.

Aguilar, C., White, D., and Ryan, D. (2005). *Domestic Water Heating and Water Heater Energy Consumption in Canada* (Technical Report CBEEDAC 2005-RP-02). Edmonton, AB: Canadian Building Energy End-Use Data Analysis Center, University of Alberta.

Arias, D., McMahan, A., and Klein, S. (2008), Sensitivity of long-term performance simulations of solar energy systems to the degree of stratification in the thermal storage unit. *International Journal of Energy Research*, 32(3), 242-254.

ASHRAE. (1993). *Development of a Design Procedure for Thermal Energy Storage Tanks Which Separate the Manufacture from the Storage of Ice* (Final Report Research Project 707). Atlanta: ASHRAE.

ASHRAE. (2005). *2005 ASHRAE Handbook-Fundamentals*. Atlanta, GA: ASHRAE.

ASHRAE. (2006). *ASHRAE GreenGuide-The Design, Construction, and Operation of Sustainable Buildings* (2nd ed.). New York, NY: Elsevier.

ASHRAE. (2007). *2007 ASHRAE Handbook:HVAC Applications*. Atlanta, GA: ASHRAE.

Behschnitt, S. A. (1996). *A Comparison of Water-Ethanol, Pure Water and Ice as Storage Media for Building Thermal Storage Applications* (M.S Thesis, University of Wisconsin-Madison).

Retrieved Dec. 5th, 2009 from <http://minds.wisconsin.edu/handle/1793/39136?show=full>.

Boerstra, A., Op'Veld, P., and Eijdem H.(2000). The Health, Safety, and Comfort Advantages of Low Temperature Heating Systems- A Literature Review. *Proceedings of Healthy Buildings*

Conference, Espoo Finland, August 6-10 2000. Retrieved Jan. 11th, 2011 from

http://www.healthyheating.com/IEQ_Radiant.htm.

California Department of Resources Recycling and Recovery (Calrecycle). (1998). *CANMET*

Advanced Houses Program. Retrieved Dec. 8th, 2009 from

<http://www.calrecycle.ca.gov/condemo/CaseStudies/CanMet/>.

Canadian Commission on Building and Fire Codes. (1997). *Model National Energy Code of*

Canada for Houses. Ottawa, Ont: National Research Council of Canada.

Chan, A., Chow, T., Fong, S. and Lin, J.(2006). Performance evaluation of district cooling plant with ice storage. *Energy*, 31(14), 2750-2762.

Dincer, I., and Konoglu, M. (2010). *Refrigeration Systems and Applications* (2nd ed). Chichester U.K: John Wiley and Sons.

Duffie, J., and Beckman, W. (2006). *Solar Engineering of Thermal Process* (3rd ed.). New York, NY: John Wiley and Sons.

Dumas, M., and Marcoux, C. (2004). *Température de l'eau dans l'aqueduc de Montréal*. Retrieved Nov. 19th, 2010 from http://www.ashrae-mtl.org/text/a_ashrae.html.

Eemax. (2010). *Eemax-Series Two*. Retrieved Oct. 10th, 2010 from <http://www.eemaxinc.com/SeriesTwo>.

Egolf, P.W, Kitanovski, A., Ata-Cesar, D., Vuarnoz, D., and Meili, F. (2008). Cold storage with ice slurries. *International Journal of Energy Research*, 32(3), 187-203.

Enermodal Engineering Ltd. (1992). *Performance of the Brampton Advanced House* (Technical Report). Ottawa, Ont.: Efficiency and Alternative Energy Technology Branch, CANMET, Energy, Mines and Resources Canada.

Engineering Toolbox. (2010). *Fittings and Minor Pressure Loss*. Retrieved Dec. 15th, 2010 from http://www.engineeringtoolbox.com/fittings-minor-pressure-loss-d_191.html.

Environment Canada. (2010). *National Inventory Report 1990-2008: Greenhouse Gas Sources and Sinks* (Technical Report). Retrieved Jul. 21st, 2011 from <http://www.ec.gc.ca/Publications/default.asp?lang=En&xml=492D914C-2EAB-47AB-A045-C62B2CDACC29>.

Feldman, D., Shapiro, M.M., Banu, D., and Fuks, C.J. (1989). Fatty Acids and Their Mixtures as Phase-Change Materials for Thermal Energy Storage. *Solar Energy Materials*, 18(3-4), 201-216.

Feldman, D., Banu, D., Hawes, D., and Ghanbari, E. (1991). Obtaining an energy storing building material by direct incorporation of an organic phase change material in gypsum wallboard. *Solar Energy Materials*, 22(2-3), 231-242.

Fischer, H.C. (1981). Seasonal ice storage for domestic heat pumps. *International Journal of Refrigeration*, 4(3), 135-138.

Flick, D., Doursat, C., and Ben Lakhdar, M. (2007). Modelling and numerical simulation of ice slurry storage tank. *Computer Aided Chemical Engineering*, 24(1), 1169-1174.

Frei, B., and Huber, H. (2005). Characteristics of different pump types operating with ice slurry. *International Journal of Refrigeration*, 28(1), 92-97.

Gerbas, D. (2000). *The Energy Performance of the NOVTEC Advanced House* (M.A.Sc Thesis, Concordia University). Retrieved Jul. 22nd, 2011 from <http://www.collectionscanada.gc.ca/obj/s4/f2/dsk3/ftp04/MQ59296.pdf>.

Government of Quebec . (2011). *Regulation Respecting Energy Conservation in New Buildings*. Retrieved Mar. 15th, 2011 from <http://www.canlii.org/en/qc/laws/regu/rq-c-e-1.1-r1/latest/rq-c-e-1.1-r1.html>.

Grozdek, M., Khodabandeh, R., and Lundqvist, P. (2009). Experimental investigation of ice slurry flow pressure drop in horizontal tubes. *Experimental Thermal and Fluid Science*, 33(2), 357-370.

Han, Z., Zheng, M., Kong, F., Wang, F., Li, Z., and Bai, T. (2008). Numerical simulation of solar assisted ground-source heat pump heating system with latent heat energy storage in severely cold area. *Applied Thermal Engineering*, 28 (11-12), 1427-1436.

Hasnain, S. (1998). Review on sustainable thermal energy storage technologies. II. Cool thermal storage. *Energy Conversion and Management*, 39(11), 1139-1153.

Hawes, D.W., Feldman, D., and Banu D. (1993). Latent heat storage in building materials. *Energy and Buildings*, 20(1), 77-86.

Hugo, A. (2008). *Computer Simulation and Life Cycle Analysis of a Seasonal Thermal Storage System in a Residential Building*(M.A.Sc Thesis, Concordia University). Retrieved from ProQuest Dissertations and Thesis (MR 45464).

IIR. (2005). *Handbook on Ice Slurries-Fundamentals and Engineering*. Paris:IIR/IIF.

Illan, F., and Viedma, A. (2009). Experimental study on pressure drop and heat transfer in pipelines for brine based ice slurry. Part I: Operational parameters correlations. *International Journal of Refrigeration*, 32(5), 1015-1023.

IPCC. (2007). Summary for Policymakers. In S. Solomon, D. Qin, M. Manning, Z. Chen, M. Marquis, K.B. Averyt, M. Tignor and H.L. Miller (Eds.), *Climate Change 2007: The Physical Science Basis. Contribution of Working Group I to the Fourth Assessment Report of the Intergovernmental Panel on Climate Change* (pp 8-22). New York, NY: Cambridge University Press.

Jenni Energietechnik AG. (2011). *Preise vollständig*. Retrieved Jul. 16th, 2011 from http://www.jenni.ch/pdf/Preise_vollst%C3%A4ndig.pdf.

Jordan, U., and Vajen, K. (2001). *Realistic Domestic Hot-Water Profiles in Different Time Scales* (Technical Report, V2.0). Marburg, Germany: Universität Marburg. Retrieved Nov. 17th, 2010 from <http://sel.me.wisc.edu/trnsys/trnlib/iea-shc-task26/iea-shc-task26-load-profiles-description-jordan.pdf>.

Kasuda, T., and Archenbach, P. (1965). Earth temperature and thermal diffusivity at selected stations in the United States. *ASHRAE Transactions*, 71(1), 61-74.

Klein et al. (2004) *TRNSYS 16 - A TRaNsient SYstem Simulation program, User manual. Getting Started* — Solar Energy Laboratory, University of Wisconsin-Madison. For more information, see <http://sel.me.wisc.edu/trnsys/default.htm>

Kondo, M., Matsuki, N., Nakano, Y., Miyanaga, T., and Oka, T. (1999). Performance of Radiant Cooling System Integrated with Ice Storage. *Energy and Buildings*, 30(2), 177-183.

Kuchen, E., and Fisch, M.N. (2009). Spot Monitoring: Thermal comfort evaluation in 25 office buildings in winter. *Building and Environment*, 44(4), 839-847.

Li, X., Zhang, X., Cao, R., and Fu, X. (2009). A novel ice slurry producing system: Producing ice by utilizing inner waste heat. *Energy Conversion and Management*, 50(12), 2893-2904.

Lund, P.D. (2005). Sizing and applicability considerations of solar combisystems. *Solar Energy*, 78(1), 59-71.

Mathworks. (2008). *Matlab R2008b*. For more information, see <http://www.mathworks.com>.

Mayo, T., and Sinha, R. (Sept./ Oct. 1996). Advanced Houses: The Canadian Experience. *Home Energy Magazine*. Retrieved Jun. 15th, 2011 from <http://www.homeenergy.org/archive/hem.dis.anl.gov/eehem/96/960909.html>.

Microsoft Corp. (1998). Microsoft Visual C++ V6.0. For more information, see <http://msdn.microsoft.com/en-us/visualc/aa336395>

Microsoft Corp. (2007). *Microsoft Office Excel 2007*. For more information, see <http://office.microsoft.com/en-ca/excel/>

Niezgoda-Zelasko, B., and Zalewski, W. (2006). Momentum transfer of ice slurry flows in tubes, experimental investigations. *International Journal of Refrigeration*, 29(3), 418-428.

Norgaard, E., Sorensen, T.A., Hansen, T.M., and Kauffeld, M. (2005). Performance of components of ice slurry systems: pumps, plate heat exchangers, and fittings. *International Journal of Refrigeration*, 28(1), 83-91.

NRCan. (2010a). *Energy Use Data Handbook, 1990 to 2007*. Retrieved Oct. 10th, 2010 from <http://oee.nrcan.gc.ca/Publications/statistics/handbook09/index.cfm?attr=24>.

NRCan. (2010b). *About R-2000*. Retrieved Dec. 18th, 2010 from <http://oee.nrcan.gc.ca/residential/personal/new-homes/r-2000/about-r-2000.cfm>.

Poirier M. (2010). Personal Communications, NRCan/CanmetENERGY, received Mar. 26th 2010.

Poirier M. (2011a). Personal Communication, NRCan/CanmetENERGY, received Jan. 20th, 2011.

Poirier M. (2011b). Personal Communications. NRCan/CanmetENERGY, received Jan. 27th 2011.

Qi, Q., Deng, S., and Jiang, Y. (2008). A simulation study on a solar heat pump heating system with seasonal latent heat storage. *Solar Energy*, 82(8), 669-675.

Silver, S.C., Milbitz, A., Jones J.W., Peterson J.L., and Hunn, B.D. (1989). Component Models for Computer Simulation of Ice Storage Systems. *ASHRAE Transactions*, 95(1), 1214-1226.

SunMaxx Solar. (2010). *TitanPowerPlus SU-2 Solar Flat Plate Collector*. Retrieved Oct. 3rd, 2010 from <http://www.siliconsolar.com/titanpowerplussu2-solar-flat-plate-collector-p-501608.html>.

SUNSYSTEM. (2011). *Solar thermal appliances*. Retrieved Jul. 16th, 2011 from <http://www.sunsystem.bg/en/slanchevi-termalni-izdelia/>.

Tanino, M., and Kozawa, Y. (2001). Ice-water two-phase flow behavior in ice heat storage systems. *International Journal of Refrigeration*, 24(7), 639-651.

TESS. (2007). *TESS Library Documentation*. Madison, USA: Thermal Energy System Specialists.

Tong, A. (2001). Improving The Accuracy of Temperature Measurements. *Sensor Review*, 21(3), 193-198.

Trinkl, C., Zorner, W., and Hanby, V. (2009). Simulation study on a Domestic Solar/Heat Pump Heating System Incorporating Latent and Stratified Thermal Storage. *Journal of Solar Energy Engineering*, 131(4), 041008-1 to 041008-8.

UNIPHIZ Lab. (2011). Findgraph V2.311. For more information, see <http://www.uniphiz.com/findgraph.htm>.

United Nations Framework Convention on Climate Change (UNFCCC). (2011). *Kyoto Protocol*. Retrieved Jul. 31st, 2011 from http://unfccc.int/kyoto_protocol/items/2830.php.

Ure, Z. (1999). Slurry ice based cooling systems. *Proceedings of 20th International Conference on Refrigeration into the Third Millenium*, Sydney, Australia, 19 -24 September 1999. Retrieved Nov. 16th, 2010 from <http://www.epsltd.co.uk/files/iiraustralia99005.pdf>.

Venmar. (2007). *Air Exchangers, Range Hoods, Attic Ventilators Product*. Retrieved Oct. 11th, 2007 from <http://www.venmar.ca/>.

Viessmann. (2010). *Vitocell-V 300 Indirect-Fired DHW Tanks*. Retrieved Dec. 1st, 2010 from http://www.viessmann.ca/en/products/speicher-wassererwaermer/Vitocell-V_300.html.

Viessmann. (2011). *System Design Guidelines*. Retrieved April 14th, 2011 from <http://www.viessmann.us/en/services/manuals.html>.

Vogelsanger, P. and Laipple S. (2006). *WP1.D1 : Summary report on today's technologies* (NGEST Technical Report WP1.D1). Retrieved Apr. 12th, 2011 from http://www.swt-technologie.de/NEGST1_D1.pdf.

Wang, M.J., and Kusumoto, N. (2001). Ice slurry based thermal storage in multifunctional buildings. *Heat and Mass Transfer*, 37(6), 597-604.

Wetter, M., and Wright J. (2004). A comparison of deterministic and probabilistic optimization algorithms for nonsmooth simulation-based optimization. *Building and Environment*, 39(8), 989-999.

Wetter M. (2009). *GenOpt: Generic Optimization Program User Manual Version 3.0.0* (Technical Report LBNL-2077E). Berkeley, CA: Lawrence Berkeley National Laboratory. Retrieved Mar. 15th, 2011 from <http://gundog.lbl.gov/GO/>.

Wilo. (2010). *Wilo Pumps*. Retrieved Dec. 12th, 2010 from <http://www.wilo.com/cps/rde/xchg/en/layout.xsl/start.htm>.

Wilson, T.M., Nicholas, B.D., Hirt, C.W., and Stein, L.R. (1988). *SOLA-DM, A numerical solution algorithm for transient three-dimensional flows* (Technical Report LA-11161-MS). Los Alamos, NM: Los Alamos National Laboratory.

Wulfinghoff, D. (1999). *Energy Efficiency Manual*. Maryland, USA: Energy Institute Press.

Zmeureanu, R., and Wu, X. (2007). Energy and exergy performance of residential heating systems with separate mechanical ventilation. *Energy*, 32(3), 187-195.

Appendix A1: Heat Pump Performance

Table A1-1 contains a summary of heat pump performance data used in the TRNSYS simulation model. Compressor performance is based on the use of an Emerson ZB38KCE-TF5 (Poirier, 2010).

Table A1-1: Heat Pump Performance Data

		Inlet Fluid Temperature to Evaporator (°C)							
		-17.3	-11.8	-6.2	-0.7	4.9	10.4	13.2	
Inlet Fluid Temperature to Condenser (°C)	50.0	Heating Capacity (kW)	10.4	12.4	14.3	16.3	18.7	21.5	23.2
		Power Input (kW)	7.6	7.6	7.6	7.6	7.6	7.5	7.5
	44.4	Heating Capacity (kW)	11.0	12.8	14.6	16.8	19.4	22.4	24.1
		Power Input (kW)	6.7	6.7	6.8	6.8	6.8	6.7	6.7
	38.9	Heating Capacity (kW)	11.4	13.0	15.0	17.3	20.1	23.1	25.3
		Power Input (kW)	6.0	6.0	6.0	6.0	6.0	6.0	6.0
	33.3	Heating Capacity (kW)	11.4	13.2	15.4	18.0	20.9	24.6	26.5
		Power Input (kW)	5.3	5.4	5.4	5.4	5.4	5.4	5.4
	27.8	Heating Capacity (kW)	11.6	13.5	15.9	18.6	21.8	25.6	27.7
		Power Input (kW)	4.8	4.8	4.8	4.8	4.8	4.8	4.8
	16.7	Heating Capacity (kW)	11.9	14.2	16.9	20.0	23.7	27.9	30.4
		Power Input (kW)	3.8	3.9	3.9	3.9	3.9	3.9	3.9
	11.1	Heating Capacity (kW)	12.1	14.5	17.4	20.8	24.7	28.7	32.7
		Power Input (kW)	3.4	3.5	3.5	3.5	3.5	3.5	3.5
	0.0	Heating Capacity (kW)	12.7	15.4	18.7	22.0	25.3	28.5	31.8
		Power Input (kW)	2.8	2.8	2.8	2.9	2.9	2.9	2.9

Appendix A2: DHW Temperature Profile

Table A2-1 contains a summary of the correlation coefficients used in the DHW temperature profile (Hugo, 2008). The value of a was fixed at 11.490452, while z was set equal to 0.0086904361.

Table A2-1: DHW Temperature Profile Correlation Coefficients

Harmonic	v_n	w_n
1	0.183995	0.090567
2	-6.77637	-7.3993
3	-0.09657	-0.20339
4	0.084369	0.882934
5	-0.00319	-0.03706
6	-0.09697	0.116119
7	0.014071	-0.02291
8	-0.33625	-0.01428
9	-0.02776	-0.01798
10	-0.03625	-0.13905
11	-0.01367	-0.05412
12	-0.01872	0.135356
13	-0.0066	-0.02064
14	-0.08932	0.084332
15	-0.04498	-0.01227
16	0.172708	0.068649
17	0.024282	0.000807

Appendix A3: Demonstration of Sample Optimization

Table A3-1 contains a detailed summary of the sample optimization.

Table A3-1: Results of Sample Optimization

Search around initial starting point, x_1				
Iterate	Sub-Iterate	Evaluation Point	Function Value	Comment
1	1	(3,7)	18	Evaluate $f(x_1)$
	2	(4,7)	25	Perform global search around x_1
	3	(2,7)	13	
	4	(2,8)	20	
	5	(2,6)	8	
Lowest value at (2,6). Set $x_2 = (2,6)$ and maintain $\Delta_2=1$.				
Make exploratory move to $x_b=(1,5)$				
2	1	(1,5)	2	Evaluate x_b
	2	(2,5)	5	Perform global search around x_b
	3	(0,5)	1	
	4	(0,6)	4	
	5	(0,4)	0	
The global search results in a reduction of the objective function.				
Set $x_2=(0,4)$, and perform local search				
2	6	(1,4)	1	Perform local search around x_2
	7	(-1,4)	1	
	8	(0,5)	1	
	9	(0,3)	1	
The exploratory move results in a reduction in the objective function. Set $x_3 = (0,4)$ and maintain $\Delta_3=1$.				
Make exploratory move to $x_b=(-1,3)$				
3	1	(-1,3)	2	Evaluate x_b
	2	(-2,3)	5	Perform global search around x_b
	3	(0,3)	1	
	4	(0,2)	4	
	5	(0,4)	0	
The global search does not result in a reduction of the objective function.				
Perform a local search around $x_3=(0,4)$				
3	6	(-1,4)	1	Perform local search around x_3
	7	(1,4)	1	
	8	(0,3)	1	
	9	(0,5)	1	
Neither the global or local searches associated with the exploratory move result in a reduction in the objective function.				
Set $x_4=(0,4)$, reduce the step size $\Delta_4=0.5$				
4	1	(0,4)	0	Evaluate x_4
	2	(-0.5, 4)	0.25	Perform global search around x_4
	3	(0.5, 4)	0.25	
	4	(0,3.5)	0.25	
	5	(0, 4.5)	0.25	
The global search does not result in a reduction in the objective function.				
Set $x_5=(0,4)$, reduce the step size $\Delta_5=0.25$				
5	1	(0,4)	0	Evaluate x_5
	2	(-0.25,4)	0.0625	Perform global search around x_5
	3	(0.25,4)	0.0625	
	4	(0, 3.75)	0.0625	
	5	(0, 4.25)	0.0625	
The global search does not result in a reduction in the objective function.				
Set $x_6=(0,4)$, reduce the step size $\Delta_6=0.125$				
Since $\Delta_6 < \Delta_{\min}$, terminate the algorithm with optimal point (0,4)				

